The electrical structure of nimbostratus clouds

Stringfellow, Michael F.

THE ELECTRICAL STRUCTURE OF NIMBOSTRATUS CLOUDS

BY

MICHAEL F. STRINGFELLOW, B.Sc., F.R.Met.S.

Presented in Candidature for the Degree of Doctor of Philosophy, in the University of Durham

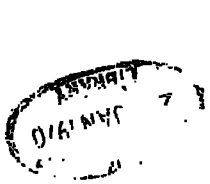

October, 1969

FOREWORD

The experimental work described in this thesis was conducted mainly at the University field centre at Lanehead in the Northern Pennines. Equipment for the measurement of precipitation current density and potential gradient was constructed and operated at Lanehead, and identical equipment was mounted upon a Land-Rover to provide mobile observations.

The author is indebted to the late Professor J.A. Chalmers who suggested and made possible the project; Dr. W.C.A. Hutchinson for his supervision and support throughout the project, Professor G.D. Rochester, Head of the Physics Department, who provided the facilities, and Professor W.B. Fisher, Head of the Geography Department, for the use of the Lanehead field centre.

The author wishes to express his thanks to fellow members of the Atmospheric Physics research group, particularly Mr. W.P. Aspinall who constructed the automatic recording system used for the project and whose assistance at Lanehead was invaluable. Thanks are also due to Mr. Jack Moralee for the construction of apparatus, Mr. Michael Lee for the photographs and reproduction of the diagrams and last, but not least, Mrs. S. Naylor for the speed and efficiency with which she typed this thesis.

This work was carried out with the support of research grants from the United States Office of Naval Research and from the Natural Environment Research Council.

ABSTRACT

Simultaneous records of precipitation current density, potential gradient and wind speed have been obtained with mobile equipment mounted on a Land-Rover and with fixed equipment located at a field station in the Pennines. Measurements were made in quiet precipitation with the two sets of equipment separated by horizontal distances of up to 8 km in a direction in line with the cloud movement. Maximum cross-correlation between the precipitation current density records at the two stations was usually for time lags corresponding to the time of travel of the clouds between the stations. On one occasion of low wind speed, simultaneous precipitation current correlation was obtained at the two stations when separated by 5 km. It was deduced that the time variations of electrical parameters observed at a ground station would normally be the result of movement of the cloud system rather than its electrical development.

Analysis of the effects of wind speed has shown that rain electrification is more intense at sites more exposed to the wind and that the effects may be due to a process operating from ground level up to a height of several hundred metres.

The persistence of potential gradient and of precipitation current density has been shown to be inversely proportional to cloud speed. The horizontal dimensions of cloud across which persistence

exists at a given point in time has been shown to be independent of wind speed and to be of the order of several kilometres. It is suggested that these dimensions may be a characteristic of cloud type and may be used as a criterion for their identification.

A theoretical model to explain the electrical structure of nimbostratus clouds has been proposed, and it has been shown to be consistent with observations. The model satisfactorily explains the inverse relation between precipitation current density and potential gradient and it explains observed differences in phase between precipitation current-time and potential gradient-time curves in terms of the periodicity of the electrical changes within the cloud.

CONTENTS

CHAPTER 1

THUNDERSTORM AND QUIET PRECIPITATION ELECTRIFICATION

1.1 Introduction

The study of thunderstorms is important for two main reasons. Firstly, as large areas of intense meteorological activity, comprising strong horizontal and vertical winds, torrential rain and hail, much electrical activity, and occasionally tornadoes, thunderstorms are a hazard to agriculture, communications, navigation and also life. Secondly, thunderstorms represent both a large and efficient heat engine and an electrical generator, and are thus of interest to the physicist.

It is now generally agreed that the electrical effect of thunderstorms is to generate a current between the earth and ionosphere, both of which are very much more conductive than the air separating them. The ionosphere is maintained at a potential of about 0.3MV with respect to earth, a quasi-static state being maintained by the leakage current to earth in fair-weather regions.

The electrical studies of atmospheric physics are carried out in an attempt to discover the nature of charge separation and transport in both the free atmosphere and clouds, and to link these with the meteorological environment. Although smaller in magnitude, the electrification of continuous quiet rain ('Landregen') and the associated clouds is similar in some ways to that of the thundercloud.

The purpose of the present research project is to clarify the nature of the charge separation in continuous precipitation and its relevance to thunderstorm electrification.

1.2 The Electrical Structure of Thunderstorms

Although it is now over two hundred years since the electrical nature of the thundercloud was firmly established by the experiments of Franklin (1752) and D'Alibard (1752), the electrical mechanisms responsible for the charging of the cloud are still not understood. By measuring the electric field intensity due to both near and distant clouds, Schonland (1928), Wormell (1939), Malan and Schonland (1950) and Smith (1954) have established the approximate magnitudes and relative positions of the main charge centres. Similar information was obtained by Appleton et al (1926), Wormell (1939), Malan and Schohland (1950) and Pierce (1955), by measuring the electric field changes brought about by lightning flashes. Simultaneous multiple-station recording of potential gradient and other parameters has enabled Workman et al (1942), Barnard (1951) and Reynolds and Neill (1955) to estimate more accurately the magnitude of the charge centres and their positions relative to the cloud. Aircraft and balloon measurements have also produced useful information, particularly those of Simpson and Scrase (1937), Simpson and Robinson (1940) and Gunn (1948).

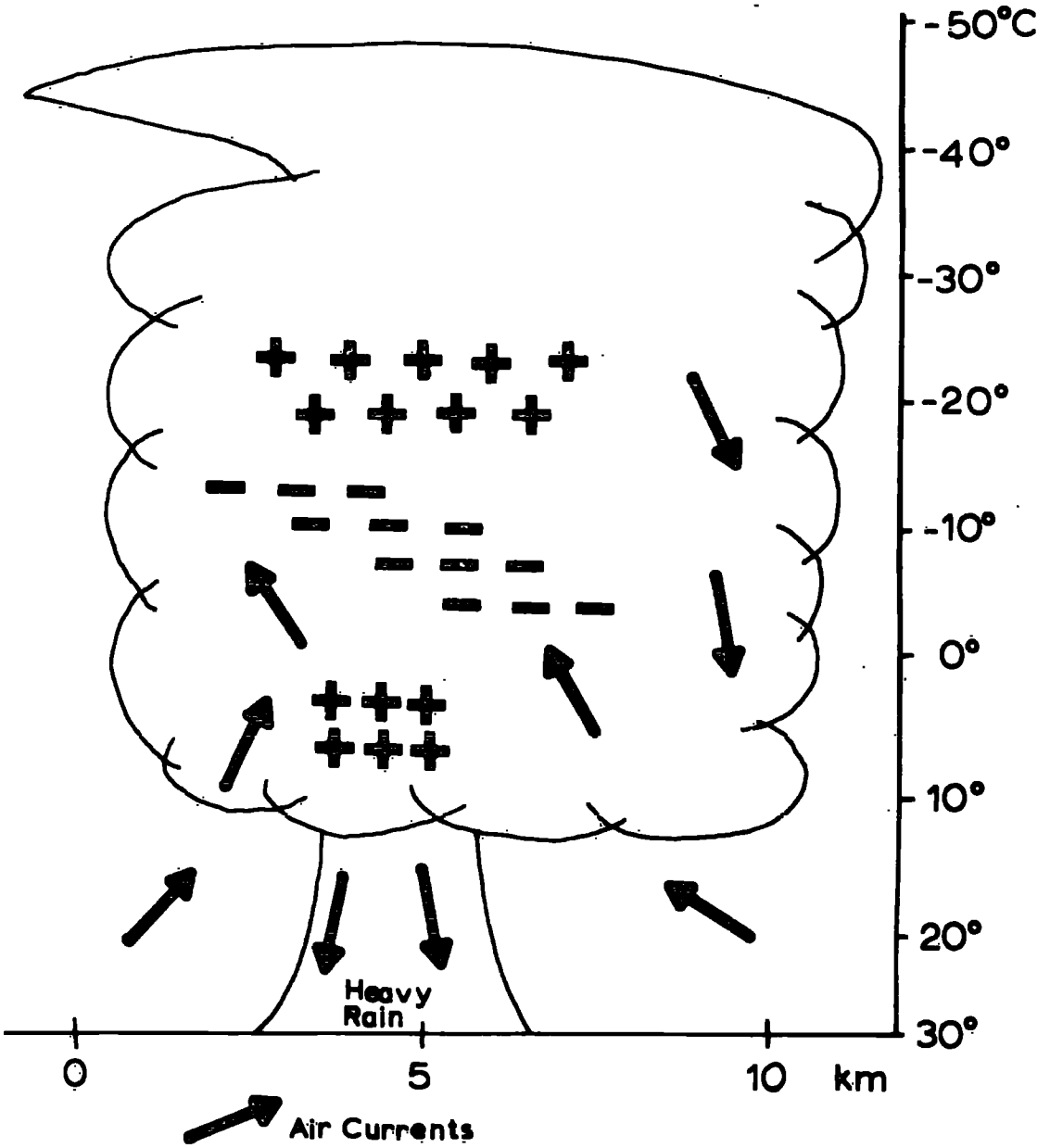

Fig. 1.1 Location of main thunderstorm charges.

The generalised electrical structure obtained from these measurements is an approximate double dipole, with the highest cloud charges being positive, the main lower charges being negative, and with a second lower positive charge of smaller magnitude (Fig. 1.1).

Earlier workers assumed the main charge centres to be distributed vertically above one another, but the measurements of Pierce (1955) and Brook (1969) suggest that considerable horizontal separation of charge centres may exist. Estimates of the quantities of charge involved vary considerably, but the excess charges in the main charge centres must be at least several tens of coulombs. The main negative and positive charge centres in the thunderclouds of temperate latitudes exist at temperatures below freezing, in regions where both solid and liquid hydrometeors exist, and the most favoured charging theories involve gravitational separation of oppositely charged particles, with the main updraught carrying the smaller particles aloft.

Examination of the recovery curve of potential gradient after lightning discharges has shown that regenerative currents of several amperes per storm cell are perhaps necessary. Aircraft measurements by Gish and Wait (1959) have shown that conduction currents of this magnitude flowing to the ionosphere do exist. The potential gradient at the ground beneath a storm reaches a maximum

value of around 10,000 Vm^{-1}, being limited by a space charge blanket of opposite sign released by point-discharge from raised objects. Precipitation current densities at the ground are found to be extremely variable in sign and magnitude, maximum values being of the order of 0.1 μAm^{-2}. It should be noted that this value is at least two orders of magnitude too small to explain the observed charges in the cloud, and it is generally thought that the charges on precipitation particles are much larger in the cloud. The most active thunderstorm cells produce flashes at a rate not normally exceeding one every five seconds, so that any theory of electrification must be able to explain these high rates of charge production.

1.3 The Electrification of Quiet-Precipitation Clouds

In conditions of steady precipitation not associated with stormy weather or showers, it was discovered by early workers that the clouds and precipitation were electrified. Potential gradient measurements often gave values different in sign or magnitude from fair-weather values, and it was soon realised that precipitation particles brought down charge also. The question then arose as to whether the charging mechanisms in quiet precipitation were similar to those in thunderstorms, but smaller in magnitude, or were quite different. It was also suggested that, if the precipitation brought down net negative charge, then since such large areas were involved,

quiet precipitation might contribute to the maintenance of the earth-ionosphere potential difference.

Simpson (1919, 1949), Reiter (1955), Adkins (1959) and other workers have found the potential gradient at the ground under clouds producing quietly falling snow not drifting at the ground to be usually positive. Simpson (1942), Chalmers and Little (1947) and Chalmers (1956) have measured the precipitation- or total-current density which they found to be usually negative. Wet snow, blowing snow and sleet were often found by many workers to be positively charged. The potential gradient at the ground does not normally exceed 1500 Vm^{-1}, and the precipitation current density 100 pAm^{-2}. The total air-earth current is nearly always of the same sign as the snow current, showing that conduction and convection currents are relatively much smaller.

Measurements in quiet rain are more numerous than those for snow, but, except in a few cases, records have not been taken continuously over long periods.

The results of Simpson (1949), Reiter (1955), Chalmers (1956), Adkins (1959) and also earlier workers show that the potential gradient at the ground in continuous quiet rain is usually negative. However, Kelvin (1860) and Chauveau (1900) discovered a negative potential gradient at the ground, with a simultaneous positive potential gradient at the top of a tower. Simpson (1909, 1949),

Scrase (1936), Ramsay and Chalmers (1960) and Reiter (1965) have found the rain current densities to be usually positive, having a maximum value of around 100 pAm^{-2}. Measurements taken above the ground of single drop charges have shown that the rain acquires a net positive charge before reaching the ground, and Reiter (1955) has shown that a significant change of sign of potential gradient takes place below the melting level (Figure 1.2).

These results indicate a minimum of two charge separation processes acting in the rain cloud, one acting in the solid phase at lower temperatures ($0^{o}c$ to $-20^{o}c$) giving negative charge to the precipitation and a positive charge to the cloud, and a lower process acting in the opposite direction. Thus the charge distribution in quiet rain clouds has the same polarity as the main charges in thunderclouds, which has led some workers to suggest that similar processes are at work, differing only in magnitude. However, Chalmers (1967) points out that the difference in magnitude between the charges of thunderclouds and quiet rain clouds cannot be explained merely in terms of the different rates of rainfall.

1.4 Thunderstorm Charge Separation Theories

Theories of charge separation in the thundercloud can be put generally into two classes, those depending on gravitational separation of charge, and those depending on non-gravitational

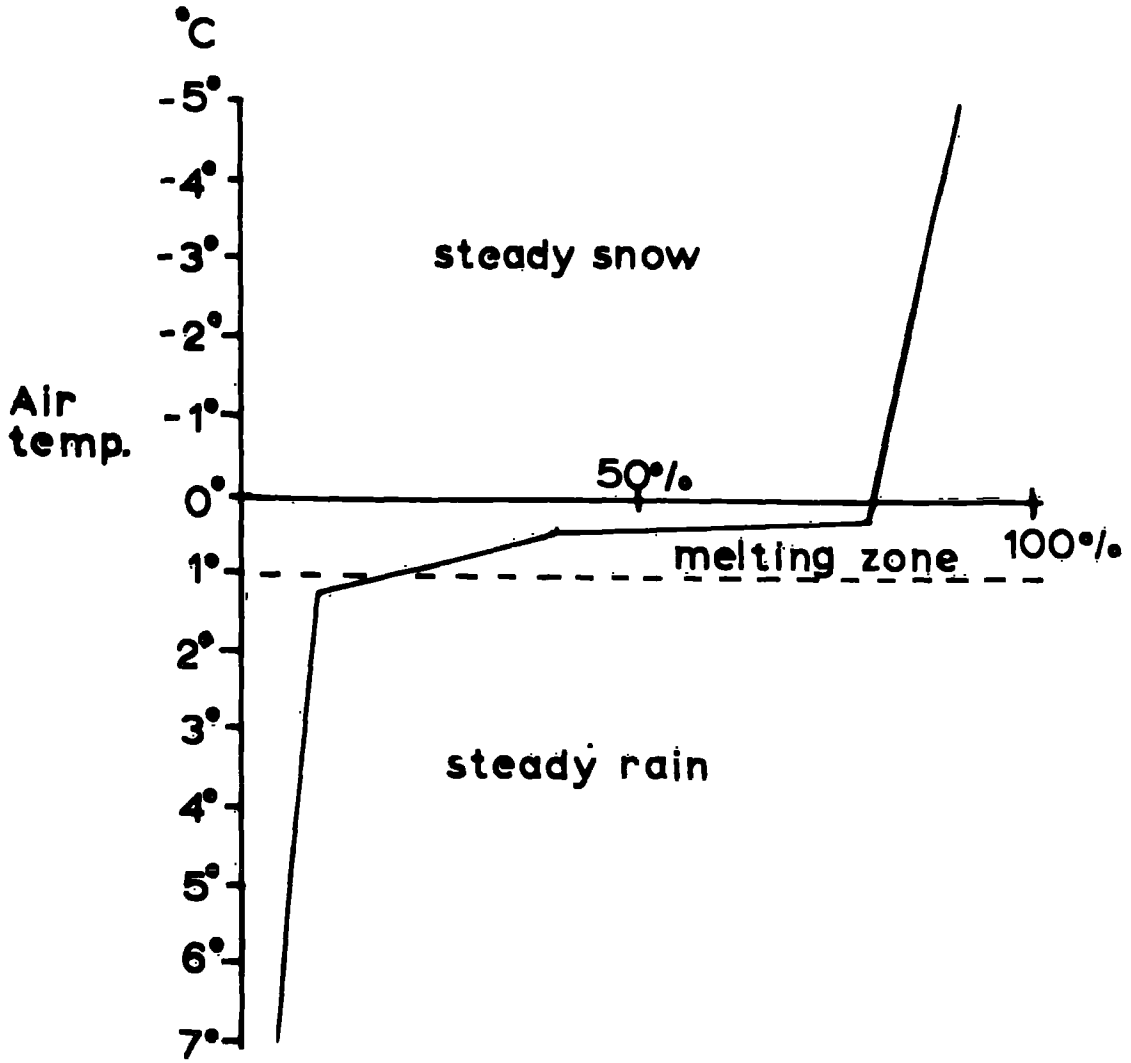

Fig. 1.2 Percentage frequency of positive extraneous potential gradient during precipitation.

separation, such as air currents. Each of these classes can be subdivided into two further classes, one utilising natural ions in the cloud, produced by cosmic rays and natural radioactivity, the other requiring charge production from originally neutral sources.

Class 1A

Theories involving gravitational separation of natural ions by selective attachment and 'influence' theories

Elster and Geitel (1885) suggested that raindrops would be polarized in an electric field, and that contact with the smaller cloud droplets as they fell would give rise to a separation of charge. If the droplets removed part of the induced charge on the bottom part of the falling raindrops, the separation is of the correct sign for thunderstorm electrification under the influence of the normal positive fair-weather potential gradient.

Wilson (1919) thought that ion capture by water drops polarised in the fair-weather field would give rise to electrification, and experiments by Gott (1933, 1935), and Muhleisen and Holl (1953) have shown that it does operate in certain conditions, but is small in magnitude. Whipple and Chalmers (1944), Wormell (1953) and Muller-Hillebrand (1954) have given detailed accounts of this process, and Chalmers (1947) has shown that similar processes can operate with ice particles.

Gunn (1935) and Frenkel (1944) have produced somewhat similar theories, but assume an electrical concentration cell to exist between the water droplets and the surrounding ions.

Many of the earlier theories were of the influence type, and of the modern theories none is thought to produce charge separation of sufficient magnitude to explain the charges found in an active thundercloud. Processes of this kind may, however, influence the early electrification of clouds, and certainly play a role in determining the charge carried on precipitation reaching the ground.

Class 1B

Theories involving charge production by precipitation particles

Lenard (1892) showed that splashing of water drops gives rise to a positive charge on the water and a negative charge on the air, and it was later shown by Simpson (1909) and Nolan (1914) that similar processes occur when water drops are broken by air currents or turbulence. Simpson (1927) and Chapman (1952) have shown that the charge production is of sufficient magnitude to produce thunderstorm charges. However, it operates at too high a temperature and in the wrong direction to explain the main thunderstorm charges, but may explain the lower positive charge, which seems to be associated with the zone of heavy rain.

Simpson (1919) found that in blizzards large positive potential gradients were produced, and Simpson and Scrase (1937) suggested that ice crystal impact might be the charging mechanism responsible, and proposed a thunderstorm charging theory which suggested that ice impacts in the cloud would give a positive ionic charge to the air and a negative charge to the ice crystals.

Reynolds (1954) found considerable charging on riming of graupel pellets in the presence of supercooled water droplets, but the results of similar experiments by Latham and Mason (1961) and Hutchinson (1960) found very much smaller effects.

Workman and Reynolds (1950, 1953) suggested that partial glazing of supercooled cloud droplets on falling ice particles would give rise to charge production, positive charges being thrown off on smaller water droplets, and a negative charge remaining on the ice. At temperatures higher than 0°c, impacts with non-supercooled cloud droplets would throw off negative charge, giving a positive charge to the ice. Mason (1953) and Reynolds (1953) have shown that experimental results are in accord with the theory, and that sufficient charge production for thunderclouds is feasible by this mechanism. Reynolds, however, pointed out that the absence of supercooled water droplets at temperatures below -15°c would mean that the process cannot operate at higher levels, whereas observations have shown active cloud electrification at temperatures well below this.

Mason (1953) has proposed a similar theory involving riming, but thinks the positive charge is carried off by ions, and that the whole of the captured droplet is frozen. Latham and Mason (1961) found this separation of charge to be present, but found the positive charge to be carried off on small ice splinters and not ions. The process was found to give sufficient charge of the correct sign to explain thunderstorm electrification, and has been shown by Latham and Mason (1962) to be unaffected by high electric fields.

Chalmers (1943) proposed a theory dependent upon the freezing of water droplets, but Mason and Maybank (1960) showed that any effects are small.

Class 2

Theories not involving gravitational separation of charge

One of the objections against gravitational separation of charged precipitation particles is that the terminal velocity of the largest particles is about 10 ms^{-1}, and with observed regeneration times of about 10 seconds in an active thundercloud, a vertical separation of particles of only 100m is possible in this time. Some workers suggest that this requires prohibitively large charge densities on the precipitation. Air currents, however, often reach speeds several

times larger than 10 ms^{-1}, and several theories have been proposed requiring charge of one sign to be carried in the updraught, and the opposite sign in the downdraught.

Grenet (1947) first suggested this idea, and Vonnegut (1955) suggested that separation is produced by the relative motion of the central updraught and peripheral downdraughts. Vonnegut proposes that the updraught brings in the positive space charge normally existing below the cloud, and carries it upwards to the cloud top. This then reverses the potential gradient in the region, and when this becomes sufficiently high, point discharge at the ground produces a continuous supply of positive ions to replace the convected space charge. The upper positive charge is then considered to bring down negative ions by conduction, and these are then carried in the downdraught to augment the negative potential gradient. Vonnegut and Moore (1958) tried to test this theory by introducing negative charges under developing thunder-clouds in an attempt to reverse their polarity, but have so far not reported any sucess.

Chalmers (1967) raises objections to Vonnegut's theory, since the downdraught is not a feature of developing thunder cells, and also he can see no reason why the positive charges should not be brought down as well as the negative charges in the downdraught. He also suggests that the high correlation between the appearance of precipitation and electrification points towards precipitation charging.

1.5 Quiet Precipitation Charge Separation Theories

In conditions of quiet precipitation, electrification is smaller in magnitude and steadier in nature than that in thunderclouds. It is believed that all precipitation from nimbostratus clouds in temperate latitudes results from the production of snow crystals in the higher portion of the clouds. Updraughts rarely exceed 0.5 ms^{-1} and the terminal velocity of the largest snowflakes is about 1 ms^{-1}. This means that charge separation due to precipitation will proceed at a lower rate than in the thundercloud. Even in the lower portions of the cloud, after the snowflakes have melted, the larger drops break up to produce smaller ones with a maximum terminal velocity of about 5 ms^{-1}.

As discussed in Section 1.3, quietly falling dry snow crystals are negatively charged, whilst the potential gradient due to the snow cloud is positive. Chalmers (1959) has shown that, since the total vertical current in the snow cloud is usually negative downwards, the potential of the cloud top must be above that of the ionosphere. The only physically reasonable solution of this involves an active charge separation process within the cloud itself.

Most of the early theories of quiet snow electrification were of the influence type, requiring the selective capture of ions or similar processes, but present day measurements show that

all these processes are at least one order of magnitude too small to account for the observed charging. Other processes, such as riming or glazing, would not appear satisfactory either, particularly in view of the slow fall speed of snowflakes which precludes large temperature gradients and many impacts. Also, evidence suggests that nimbostratus electrification exists at temperatures below $-15^{\circ}c$, in the absence of many supercooled water droplets.

The only processes which seem feasible for the upper mechanism thus require ice to ice impact or contact, although meteorological conditions obviously exclude processes requiring large updraughts or the presence of graupel. Most ice-ice impact experiments have shown that the smaller particles produced are positively charged, whilst the larger fragments are negatively charged. The existence of large positive space charges and positive potential gradients near the ground in blizzards seems to support this. However, some workers have found opposite effects, and it appears that several mechanisms are responsible for impact charging.

Observations of quiet rain clouds have shown a large excess of positive rain charge and a predominance of negative potential gradients. Thus since the precipitation has presumably begun its existence as snow, there must be another charging process operating lower in the cloud which reverses the sign of the charge acquired

higher up. Measurements made by Reiter (1965) in mountainous regions have shown a distinctive sign change of potential gradient to take place between the 0°C and 1°C levels. Laboratory measurements of Dinger and Gunn (1956), Nakaya and Terada(1934), and Magono and Kikuchi (1963) have shown that snow becomes positively charged on melting. This evidence strongly suggests that the positive charge found on quiet rain is a result of the melting of snow.

However, the potential gradient results of Kelvin (1860) and Chauveau (1900) suggest a shallow layer of negative space charge near the ground. Smiddy and Chalmers (1959) found negative space charges near the ground in heavy rain, and Sharpless (1968) found the space charge density in quiet rain to be normally negative near the ground, and also found a high correlation with potential gradient. Smith (1955) suggested that the raindrop charging could be explained by the Lenard splash charging effect at the ground, which would also release negative space charges. Simpson (1915) thought that drop rupture in wind gusts close to the ground might account for the charging.

Chalmers (1959) pointed out that the charging processes acting in the nimbostratus cloud operate at similar temperatures and in the same direction as the chief thundercloud processes, although the lower process is relatively more important in the nimbostratus cloud. He thinks it would be fortuitous if these processes were of different origin in the two clouds.

CHAPTER 2

THE ELECTRIFICATION OF QUIET RAIN AND SNOW

2.1 The Origin and Structure of Nimbostratus Clouds

For atmospheric electrical purposes, quiet rain and snow are usually regarded as having fallen from stratiform clouds which are much more stable and long-lived than than thunderclouds, and which give rise to steady precipitation of long duration rather than showers. In temperate latitudes these conditions are usually associated with nimbostratus clouds produced by the gradual forced ascent of the air preceding a warm front. This ascent is slow but prolonged, and takes place throughout a deep and extensive layer of air.

It is now generally considered that the principal process of initiation of precipitation in all nimbostratus clouds is ice crystal growth by the Bergeron process. Bergeron (1933) showed that ice crystals, produced by the freezing of supercooled water droplets in an environment containing many supercooled water droplets, would grow at the expense of the droplets because of the difference in vapour pressure between water and ice. These ice crystals either grow or aggregate till they reach a sufficient size to overcome the updraught. Mason (1952) has shown that the coalescence process cannot be the main one in a nimbostratus cloud

unless the water content or updraught are much larger than those usually observed. When the cloud extends downwards to below the 0°C level, the snowflakes melt to produce raindrops. This has been confirmed by the presence of increased radar reflection in the few hundred metres below this level; melting snowflakes having a higher radar reflectivity than the raindrops found lower in the cloud.

A general outline of altostratus and nimbostratus clouds and a comparison with cumulonimbus clouds is given in Table 2.1, and typical cross-sections of a warm front in Figure 2.1.

2.2 Electrical Models of the Nimbostratus Cloud

It has been shown in Section 1.2 that the nimbostratus snow cloud usually gives rise to a negative precipitation current and a positive potential gradient. By assuming a total current flow uniform with height from the ground, through the cloud, to the ionosphere, Chalmers (1959) has shown that the potential of the cloud top must be higher than that of the ionosphere. As a result of this, he has shown that a charge separation process within the cloud and not at ground level is essential.

However, in the nimbostratus rain cloud the total current flow is in the opposite direction to that in the snow cloud, so Chalmers concludes that the potential of the cloud top must be lower than that of the ionosphere. As nimbostratus rain

Cloud Type	Typical Vertical Windspeed (ms^{-1})	Cause of Vertical Motion	Typical Horizontal Extent (km)	Typical Cloud Thickness (km)	Average Particle Lifetime (s)	Precipitation
Altostratus	0.05 to 0.2	Widespread regular ascent	10^3	1	5×10^4	Intermittent light rain or snow
Nimbostratus	''	''	''	10	''	Prolonged rain or snow precipitation Rate 1-5 mm hr^{-1}
Cumulonimbus	3 to 20	Intense local convection	10	10	10^3	Intermittent heavy rain or snow. Ppn. Rate 5-60 mm hr^{-1}

TABLE 2.1

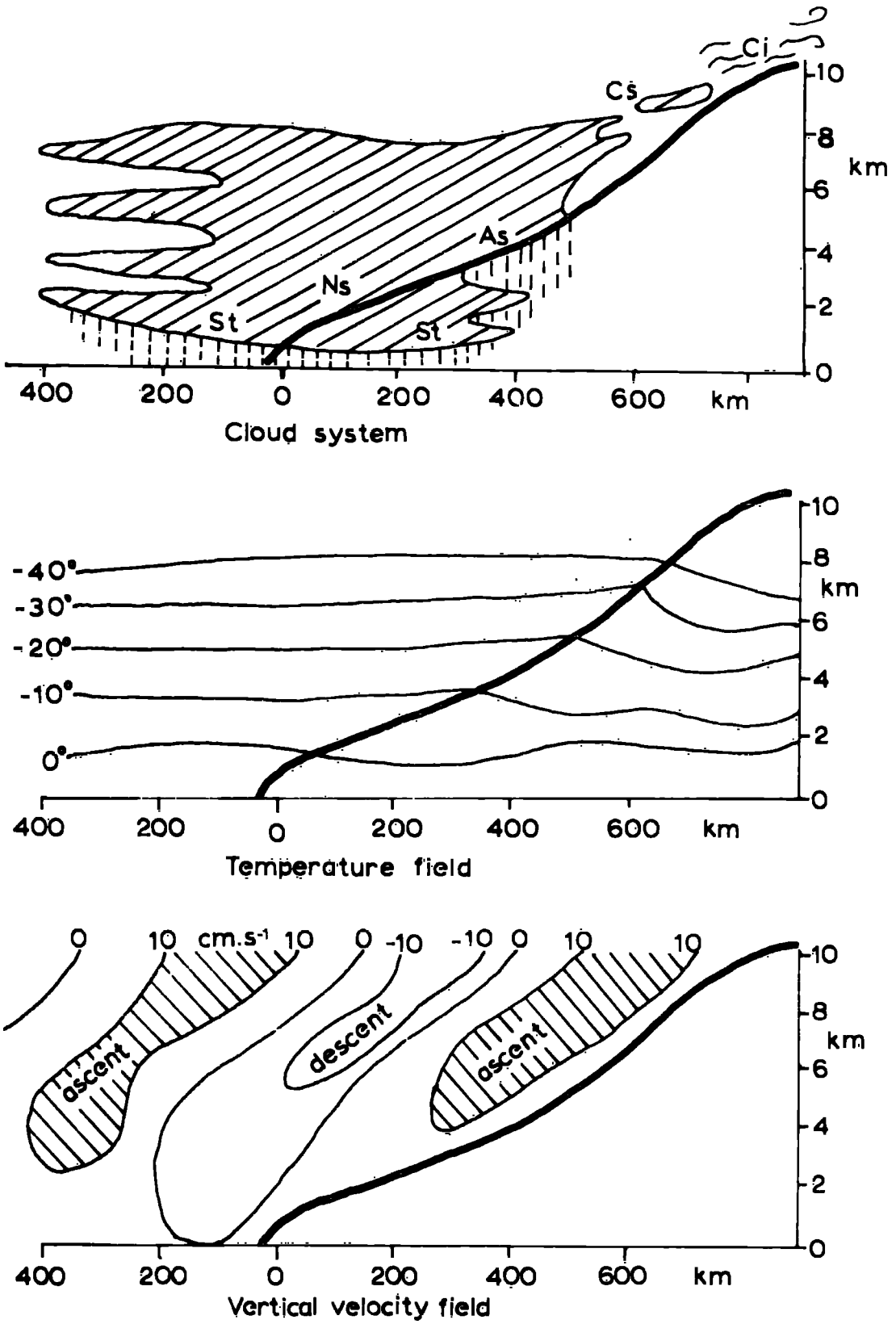

Fig. 2.1 Cross section of a typical warm front.

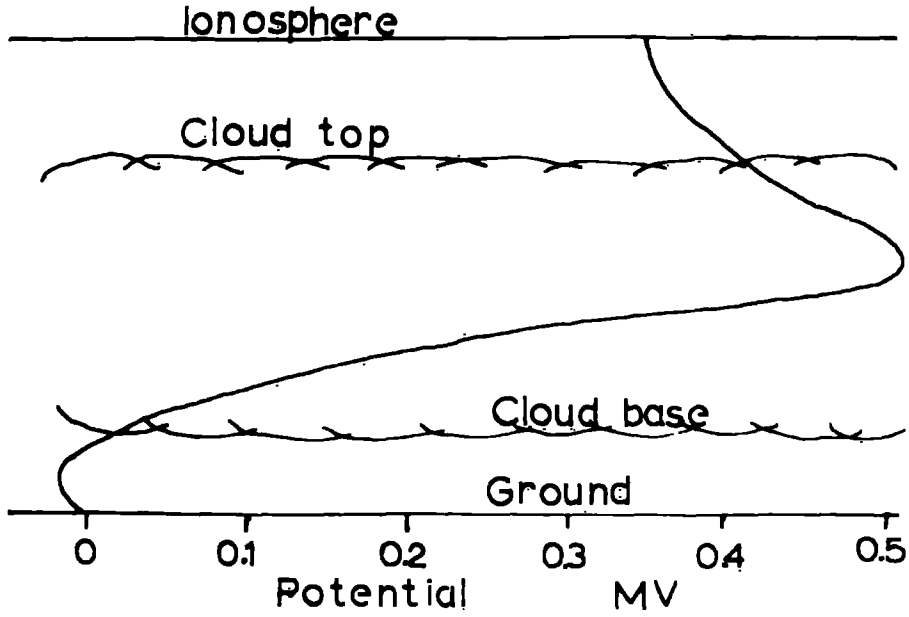

SNOW CLOUDS

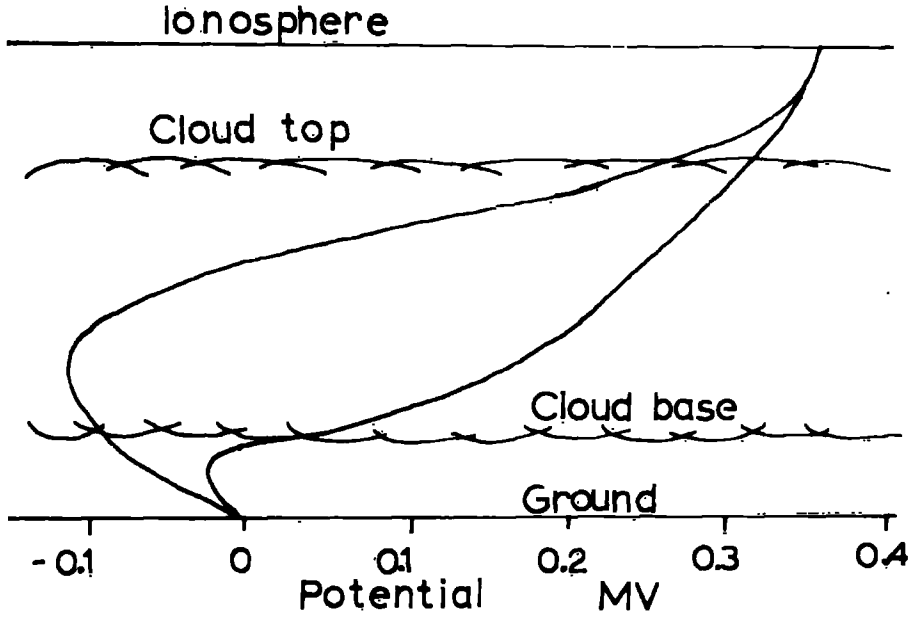

RAIN CLOUDS

Fig. 2.2 Chalmers' nimbostratus models

clouds always contain an upper snow portion, we are led to the surprising conclusion that the electrical conditions in the upper portion of the cloud depend on whether the precipitation reaches the ground as rain or snow.

The positive charging of the rain necessitates a negative ionic or cloud space charge to be produced also, and contradictory evidence points towards either charging on melting in the cloud or charging on drop-shattering near the ground. Chalmer's models of cloud potential versus height in nimbostratus clouds, including the two possible cases for rain, are shown in Fig. 2.2.

2.3 A Proposed Model for Nimbostratus Clouds

Instead of including the clouds in the earth-ionosphere current network, it is now proposed that we can consider the cloud charges to be independent of outside electrical effects. It is here assumed that any ionic or cloud space charges dissipate only by ionic conduction, and that the rate of dissipation of these charges depends only on their magnitude and the conductivity in the immediate environment. It is further assumed that any charge separation process gives rise to an ionic or cloud charge and a precipitation charge of opposite sign.

The charged precipitation is then assumed to fall to the ground, and the total precipitation current at the ground is considered to represent the total current flowing downwards from the charging region.

If we know the horizontal and vertical dimensions of the cloud system, and if we can measure the precipitation current density, we can calculate the value of the cloud ionic charge, and hence its contribution F_ρ to the potential gradient at the ground. To calculate the potential gradient at the ground due to the whole system, we must take into account the space charge on the falling precipitation. If the contribution to the potential gradient at the ground due to the precipitation space charge is F_s, then the total potential gradient at the ground is given by

$$F = F_\rho + F_s \qquad \ldots\ldots\ldots (1)$$

By assuming quasi-static equilibrium, that is charges and currents that are not changing with time, it is possible to explain the inverse relation between potential gradient and precipitation current density using this theory. Moreover, the mirror-image effect, where potential gradient and precipitation current density vary with time in a similar manner, can also be explained by the theory. The analytical derivations of these cases will be given in the following sections.

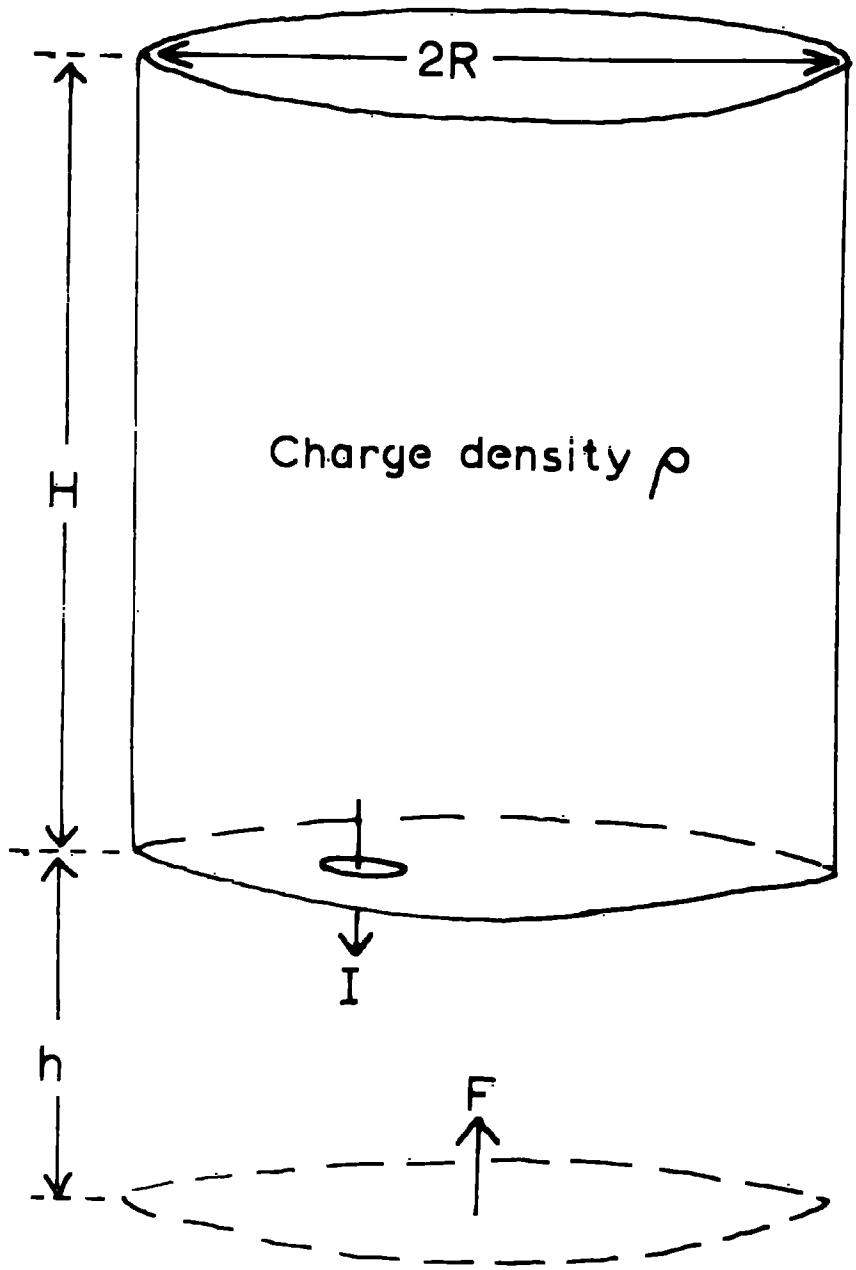

Fig. 2.3 Cylindrical cloud model.

2.4 The General Case

If we consider a cylindrical cloud zone of depth H, radius R and cloud base height h (Fig. 2.3), then if precipitation with uniform current density I is leaving the cloud base, the total precipitation current leaving the cloud is $\pi R^2 I$. If the cloud charge density at any time is ρ, the total cloud charge will be $\pi R^2 H\rho$, and the ionic conduction current out of the cloud region will be $(\pi R^2 H\rho)\lambda/\varepsilon_0$. Thus the total current out of the cloud zone will be $\pi R^2 I + (\pi R^2 H\rho\lambda/\varepsilon_0)$. This is equal to the rate of decrease of cloud charge, $-\frac{d}{dt}(\pi R^2 H\rho)$, which is then given by

$$-\frac{d}{dt}(\pi R^2 H\rho) = \pi R^2 I + \pi R^2 H\rho\lambda/\varepsilon_0$$

Thus the rate of accumulation of cloud charge density in the cloud zone is given by

$$H\frac{d\rho}{dt} = -I - \frac{H\rho}{\tau} \quad \ldots\ldots \quad (2)$$

where τ is the relaxation time (ε_0/λ) in the cloud.

The potential gradient at any point due to the cloud charges can be obtained by integrating over the cloud volume. The potential gradient at the ground under the centre of the cylinder is found to be given by

$$F_\rho = \frac{\rho}{\varepsilon_0}\cdot\left\{H + \sqrt{(H+h)^2 + R^2} - \sqrt{(h^2 + R^2)}\right\}$$

... (3)

If R is very large compared with H and h, the potential gradient at the ground due to the cloud charges is then given by

$$F_\rho = \frac{\rho H}{\varepsilon_o} \qquad \ldots\ldots\ldots \qquad (4)$$

In order that a charge separation process should produce a cloud charge density uniform with height, it is necessary that the precipitation current density should increase linearly with decreasing height throughout the charging region. If the precipitation obtains its charge uniformly throughout the depth H, and then falls through height h to the ground without charge loss, then the potential gradient at the ground under the cloud centre due to the precipitation space charge is found by integration (Appendix 1) to be given by

$$F_s = \frac{I}{2\varepsilon_o V}\left\{H + 2h + 2R + \frac{h}{H}\sqrt{h^2 + R^2} - \left(1 + \frac{h}{H}\right)\sqrt{(H + h)^2 + R^2} - \frac{R^2}{H}\log\left(\frac{H + h + \sqrt{(H + h)^2 + R^2}}{h + \sqrt{h^2 + R^2}}\right)\right\} \qquad \ldots\ldots (5)$$

If R is very large compared with H and h, the contribution to the potential gradient at the ground by the precipitation space charge is given by

$$F_s = \frac{I}{2\varepsilon_o U}(H + 2h) \qquad \ldots (6)$$

Thus if we know the precipitation current density, the conductivity of the cloud, and the dimensions of the charging region, it is possible to calculate the potential gradient at the ground due to the charge system.

This model is of necessity oversimplified. Charged cloud systems would be expected to interact electrically with each other, and the existence of wind shear and precipitation particles of different sizes will also complicate matters. However, provided the precipitation current density is greater than the ionic conduction current density to ground, and provided the potential gradient is not sufficiently high to give point discharge near the ground, then this model is perhaps a fair representation of conditions.

2.5 The Inverse Relation

Many workers have found that the precipitation current density and the potential gradient at the ground are frequently opposite in sign and proportional in magnitude. Statistical analysis of a large number of observations has enabled a straight line to be fitted in many cases. The relationship between precipitation current density I and potential gradient F is usually written

$$I = -a(F - C) \qquad \ldots\ldots \qquad (7)$$

where a and C are constants. When a is positive, the relationship is known as the inverse relation. The constant C has often been found to be close to the value of the fair-weather

potential gradient at the recording site. If we write F_D as the excess of the potential gradient over the fair-weather value, then equation (7) becomes

$$I = - a F_D \quad \ldots\ldots \quad (8)$$

In explaining the inverse relation, many workers have preferred to assume that the potential gradient is somehow set up in the cloud, and that the precipitation subsequently acquires its charge as it falls, under the influence of this electric field. The mechanism responsible for the precipitation charging is usually assumed to be ion capture or an influence mechanism, and it is assumed to depend on the precipitation rate.

Ion capture by falling raindrops under the influence of an electric field has been treated theoretically by Whipple and Chalmers(1944), and Wormell (1953) but the process appears to be too slow and not to give the observed magnitudes of precipitation current density in quiet conditions.

It is now suggested that looking upon the potential gradient as a fundamental characteristic of the cloud and the precipitation current as a secondary effect is physically the wrong way round, and that they are both the result of a single cause, namely charge separation in the cloud. The whole system of charges then gives rise to the potential gradient at the ground, which should therefore be regarded as a dependent, not independent, variable.

THE NIMBOSTRATUS SNOW CLOUD

If we make the basic assumptions of the proposed model outlined in Section 2.3, and in addition make the following assumptions

(1) The cloud is in electrical quasi-static equilibrium.

(2) The horizontal dimensions of the charge system are larger than the vertical dimensions.

then it is possible to solve the equations (2), (4) and (6) analytically.

If, at a time t = 0, a precipitation current of uniform density I_o begins to flow from the cloud and is then constant, the rate of cloud charge increases after this time will be given by

$$\frac{H\, d\rho}{dt} = -I_o - \frac{H\rho}{\tau}$$

where ρ is the cloud charge density at time t. By integration, ρ is found to be given by

$$\rho = \frac{\tau I_o}{H}\left(e^{-t/\tau} - 1\right) \qquad \ldots\ldots(9)$$

Thus for times in excess of about 5τ, the cloud charge density will be constant and equal to $-\frac{\tau I_o}{H}$

From equation (4), the potential gradient at the ground due to the cloud charge sheet will be given by

$$F_\rho = -\frac{\Upsilon I_o}{H} \cdot \frac{H}{\varepsilon_o} = -\frac{I_o}{\lambda} \quad \ldots (10)$$

Since $\Upsilon = \varepsilon_o/\lambda$.

If the precipitation is uncharged at the top of the charging region, and obtains its charge linearly in falling through the region, then the potential gradient at the ground due to the precipitation space charge, from equation (6), will be given by

$$F_s = \frac{I_o}{2\varepsilon_o v} (2h + H) \quad \ldots\ldots (11)$$

where v is the average precipitation fall speed (Fig. 2.4).

Thus the potential gradient at the ground due to the whole charge system, $F_\rho + F_s$, will be given by

$$F = I_o \left\{ \frac{(2h + H)}{2\varepsilon_o v} - \frac{1}{\lambda} \right\} \quad \ldots\ldots\ldots (12)$$

It can be seen that if

$$\frac{(2h + H)}{(2\varepsilon_o v)} < \frac{1}{\lambda}$$

then the inverse relation obtains. This inequality may be rewritten

$$\frac{h}{v} + \frac{H}{2v} < \varepsilon_o/\lambda$$

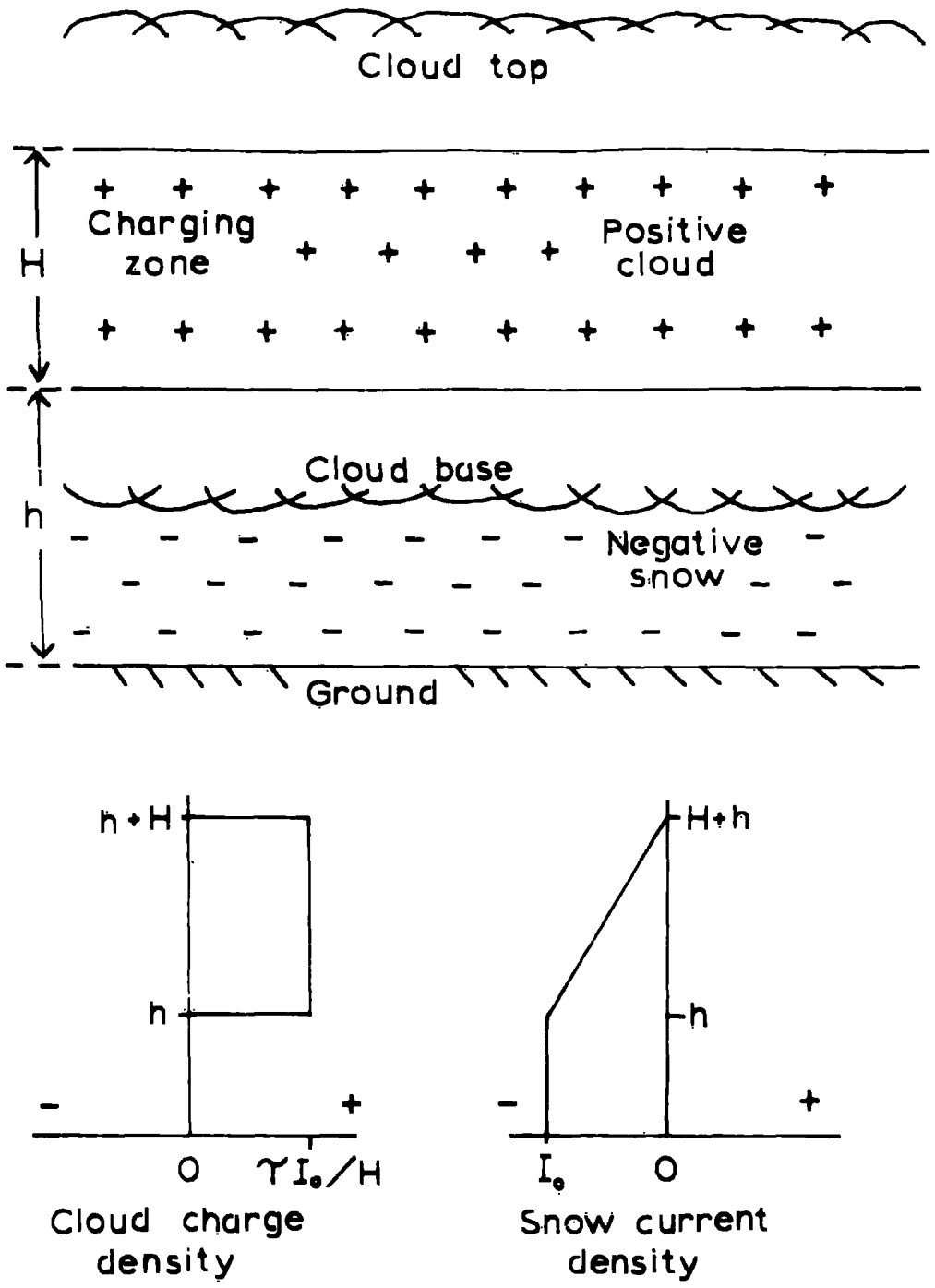

Fig. 2.4 Proposed nimbostratus snow cloud model.

Physically, ε_0/λ is the electrical relaxation time of the cloud charges, h/v is the average fall time of the precipitation from cloud base to ground, and $H/2v$ represents the average charging time of the precipitation.

This represents the case for a steady, uniform single charge separation process, as is believed to be the case in the quiet nimbostratus snow cloud.

Equation (12) may be rewritten

$$F = -I_0 \cdot K \qquad \ldots\ldots\ldots \quad (13)$$

where K is to be called the constant of proportionality between potential gradient and precipitation current density. It can be seen that different cloud base heights or different depths of the charging region will give rise to variations in K, even if all the other parameters are constant. It is therefore suggested that it might be possible to explain deviations from the inverse relation in terms of the cloud dimensions rather than rate of precipitation.

In a nimbostratus snow cloud, the velocity of fall of the snow particles hardly depends on their size (Appendix 2), and the overall range of values for different crystal structures is quite small. Several workers have obtained experimental values for the constants a and c in equation (7). The proposed theory should be in agreement with these experimental values

if C is the fair-weather potential gradient and if $K = {}^{1}/a$. This latter condition requires that

$$\left(\frac{1}{\lambda} - \frac{2h + H}{2\varepsilon_o v} \right) = {}^{1}/a \quad \ldots\ldots\ldots \quad (14)$$

The average value of a found experimentally is 0.93×10^{-14} Ω^{-1} m^{-1}, and so for agreement of the theory with the experimental results, $K = 1.075 \times 10^{14}\,\Omega$ m.

Equation (14) was solved for λ using this experimental value, for values of H between 0 and 10km. Cloud base height h was taken as 0.5km, and the equation was solved for three different values of snow fall speed, 0.3, 1.0 and 2.0 ms^{-1}. The results are shown in Table 2.2.

As far as is known, the conductivity with a precipitating snow cloud has not been measured, but estimates suggest that it lies between $\frac{1}{4}$ and $\frac{1}{2}$ of the conductivity in clear air at the ground. This suggests values of the order of 0.25×10^{-14} to 1.0×10^{-14} Ω^{-1} m^{-1}. From Table 2.2 it can be seen that this is consistent with charging heights of up to 10km. It can also be seen from the table that the results for different fall speeds all satisfy equation (14), the slower particles requiring smaller charging depths than

TABLE 2.2

Experimental values of slope (a) of line of snow current density versus potential gradient

Author	Date	$a(\Omega^{-1}m^{-1}\times10^{-14})$	$^1/a(\Omega m\times10^{14})$
Chalmers, J.A.	1956	0.92	1.087
Ramsay, M.W. and Chalmers, J.A.	1960	0.94	1.064
Reiter, R.	1965	0.93	1.075

Solutions of Eqn. 14 for cloud conductivity

Charging Height (km)	CONDUCTIVITY ($\Omega^{-1}m^{-1}\times10^{-14}$)		
	Snow fall speeds ($m\ s^{-1}$)		
	0.3	1.0	2.0
0	0.34	0.61	0.74
1	0.26	0.44	0.61
2	0.15	0.36	0.52
3	0.12	0.30	0.44
4	0.10	0.26	0.40
5	0.08	0.22	0.36
6		0.20	0.33
7		0.18	0.30
8		0.16	0.28
9		0.15	0.26
10		0.14	0.24

the faster ones. It is an observed fact that larger clouds generally have greater updraughts, and thus generate faster snowflakes, so the inferred result is what we would expect.

It seems, therefore, that the proposed theory can satisfactorily explain the inverse relation in the case of the nimbostratus snow cloud. It should be noted that one assumption of the theory is of steady state, which is probably never attained in any cloud. However, the required time for equilibrium to be attained, according to the theory, is of the order of one hour (approx. $5\xi_0/\lambda$), and a normal well-developed nimbostratus will precipitate for periods usually longer than this, maybe periods two orders of magnitude higher in certain cases. The case of snow clouds whose activity varies over periods shorter than this will be discussed in Section 2.6.

THE NIMBOSTRATUS RAIN CLOUD

The evidence discussed in Section 1.2 suggests that the charging of the nimbostratus rain cloud involves the upper charging process in the snow region, giving net negative charge to the falling snow and positive charge to the cloud, and a lower process which reverses the charge on the snow to give positively charged rain. The fall speed of the raindrops also varies through much wider limits than that of snow, and also depends on particle size to a much greater extent than snow (Appendix 2). As has been shown earlier, the fall speed has a considerable influence on the space charge of falling precipitation, and hence on the inverse relation. Thus it might be expected that the results for quiet rain are more diverse and complex than those for quiet snow.

The model now proposed is that the nimbostratus rain cloud consists of an upper charging region identical to the snow cloud described earlier, together with a rain charging region immediately below it (Fig. 2.5). If the snow current density at the interface of the charging regions is I_s, the snow charging depth H_s, and the average snow fall speed $\bar{v}_s$, then the potential gradient at the ground due to the upper cloud charge and snow space charge, from equation (12), will be given by

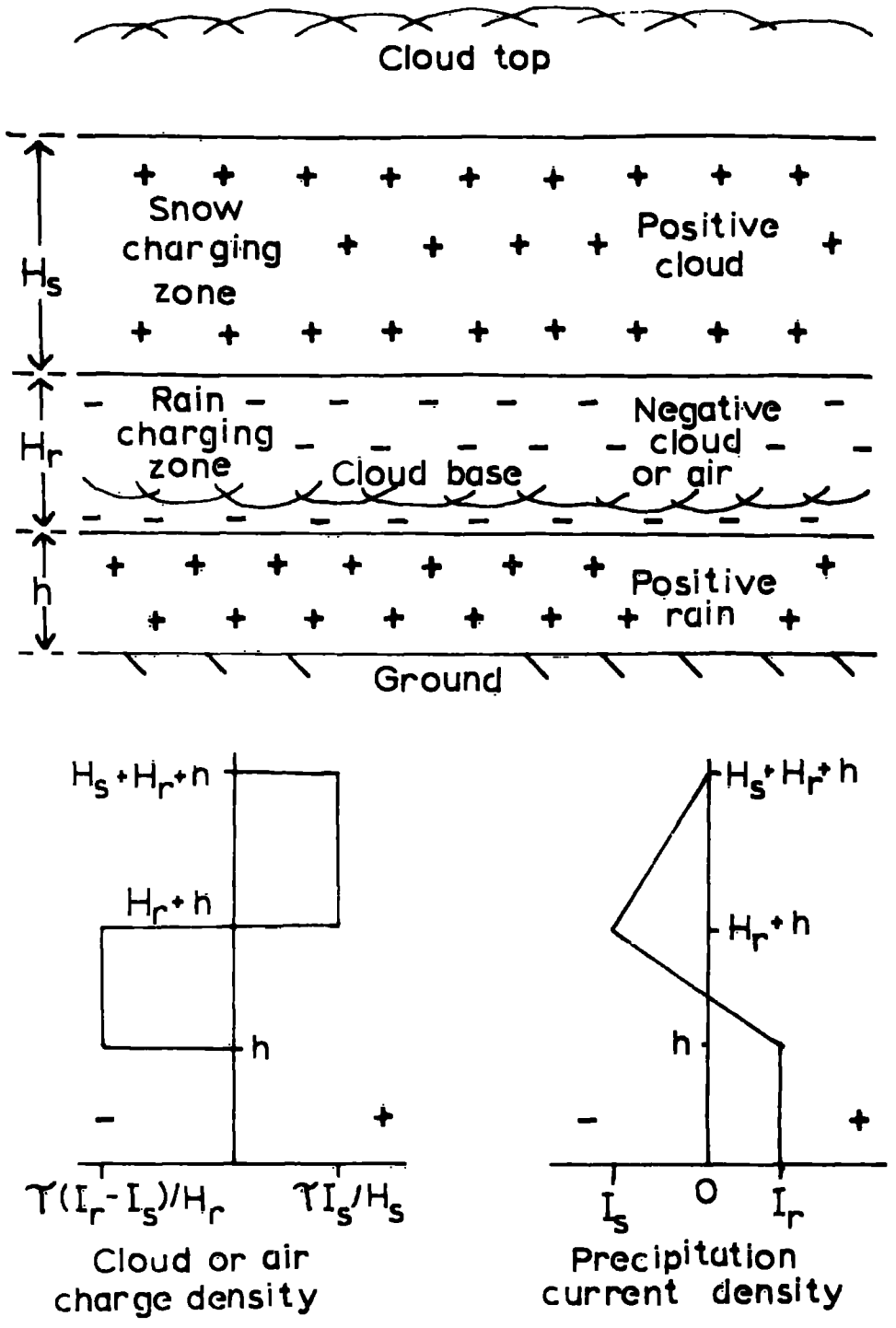

Fig. 2.5 Proposed nimbostratus rain cloud model.

$$F_s = I_s \left(\frac{H_s}{2\varepsilon_o \upsilon_s} - \frac{1}{\lambda} \right) \quad \ldots\ldots \quad (15)$$

The precipitation current density flowing into the rain charging region is I_s, the precipitation current density flowing out of the region is I_R, so that net rain charging current density is $I_R - I_S$. If the rain charging occurs linearly throughout the region of thickness H_R, and the cloud base height is h, then the potential gradient at the ground from equation (12) will be given by

$$F_R = (I_R - I_S) \cdot \left(\frac{2h + H_R}{2\varepsilon_o \upsilon_R} - \frac{1}{\lambda} \right) \ldots (16)$$

The conductivity is assumed constant throughout the cloud.

By adding equations (15) and (16), we find the total potential gradient at the ground due to the whole nimbostratus rain cloud charge system is given by

$$F = I_S \left(\frac{H_s}{2\varepsilon_o \upsilon_s} - \frac{2h + H_R}{2\varepsilon_o \upsilon_R} \right) + I_R \left(\frac{2h+H_R}{2\varepsilon_o \upsilon_R} - \frac{1}{\lambda} \right) \quad \ldots (17)$$

The second term is the contribution from the rain charging process alone, and is what we would expect if only one charging

process occurs. The first term appears as a result of the upper charging process, and as can be seen comprises a large number of variables. Unfortunately this latter fact precludes any more exact analysis, as was possible with the simpler snow cloud, but we can make simplifying assumptions in certain cases. For example, measurements made when conditions are quiet suggest that the snow and rain current densities are of the same order of magnitude, but opposite in sign. Thus a not unreasonable simplification would be to assume constant proportionality between them,

i.e. $I_S = -b\, I_R$, where b is a positive constant.

Substituting for I_S in equation (17) then gives us

$$F = I_R \left\{ (1 + b) \left(\frac{2h + H_R}{2\varepsilon_o \upsilon_R} \right) - \frac{bH_S}{2\varepsilon_o \upsilon_s} - \frac{1}{\lambda} \right\} \quad .. \quad (18)$$

Measurements of precipitation current density at the ground in conditions of quiet rain and quiet snow suggest that b will lie somewhere between 0.25 and 4.0.

Now if the rain charging process takes place near the ground, h and H_R will be very small compared with H_S, and since υ_R will usually be larger than υ_S, we can simplify Eqn.(18) to give

$$F = -I_R \left(\frac{b\, H_S}{2\varepsilon_o \upsilon_s} + \frac{1}{\lambda} \right) \quad ..... \quad (19)$$

If the previous assumptions are correct, then this means that the inverse relation will always be present, whatever the values of H_S σ_S, λ or b.

However, if the rain charging takes place upon the melting of the snow, then H_R will be approximately 1 km and h 2 km at most, so the first two terms in Eqn.(18) will be more nearly equal. If b = 1, then the potential gradient at the ground is given by

$$F = I_R \left(\frac{2h + H_R}{\varepsilon_0 \sigma_R} - \frac{H_S}{2\varepsilon_0 \sigma_S} - \frac{1}{\lambda} \right) \quad .. (20)$$

If we further assume $\sigma_R = 4\ ms^{-1}$, $\sigma_S = 1\ ms^{-1}$, $H_R = 1$ km, h = 2km, then the inverse relation will be obtained for all values of H_S if the conductivity in the cloud is less than $0.75 \times 10^{-14}\ \Omega^{-1}\ m^{-1}$. It seems likely that the cloud conductivity will normally be lower than this, and since H_S will probably also be quite large, the inverse relation should always be obtained.

Thus it can be seen that within the limits of the model, the inverse relation can nearly always be explained. It would be expected from the above analysis that we should find more variations in the constant of proportionality in the case of rain, and this is in fact found. Ramsay and Chalmers (1960) have found values experimentally for different rates of rainfall,

and these are shown in Table 2.3. It can be seen that a increases with increasing rainfall rate, and hence the constant of proportionality K decreases. Thus the assumption that the snow current density and rain current density are directly proportional is probably not correct. If, for example, the snow current density depended on the area of snowflakes impacting, and the rain current density depended on the volume of snow melted, then I_S = const. $(I_R)^{\frac{2}{3}}$. This gives us the same result as a value of b which decreases with precipitation rate.

Measurements of the conductivity in the cloud and the height and depth of the charging regions should enable these problems to be solved, and the theory tested more rigorously.

2.6 The Mirror-Image Effect

In conditions of steady precipitation, it has often been noted that the potential gradient and precipitation current density are opposite in sign and change in a somewhat similar manner. Moreover, with a suitable scale adjustment, the curves of potential gradient and precipitation current density versus time have appeared to be a mirror-image of each other. Sometimes the curves change sign simultaneously, on other occasions one shows a lead or lag against the other.

TABLE 2.3

Experimental values of slope (a) of rain current density versus potential gradient

Rainfall Rate ($mm\ hr^{-1}$)	a ($\Omega^{-1}m^{-1}$ x 10^{-14})	$1/a$ (Ωm x 10^{14})
< .18	0.32	3.13
.18 - .6	3.00	0.33
.6 - 1.2	3.93	0.25
1.2 - 1.8	5.18	0.19
1.8 - 2.4	7.09	0.14
> 2.4	6.53	0.15
All	2.19	0.46

Previous assumptions have been that the potential gradient and precipitation current density are related by an inverse relation at or below cloud level, and hence change in a similar way. The time lags between maxima and minima of the two curves have been explained in terms of purely mechanical separation of the charged cloud and the falling precipitation by wind shear or similar mechanisms. If the changes of potential gradient and precipitation current density are brought about merely by the passage of more or less electrically active portions of cloud, which themselves are in electrical quasi-static equilibrium, then this explanation is probably correct. If, however, these changes are brought about by electrical development of the cloud, then this simple picture will no longer apply, and a more rigorous analysis will be necessary.

THE DEVELOPING SNOW CLOUD

If we consider a cylindrical portion of a cloud, as discussed in Section 2.4, and a precipitation current of density I (t) is leaving the cloud at a time t, then the cloud charge density ρ will be increasing at a rate $\frac{d\rho}{dt}$ given by Eqn. (2)

$$\text{i.e.} \quad \frac{H\,d\rho}{dt} = -I(t) - \frac{H\rho}{\tau} \qquad \ldots\ldots \quad (21)$$

where H is the depth of the charging region and τ the electrical relaxation time.

For illustration, I(t) will be taken as a sinusoidal variation, such that $I(t) = I_o \sin wt$. We can then solve Eqn. (21) by integration to obtain

$$\rho = \frac{I_o}{H(w^2 + 1/\tau^2)} \left\{ \frac{1}{\tau} \sin wt - w \cos wt - we^{-t/\tau} \right\} \qquad \ldots\ldots \quad (22)$$

If we write $T = 2\pi/w$, then ρ is given by

$$\rho = \frac{I_o}{H\left(\frac{4\pi^2}{T^2} + \frac{1}{\tau^2}\right)} \left\{ \frac{1}{\tau} \sin\left(\frac{2\pi t}{T}\right) - \frac{2\pi}{T} \cos\left(\frac{2\pi t}{T}\right) - \frac{2\pi e^{-t/\tau}}{T} \right\} \qquad \ldots\ldots \quad (23)$$

Physically, T represents the periodicity of the change of precipitation current density.

For slow changes, that is $T \gg \tau$, Eqn.(23) simplifies to

$$\rho = \frac{\tau I_o}{H} \sin\left(\frac{2\pi t}{T}\right)$$

or $$\rho = \frac{\tau I(t)}{H}$$

This is the result obtained for the quasi-static case described in Section 2.5, and the mirror-image effect would then be expected to be in accordance with the classical theory.

However, if fast changes are taking place, that is $T << \tau$, then Eqn.(23) simplifies to

$$\rho = \frac{I_o T}{2\pi H} \cos\left(2\pi t/T\right)$$

Thus the cloud charge will be 90° out of phase with the precipitation current density leaving the charging region, and mechanical effects will complicate matters further. In between the two extremes outlined above, any phase changes between 0° and 90° can be expected, depending upon the rapidity of the change as well as wind shear.

Numerical solutions of Eqn.(23) were obtained by digital computer using the values of cloud parameters calculated from

Section 2.6 for the case of the quasi-static snow cloud. The potential gradient at the ground due to both the cloud charge and precipitation space charge was computed, and the result is shown in Fig. 2.6. A sinusoidal change of precipitation current density was assumed, with a periodicity equal to the relaxation time. For comparison, the computed potential gradient due to a moving quasi-static snow cloud system is also shown. A detailed analysis of these cases is given in Appendix 3.

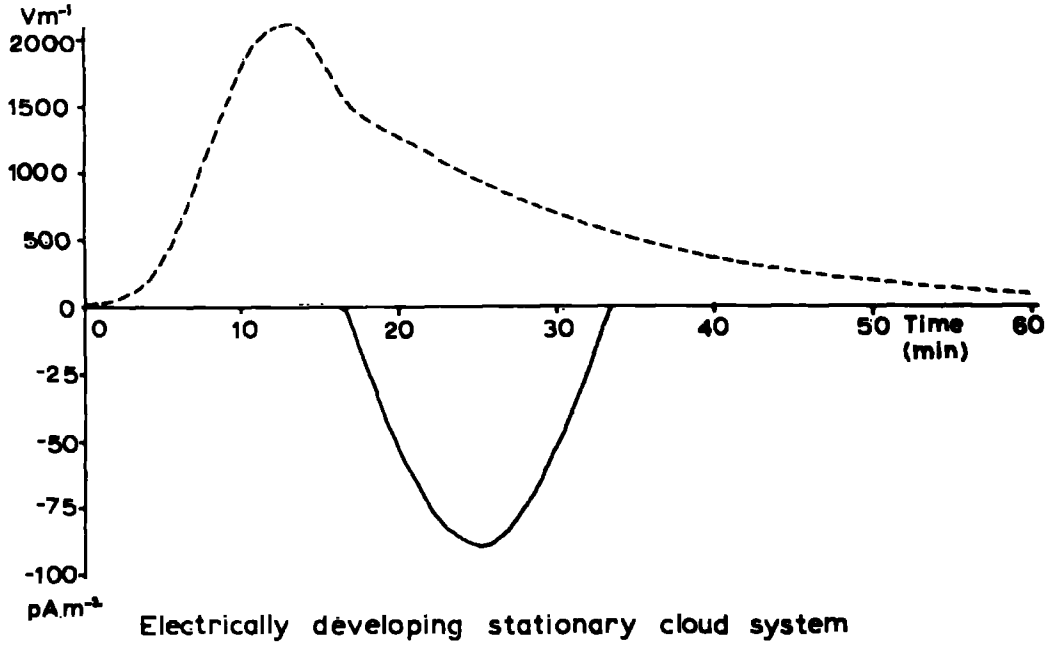

Electrically developing stationary cloud system

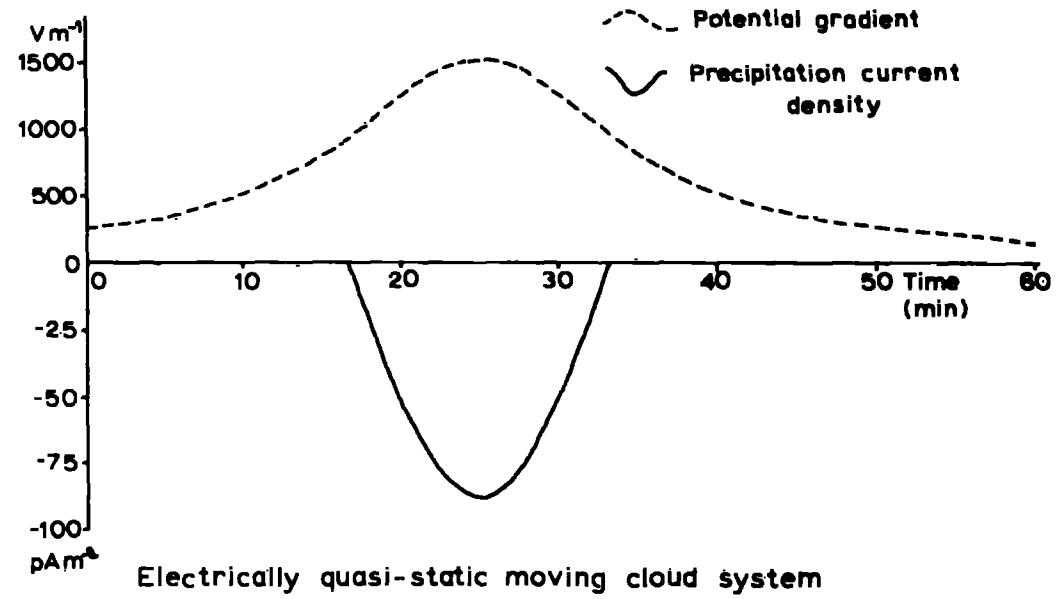

Electrically quasi-static moving cloud system

Fig. 2.6 Computed variations of potential gradient due to developing stationary and quasi-static moving nimbostratus snow cloud systems.

CHAPTER 3

MEASUREMENT OF PRECIPITATION CURRENT DENSITY

3.1 General Considerations

As has been discussed in Chapter 2, the most useful parameters of cloud electrification which can be measured are vertical electric current densities. The vertical currents which may exist are conduction currents, convection currents, point-discharge currents, lightning currents and precipitation currents. Conduction currents are the ohmic electric currents produced by the migration of atmospheric ions in the existing vertical electric field. Measurements of these currents are difficult to interpret due to the relatively low mobility of the ions. The component of the ionic velocity produced by the electric fields normally existing in the atmosphere is often small compared to the component produced by air movement.

Convection currents are caused by convective or eddy diffusive transfer of ionic charges from one level to another. Thus vertical air velocities greater than the ionic velocities are required for these currents to be significant, together with a vertical space-charge gradient. Point discharge currents are the result of the production of ions by a process of collision

when the electric field is sufficiently high. Raised metallic points several metres high begin to discharge by this process when the electric field strength reaches about 1000 Vm^{-1} at the surface of the earth. However, the latest evidence suggests that widespread point discharge does not occur from natural objects such as trees until the electric field strength is several times this value, which means that the process will not normally be important in nimbostratus conditions.

The precipitation current density is defined as the net precipitation charge arriving at unit area of the earth's surface in unit time. Precipitation charges of both signs are nearly always present, as has been shown by single-drop charge measurements, and this is true even when the net precipitation current density is relatively steady. It is generally considered that precipitation currents are larger than all other currents found in nimbostratus clouds, having a maximum current density of around 100 pAm^{-2}. The conduction current density has a maximum value of about 10pAm^{-2}, and the convection current density is estimated to be of about the same order of magnitude.

Any conducting surface exposed to the vertical electric field will have a bound charge proportional in magnitude to

the electric field strength. Changes in electric field intensity will produce corresponding changes in bound charge, and any current measuring instrument connected to the surface will detect currents as a result. These currents, known as displacement currents, are indistinguishable from other currents as far as the measuring instrument is concerned. They are a disturbing factor to be eliminated when measuring vertical currents with a collecting surface exposed to the electric field. A rate of change of electric field as small as 10 $Vm^{-1}s^{-1}$ will produce a displacement current of about 100 pAm^{-2}. Displacement currents of several times this value are found in nimbostratus conditions.

3.2 Apparatus Design Criteria

Having decided that of the vertical currents the precipitation current is the most important, the problem arises of how best to measure it. Previous measurement techniques have fallen into two main classes, those using rain collectors which are exposed to the vertical electric field, and those using collectors shielded from the electric field.

Apparently the simplest method would be to isolate a portion of the earth's surface on insulators and measure

directly the current to earth, or the net charge arriving in a given time. Unfortunately all currents are measured by this method, and displacement currents, which are not responsible for atmospheric charge transfer, must be eliminated or taken into account. Short-term electric field variations of the order of seconds are the most difficult to compensate for, and this has usually been overcome by averaging readings over periods of minutes, taking into consideration only longer term field variations. Automatic displacement current compensation, using the differentiated output from a field measuring instrument or the output from a plate exposed to the electric field but shielded from rain, has been used by several workers with some success.

Shielded collectors generally have the form of a collecting surface which is mounted on insulators and surrounded by a raised metallic shield to protect it from the electric field. Displacement, conduction and convection currents are thus not measured by these instruments. Their chief advantage is that no compensation for displacement currents is required. Their main disadvantage is that the shielding prevents some precipitation from entering the collector in windy conditions, and in certain cases the rain collected may be only $\frac{1}{2}$ of that falling on level ground.

In particular, they tend to collect only the larger drops, so that if precipitation charge depends greatly on particle size, severe errors may occur.

One of the principal aims of this research project was to obtain comparisons of precipitation current densities at two recording sites separated horizontally in a direction in the line of cloud movement. It was thought that this information would enable the identification of electrically active cloud cells moving with the wind, as well as detecting simultaneous large-scale effects. Thus, since time-variations of precipitation current densities were to be investigated, it was thought necessary to have recording equipment with a fast time response, of the order of seconds rather than minutes.

3.3 The Exposed Collector

Since there had been some measure of success by previous workers with displacement current compensation systems, it was decided to build a collector completely exposed to the electric field, and to obtain displacement current compensation by means of an inverted plate exposed to the electric field but shielded from rain. A collector was constructed according to a design by Wilson (1916), but incorporating improvements suggested by

Groom (1966). The collecting surface was made from aluminium in the form of a shallow circular dish, 0.5 m^2 in area, with 5 cm high walls. The collecting dish was supported upon an aluminium baseplate 1.25 m square by four P.T.F.E. insulators, 10 cm long and 2.5 cm in diameter. Horizontal grooves were cut in the insulators to increase their surface area, and each insulator was heated electrically by a wire coil mounted on the baseplate. Insulator weather protection was afforded by means of three circular skirts, two of which were attached to the baseplate and one to the collector dish (Fig. 3.1). A circular guard ring 18 cm wide was mounted concentrically with the collector dish, to provide compensation for any possible charging effects caused by drops splashing out of the collector. Theoretically, drops will splash into the collector from the guard ring, which will compensate for any which splash out of it.

As it was intended to install a similar collector on the roof of a Land-Rover to provide mobile observations, the prototype collector was mounted on a 2 m high metal frame to simulate these conditions. An aluminium housing to provide weather protection for the amplifiers and power supplies was constructed underneath the baseplate. The whole apparatus was then erected in a large clear area in the grounds of Durham University Observatory, which is situated just outside Durham

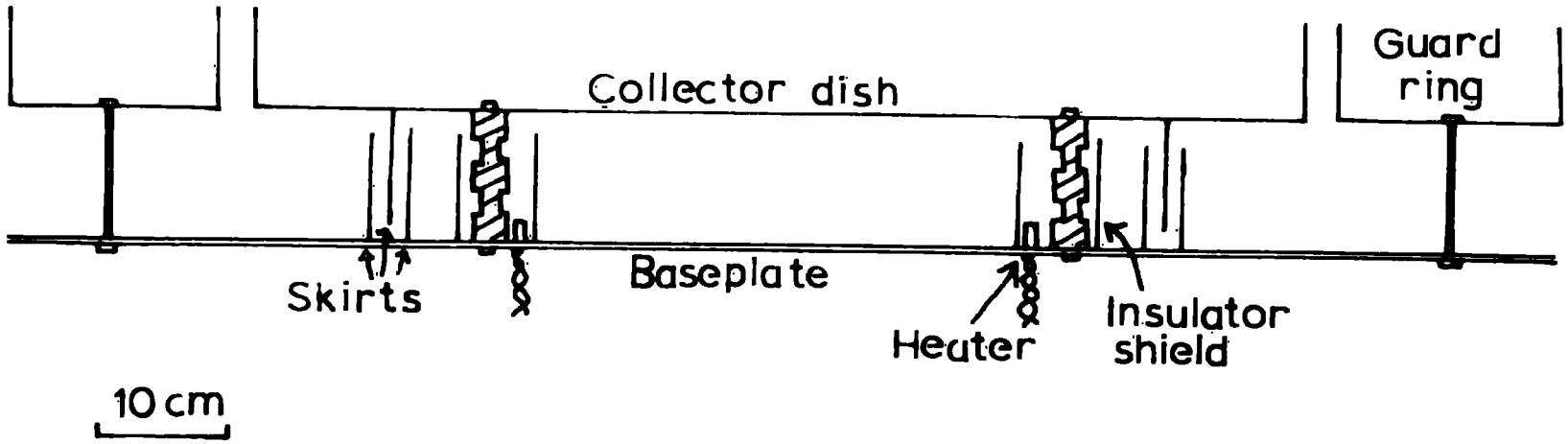

Fig. 3.1 Exposed-collector dish and guard ring.

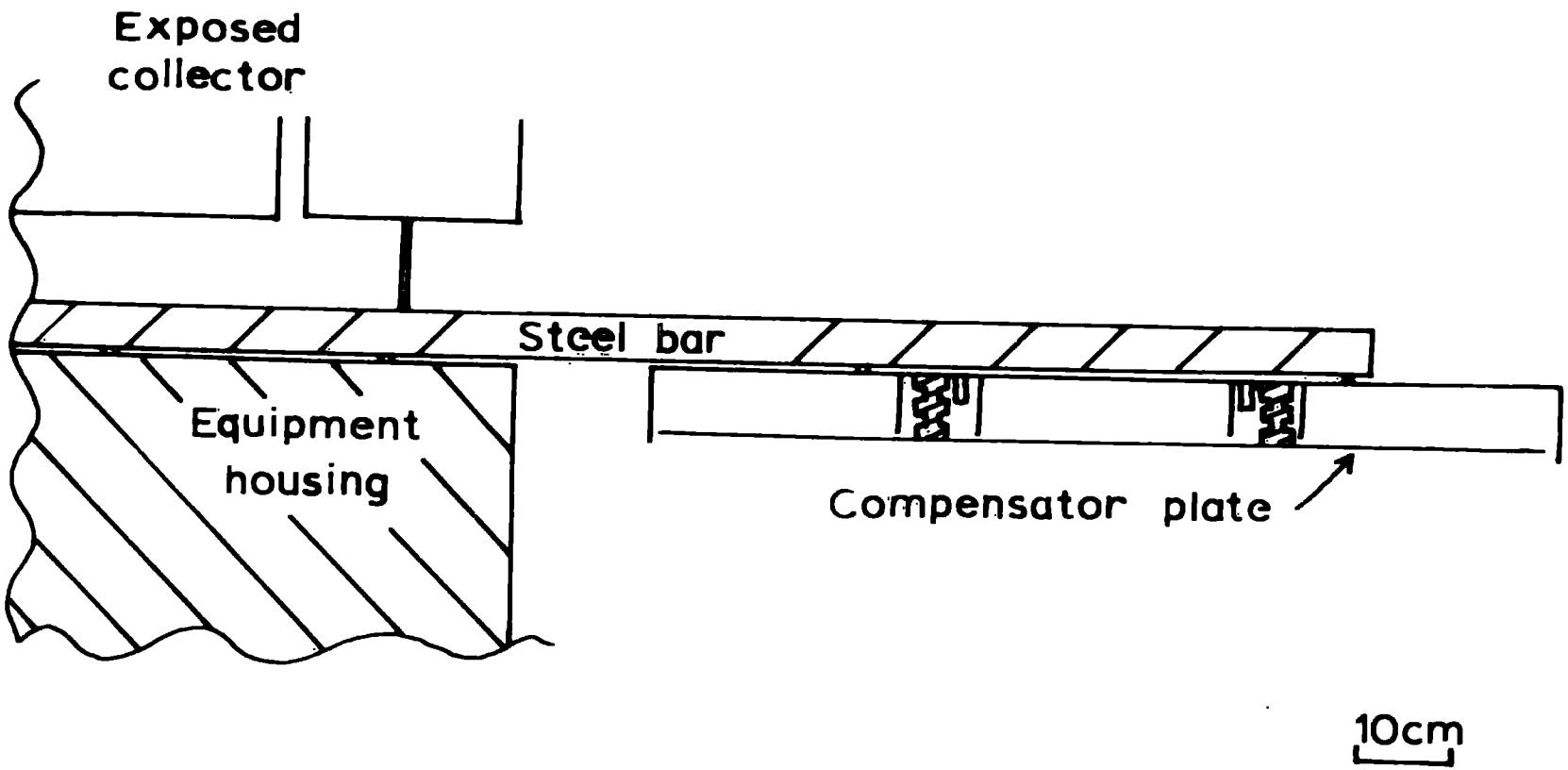

Fig. 3.2 Exposed-collector compensator plate.

City. An inverted plate for displacement current compensation was then built onto the collector frame. A circular aluminium plate, slightly larger in diameter than the collector dish, was bolted to two steel bars attached to the collector frame, at a height of 2 m above ground level. Another circular aluminium plate of 0.5 m^2 area was then attached underneath the first plate by means of four P.T.F.E. insulators, 3 cm long and 2.5 cm in diameter. The insulators were heated by wire coils, in a similar manner to the collector insulators. An aluminium skirt 3 cm deep was then attached around the circumference of the upper plate to protect the edges of the lower plate from rain (Fig. 3.2).

The collector dish and compensating plate were then connected by means of solid coaxial cable to Rank Nucleonics d.c. amplifiers, which were situated in the weatherproof housing. These amplifiers have six decade current ranges, giving a maximum full scale sensitivity of 0.2 pA. A differential d.c. amplifier was then constructed and mounted on an aluminium panel inside the housing, and the outputs from the Rank amplifiers were connected to its inputs (Fig. 3.3). The differential amplifier produces an output voltage proportional to the difference in output voltage between the collector and

compensater amplifiers. It was hoped that the compensator would be exposed to identical conduction and displacement currents to the collector, and that the difference in their outputs would be equal to the precipitation current density and would be zero in fair weather.

It became immediately evident that the two currents were not the same in fair weather, and the differential amplifier indicated very large differences between them. Comparison with a plate mounted at the earth's surface showed that the exposure factor of the collector dish was about 2 and that of the compensator plate was about 1. The gain of the compensator amplifier was then increased by a factor of 2, but it was still found impossible to obtain zero output from the differential amplifier in fair weather. Displacement currents found in nimbo-stratus conditions did not usually exceed 200 pAm^{-2}, but the difference in outputs from the two amplifiers was frequently in excess of 25 pA when there was no precipitation. The output of the differential amplifier would usually gradually increase in one direction, then decrease to zero and increase in the opposite direction. It was thought that the cause of these currents was mis-match of the displacement current compensation system due to its different exposure factor to the collector,

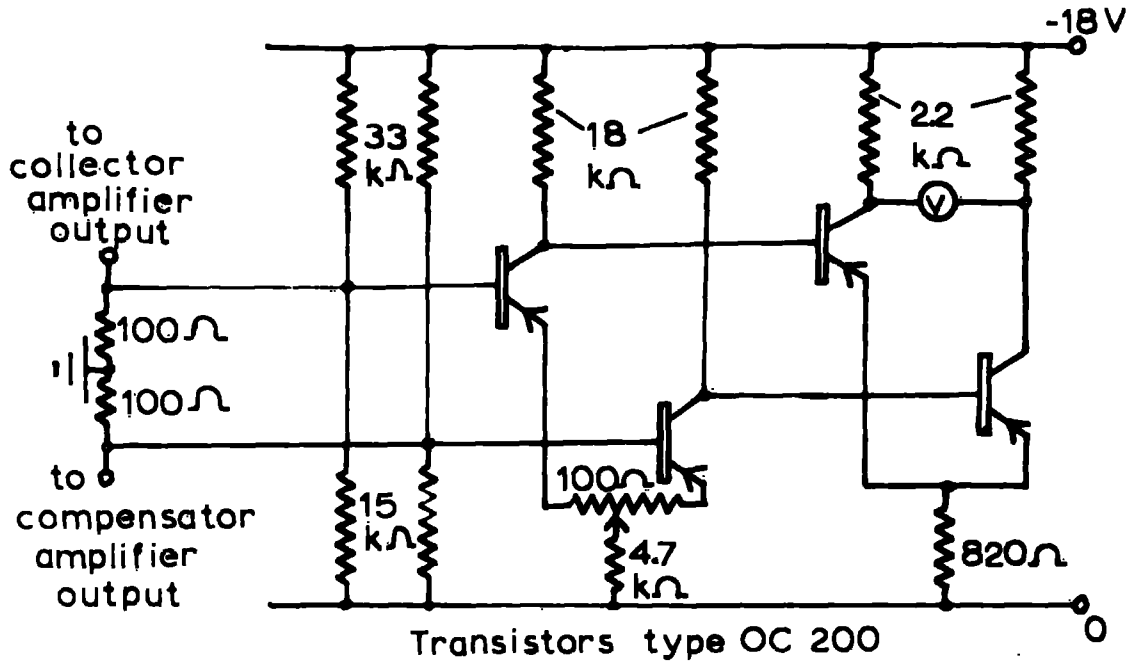

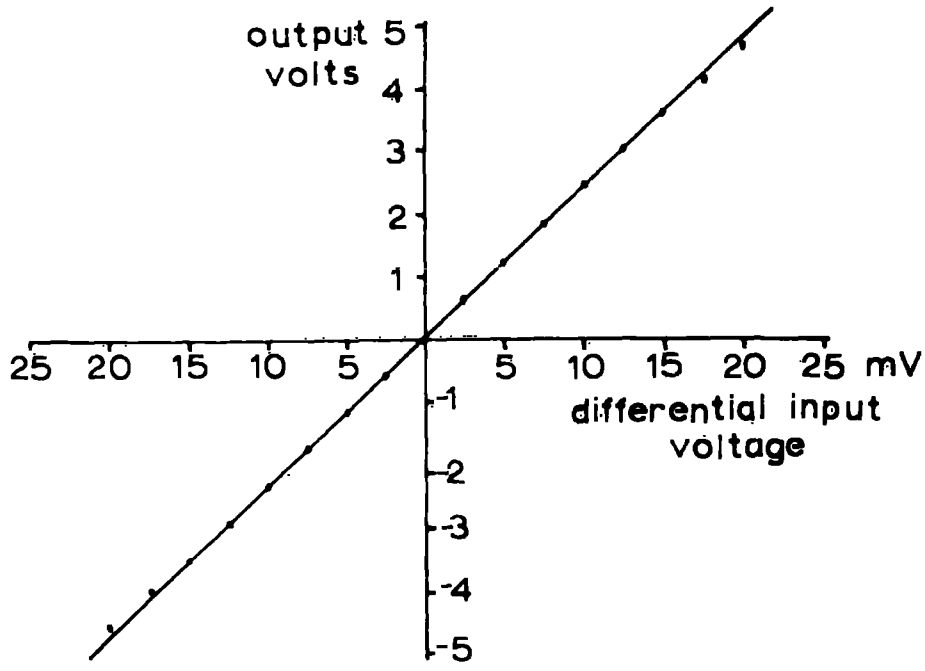

Fig. 33 The differential amplifier.

together with the influence of low-level space charge packets moving in the wind. The latter speculation was supported by the fact that the displacement currents were larger and more rapidly varying in stronger winds.

It was thought that some of the space-charge effects might be a result of vehicular exhausts, and since the Observatory site is situated close to a trunk road carrying heavy traffic, it was decided to move the equipment to a less polluted environment. Consequently, the apparatus was removed and reconstructed at the Lanehead Field Centre, which is situated 35 miles west of Durham City in the Pennines. The environment at Lanehead is almost completely unpolluted and traffic free, and ideally suited to atmospheric electric observations. Nevertheless, displacement currents similar in character to those in Durham were found, and it was not found possible to adjust the gain of the compensator amplifier to obtain perfect compensation. It was estimated that space charge packets some metres or tens of metres in diameter existed near the ground and that these travelled with the wind, producing small-scale electric field changes. Although the average exposure factors of the collector dish and compensator plate are 2 and 1 respectively, the exposure factors with respect to low-level

charges will be more nearly equal. This results in over-compensation for displacement currents produced by low-level charges. Although it was feasible to raise the compensator plate even further to give it the same exposure factor as the collector, it was thought that good compensation might still not be achieved as a result.

It was then decided to abandon the compensating system and to use the exposed collector with the system of displacement current compensation developed by Kasemir (1955). This method consists of equating the time-constant of the current measuring circuit to the electrical relaxation time of the atmosphere (Fig. 3.4). The latter depends on the conductivity, which is constantly varying, so a good match can never be achieved. However, consultation of the positive and negative conductivity records obtained at the Lanehead station in nimbostratus conditions suggested that the variations were only of the order of 30%. Even with a mis-match of this order of magnitude, the errors arising are not very large if the electric field does not change too rapidly. From the conductivity records, the relaxation time was estimated as being between 600 and 1000s. The input time-constant of the Rank amplifier was set to 600s by introducing a 12,000 pF capacitor across the $5 \times 10^{10}\,\Omega$ input resistor. At no time

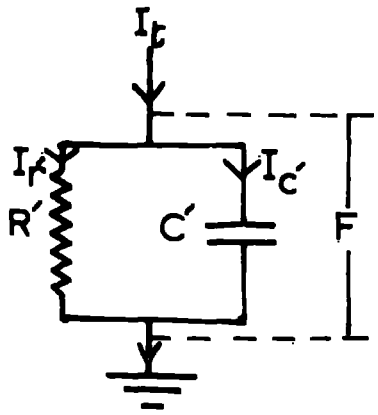

Equivalent circuit of bottom 1 metre of the atmosphere

Potential gradient = F

Total conductivity = λ

Conduction current density = $I_{r'} = F\lambda = F/R'$

Displacement current density = $I_{c'} = (dF/dt)/\varepsilon_0 = C'dF/dt$

$R'C' = \varepsilon_0/\lambda$

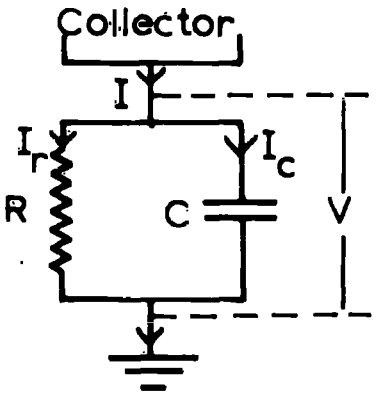

Input circuit of the measuring apparatus

$I_t = I_c + I_r = I_{c'} + I_{r'} = V/R + C\,dV/dt = F/R' + C'dF/dt$

If $RC = R'C'$, $I_r = I_{r'}$ and $I_c = I_{c'}$

Fig. 3.4 Kasemir's method of displacement-current compensation.

in subsequent recording periods was any serious displacement current noticed, and this form of compensation seemed quite satisfactory.

A similar collector was then constructed and mounted on the roof of the Land-Rover, in order to obtain mobile observations. The Rank d.c. amplifier was mounted on a rack inside the Land-Rover and connected to the collector by a rigid copper wire which passed through a small hole in the roof. Additional weather protection in the form of a deflector plate was attached to the front of the collector when it was discovered that rain was being forced around the skirts when the Land-Rover was being driven. Provision was also made for the insulator heaters to be operated from a battery, instead of the usual mains-operated power supply when the vehicle was in motion.

Unfortunately, although Kasemir's displacement current compensation system provides instantaneous response to conduction current changes, it integrates the precipitation current with a time constant equal to that of the input circuit. Hence the exposed collectors did not satisfy one of the design criteria, namely, that which required a rapid response to precipitation current changes. It was then

decided to attempt to measure precipitation current density by another means in addition.

3.4 The Experimental Collector

In addition to the separate objections to the exposed and shielded collectors, there is still the problem of wind gusts near the earth's surface, which is common to them both. In precipitating conditions, the effect of varying wind speed is to vary the proportion of the rain falling on a particular piece of ground. For example, 1 mm diameter raindrops have a terminal velocity of about 4 ms^{-1}, so if the wind speed near the ground rises from zero to 4 ms^{-1}, their angle of fall will increase from zero to 45^{o}. The proportion of the rain collected by a small horizontal surface will then fall from unity to about 0.7. Since most frontal systems in the British Isles are associated with depressions, surface winds are often as high as 10 ms^{-1} and very variable. This means that any collecting surface, even if it is a representative section of the ground, may not collect a representative sample of precipitation. The only method of overcoming this problem is to have a collecting surface which presents an equal projected area to falling precipitation, at whatever angle it might fall. The only geometric shape which satisfies this criterion is a raised sphere, and it was

decided to attempt to construct a rain collector of this shape.

In order to overcome the difficulty of collecting raindrops on a convex surface without splashing, several materials were tested qualitatively in the laboratory. The most satisfactory material that was readily available was found to be phosphor-bronze wire mesh of 1 mm spacing. Water drops of diameters from 1 to 4 mm were allowed to fall through a height of several metres before impinging upon a sample of the mesh, whose angle was varied from horizontal to near vertical. At large angles of impact the drops splashed through the mesh, breaking up into many smaller droplets. If these smaller droplets were allowed to fall onto a second, similar mesh, they became absorbed on its surface to form a continuous water layer. At very shallow angles of impact the drops did not splash so readily, but tended to become absorbed immediately. Splashing away from the mesh was almost absent and not thought to be serious. Tests were also carried out using small water droplets of diameter less than 100μm produced from a vibrating hypodermic needle. These droplets were found to adhere to the mesh in some cases, to bounce off in others. At shallow angles of impact nearly all of the incident droplets were found to bounce off the mesh, even when it was wetted.

Since the rain collecting characteristics of the wire mesh seemed satisfactory for the purpose, an experimental rain collector was designed using this material. Unfortunately, it was found extremely difficult to form a sphere from the mesh, so the experimental collector was constructed in the form of a cylinder. It was intended to test the experimental collector attached to the Land-Rover, which could be directed facing into the wind, so a cylindrical shape was quite satisfactory. The experimental collector consisted of a cylinder, 76 cm long and 38 cm diameter, mounted with its axis horizontal by means of two pairs of P.T.F.E. insulators attached to brackets at each end of the cylinder (Fig. 3.5). This was then bolted to a frame attached to the Land-Rover roof.

During periods of quiet rainfall of varying intensity, observations of the collecting characteristics of the collector showed that it was quite satisfactory. Splashing from the cylinder surface did not seem to occur in quiet rain, even in windy conditions. The mesh became uniformly wetted after a few minutes' exposure to rain and formed a good collecting surface. The collected water eventually ran around the mesh and fell away from the bottom of the cylinder. The collector was then connected by means of coaxial cable to a Rank d.c.

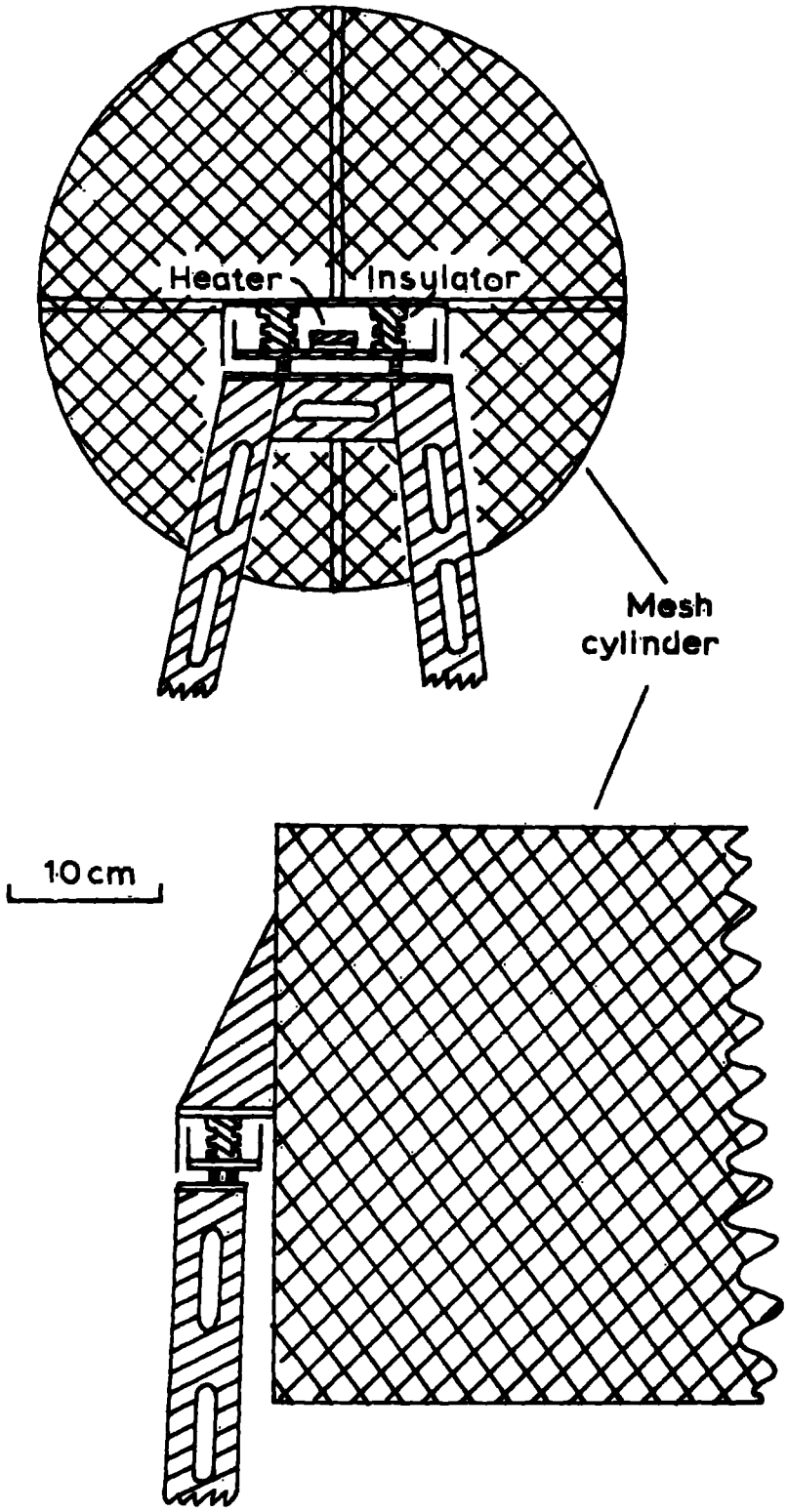

Fig. 3.5 The cylindrical rain collector.

Fig. 3.6 The Land-Rover experimental and exposed rain collectors.

amplifier mounted inside the Land-Rover. Experiments were conducted in fair-weather conditions to detect any possible charging produced by the drops falling from the bottom of the cylinder. After wetting the collector with a water spray, the water continued to run off for up to a minute, mainly in the form of very large drops. With the amplifier on maximum sensitivity, no significant deflection higher than the ambient noise level (1pA) could be detected.

The water spray was also electrified by passing the water through a brass nozzle whose voltage could be varied, and the charged droplets were directed simultaneously onto both the collectors on the Land-Rover roof. Some difficulty was encountered in obtaining a uniformly charged spray, as the spraying process itself gave rise to charge separation, but by trying differently shaped nozzles and varying the water pressure, consistent results were obtained. During one ten-minute period, the current densities measured by the two collectors agreed to within 10%, and the amplifiers indicated a steady output of about 150 pA.

The experimental collector was, however, exposed to the electric field, and in an attempt to shield the collector from displacement currents, a 5 cm spacing thin wire mesh was erected surrounding the collector (Fig. 3.6). It was calculated that

this outer shield would reduce the mesh cylinder's exposure factor from 2.5 to 0.1, whilst it would only intercept 5% of the incident rain. It was also calculated that drops impacting on the outer shield and falling onto the mesh cylinder would not transfer a significant amount of charge, provided the potential gradient at the ground did not exceed about 1000 Vm^{-1}. In actual fact, very few raindrops intercepted by the shielding mesh fell from it onto the collector, but instead they ran along the wires of the mesh. However, in the first conditions of quiet rain that occurred after completion of the apparatus, it became obvious that the electrical shielding provided by the outer mesh was nowhere near as good as that predicted. Large currents of up to 50 pA were found when rain was not falling, and these were directly attributable to potential gradient changes. Further experiments were conducted with earthed rods and other forms of shielding, but it was not found possible to improve the results. It was therefore decided to abandon the use of the experimental cylindrical collector.

3.5 The Shielded Collectors

Despite the disadvantages of the shielded rain collector, the necessity for a fast time-response measure of precipitation current density led to the adoption of this apparatus. The design

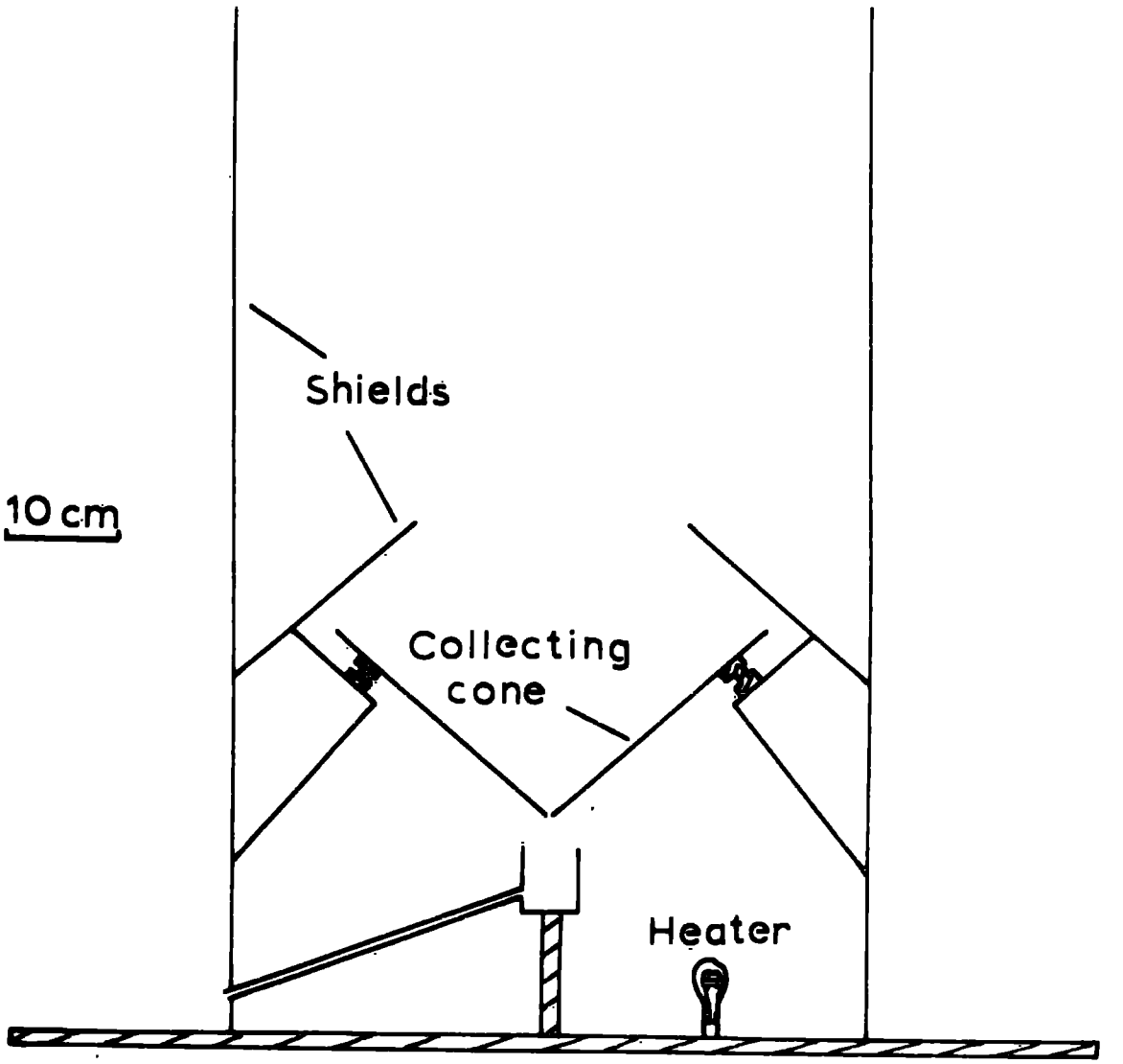

Fig. 3.7 The shielded rain collector.

of the equipment used is based on the apparatus used by SCRASE (1938), but incorporating a relatively larger diameter shield and modern insulators. A conical aluminium collecting bucket was mounted on three 2.5 cm long P.T.F.E. insulators inside a 1 m high, $\frac{1}{2}$ m diameter aluminium shielding cylinder. Protection from drops splashing from the rim of the cylinder into the bucket was provided by a truncated cone with a 25 cm diameter aperture (Fig. 3.7). The water falling from the bottom of the collecting cone was collected in a can below and run off through a brass tube. Insulator heating was provided by means of two mains-operated light bulbs connected in series.

Two identical collectors were constructed, one was mounted on the Land-Rover roof behind the exposed collector, the other was situated close to the exposed collector at Lanehead. In both cases the current was measured by a Rank nucleonics d.c. amplifier. The Lanehead shielded collector amplifier was mounted in the collector itself, below the cone (Fig. 3.8). The Land-Rover shielded collector amplifier was mounted on a rack inside the Land-Rover immediately beneath the collector base. The amplifiers were connected to the collecting cones by rigidly attached coaxial cable.

The displacement current shielding in both collectors was found to be extremely good, and even with rapid potential gradient changes associated with showers no discernible deflections have been obtained. It was hoped to make calculated compensations for the reduction in precipitation collection due to wind by taking simultaneous anemometer records.

Fig. 3.8 The Lanehead shielded collector interior

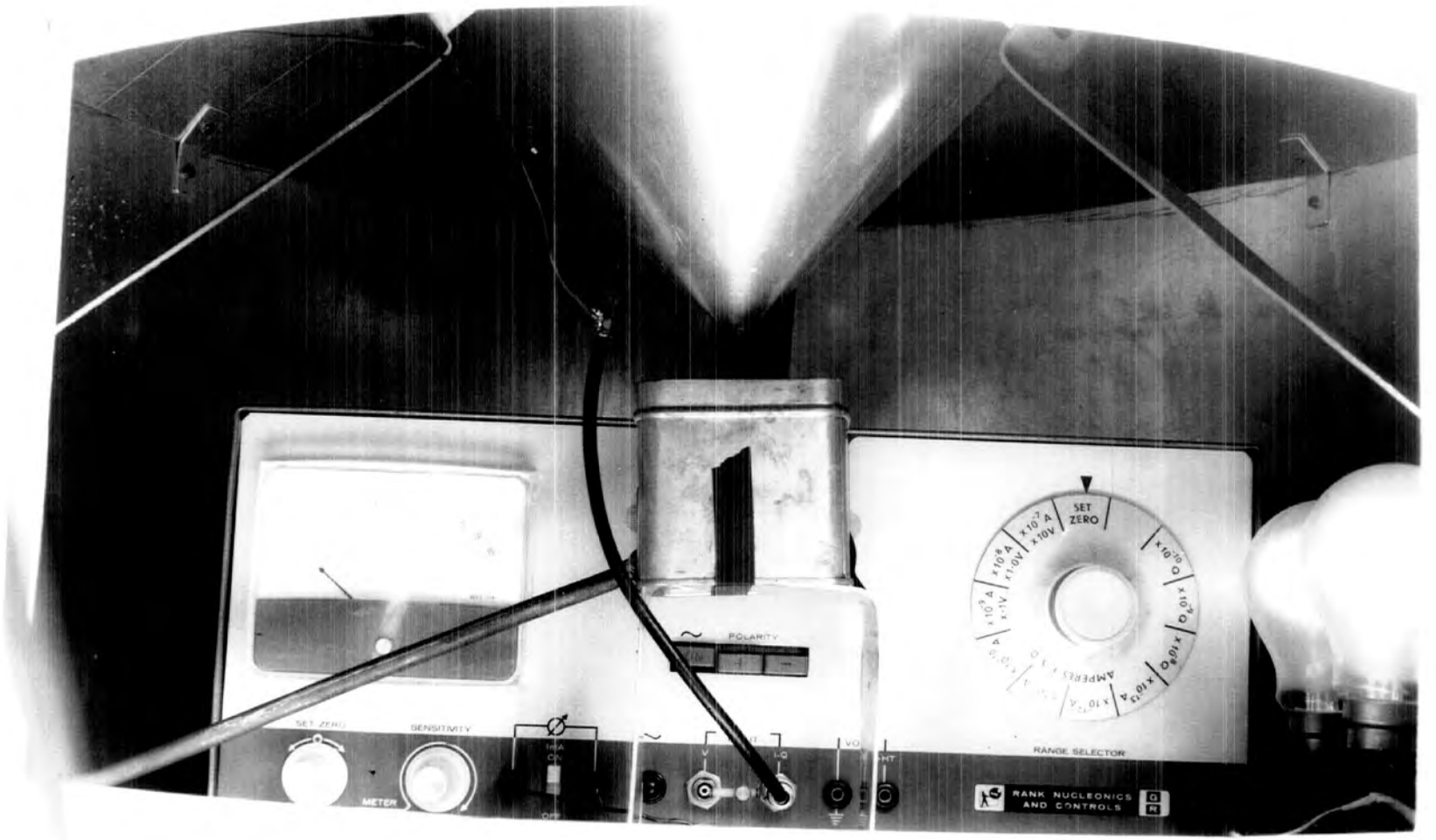
SET ZERO
POLARITY
SET ZERO
SENSITIVITY
METER
RANGE SELECTOR
RANK NUCLEONICS AND CONTROLS

CHAPTER 4

THE DESIGN AND CONSTRUCTION OF APPARATUS

4.1 The Automatic Recording Systems

Since readings were to be taken simultaneously at the Lanehead field centre, and at a mobile site using the Land-Rover and since the taking of readings by hand is laborious, liable to error, and difficult to maintain for long periods, it was decided that some form of automatic recording system was essential. Although pen recorders were in use at Lanehead with previously installed equipment, it was not considered possible to obtain sufficient time resolution by chart inspection for this research project, and the laborious task of chart analysing by hand would introduce human error also. In addition, the recording system to be installed in the Land-Rover had to withstand the shocks and vibration produced by travel and this precluded the use of pen recorders.

As a result, another member of this Research Group, Mr. W.P. Aspinall, designed and constructed an automatic recording system for use both at the Lanehead field station and in the Land-Rover. Basically the system comprises two units. The first unit samples the voltage input of each of ten channels and produces a sequence of rectangular pulse

trains whose repetition frequency is proportional to the input voltage. The pulse train of each channel is gated for 100 ms and fed to the output of the unit preceded by a 1 ms trigger pulse (Fig. 4.1). The output consists of a sequence of these 100 ms pulse trains and trigger pulses at intervals of 3s, giving a maximum cycling time of 30s. It was arranged that the number of sampled channels could be varied from one to ten, which meant a smaller number of parameters could be sampled at more frequent intervals.

Seven of the input channels were arranged to have an input range of 0 to -10V, the pulse repetition frequency varying from 0 to 10,000 pulses per second (p.p.s.). Three channels were provided with offset-voltage inputs so that positive and negative input voltages could be handled. Zero input voltage on these channels was arranged to give 5,000 p.p.s. output, and the input voltage range was thus $\pm$ 5V. Two identical models of this unit were constructed, one for the Land-Rover and one for the field station. Both models were mounted on 19" rack-mounting panels, with all the circuits on plug-in boards for rapid servicing and fault-tracing. In the Land-Rover, the output sequence of pulse trains was recorded directly on an E.M.I. battery-powered portable tape recorder, after the pulses had been smoothed to render them quasi-sinusoidal.

Fig. 4.1 **Recording system trigger and data pulses**

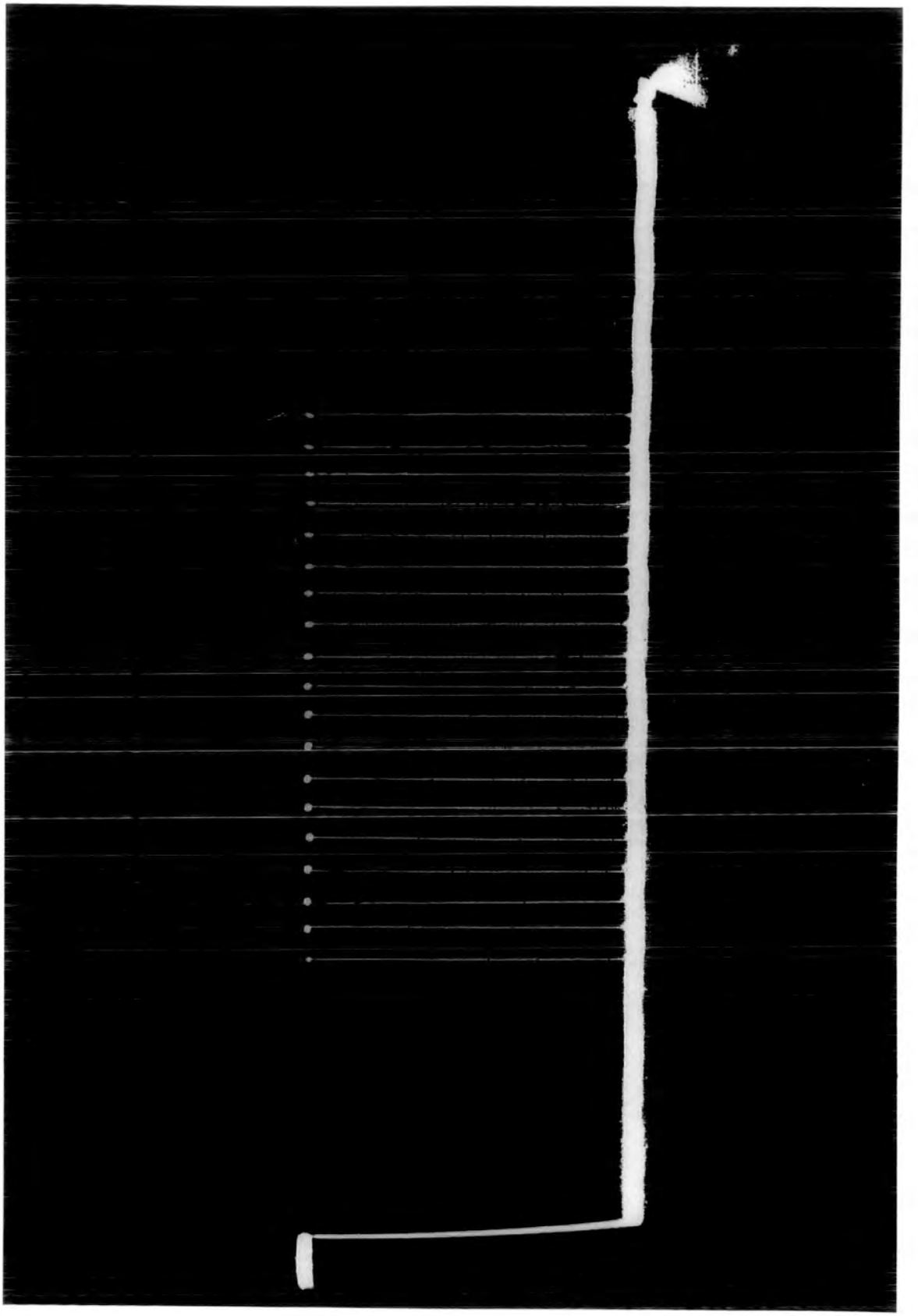

The Lanehead field station unit output was fed directly to the second output unit, which was permanently situated at the field station.

The second unit comprises electronic counters, digitizing circuits, paper tape punch and driving circuits. The output of the first unit, or the recorded output from the tape recorder, is first squared to ensure good triggering of the counting circuits, and then the number of pulses in each 100 ms train is counted electronically. The value of the count is displayed on numerical indicator tubes, as is also the number of the sampled channel. The count is simultaneously converted into Elliott binary code, and the coded number punched onto five-hole paper tape. The number of pulses in each train varies from 1 with zero input on the 0 to -10V channels, or +5V on the ±5V channels, to 999 with about -10V on the 0 to -10V channels or -5V on the ± 5V channels. The paper tape thus consists of a sequence of three-digit numbers, together with spaces and line printer carriage control characters. If the maximum count of 999 is exceeded, the counters reset to zero and continue counting. If there were 1200 pulses in a 100 ms train, for example, a count of 200 would be obtained. As most of the circuits were linear beyond full scale, no loss of

information occurred if the signal only exceeded full scale for a short period. The times when this happened were infrequent and easily identifiable.

The units were calibrated by applying known voltages to the inputs of the various channels, typical curves being shown in Fig. 4.2. The calibration curves are linear within 2%, and were found to be reproducible. Drift in the recording system as a whole produced long term variations of the order of 1%. A fixed input voltage produces a count consistent to within $\pm$ 1 or $\pm$ 0.1% of full scale. The performance of the system well exceeds that which may be expected of recording by hand, and in particular allows rapid sampling of parameters.

4.2 The Field Mills

For the measurement of potential gradient, it was decided to construct two identical field mills, one for each of the recording stations. Because of the nature of the project, simplicity and ruggedness were considered to be paramount. A single range with a maximum sensitivity of 1500 Vm^{-1} was thought to be most useful for the project. Tests were first carried out with a field mill of conventional design, comprising a stator of four 45° sectors of a disc and a similar earthed rotor above it. The alternating current

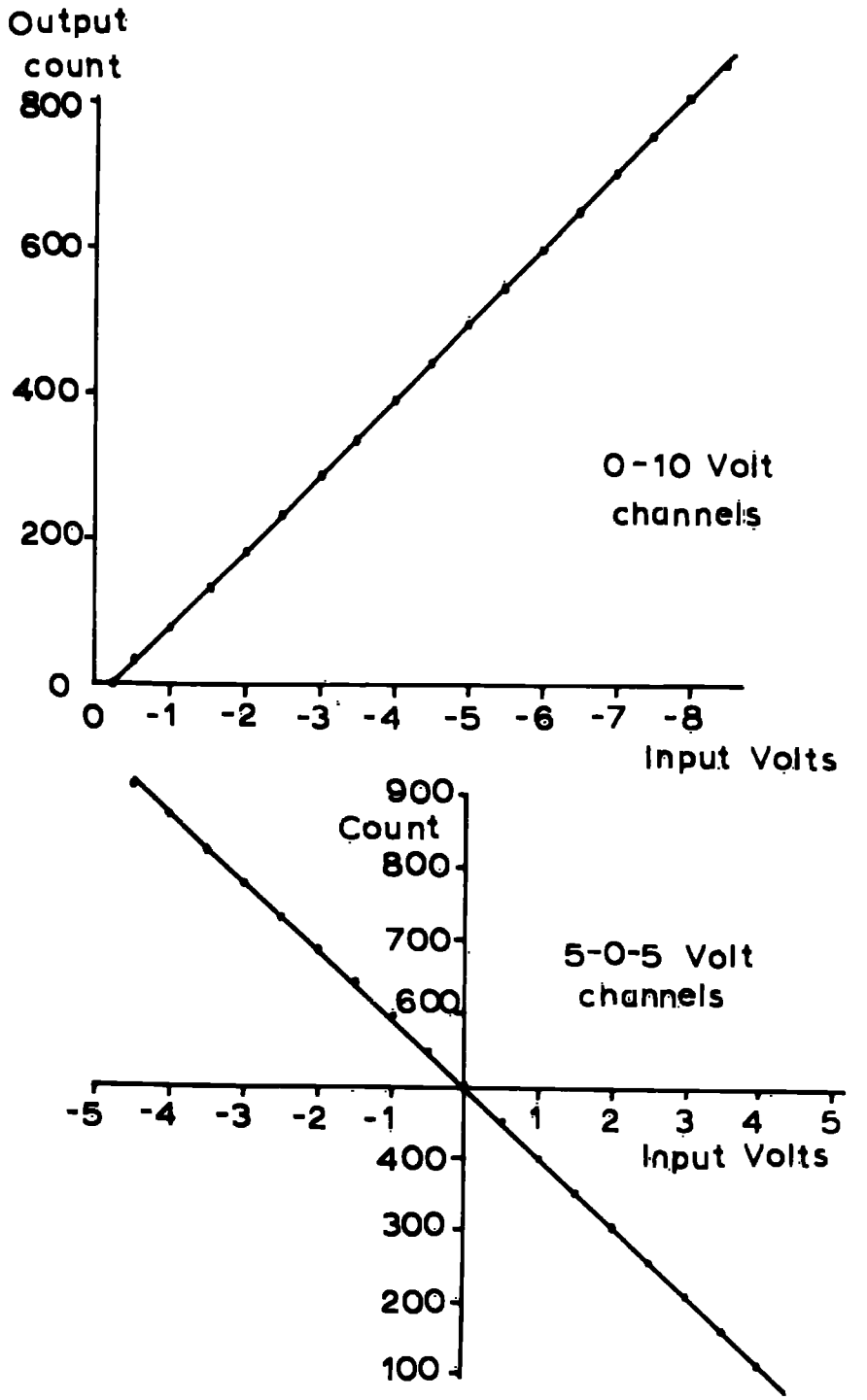

Fig. 4.2 Recording system calibrations.

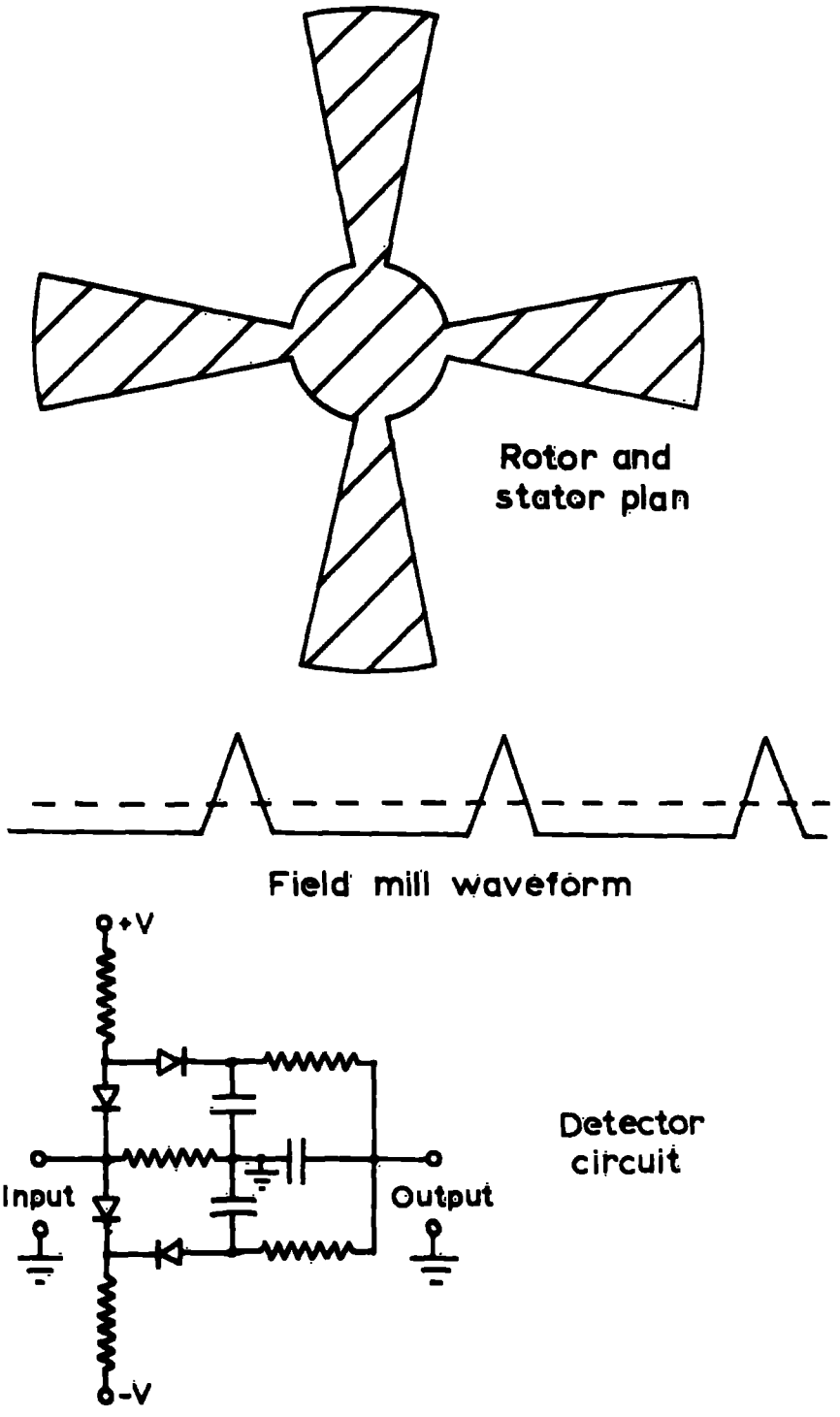

Fig. 4.3 Principle of operation of the assymetric field mill.

induced between the stator and earth was amplified by means of a two-transistor stage designed for the purpose by a colleague, Mr. I.M. Stromberg. Sign discrimination by means of an offset voltage or artificial electric field was not considered suitable for portable apparatus, so various methods of phase-sensitive detection were tried, including commutator-brush assemblies and magnet-reed switch arrangements. However, all were found to be unreliable and very sensitive to position and mechanical effects.

It was then decided to test a new design of field mill which relies on purely electronic detection and sign discrimination. This field mill, first developed by Lane-Smith (1968), comprises a stator and rotor of shape different from that normally employed, each being composed of four $22\frac{1}{2}^{\circ}$ sectors of a disc. The voltage induced on the stator in the presence of an electric field is an asymmetric triangular waveform whose amplitude is proportional to the field strength (Fig. 4.3). After amplification, the signal is detected by a four-diode network, which produces an output proportional in sign and magnitude to the electric field. High frequency spurious noise or low frequency sinusoidal pickup do not affect the output of the detector.

The prototype field mill of this type was constructed with a stainless steel rotor and stator of diameter 20 cm. The stator was mounted on an aluminium base plate by nylon bolts, and the rotor mounted on the shaft of a 27V d.c. electric motor bolted to the base plate (Fig. 4.4). Preliminary tests showed that the waveform obtained was not sufficiently asymmetric and in fact was almost sinusoidal. This was remedied by the insertion of earthed sectors in between the stator arms and a guard ring around the outside of the stator, to present a more nearly plane surface (Fig. 4.5).

A four-transistor amplifier was built to obtain current and voltage amplification of the stator signal. The first two transistors form a bootstrapped current amplifier stage, the third forms a simple voltage amplifier stage of gain 100, and the fourth forms an emitter follower 'buffer' stage between the amplifier and detector. The final amplifier and detector circuit is shown in Fig. 4.6.

The first field mill was rendered weatherproof by enclosing the motor in a watertight aluminium box, and it was then fastened in an inverted position by rubber mountings to a bracket on the side of the exposed collector equipment

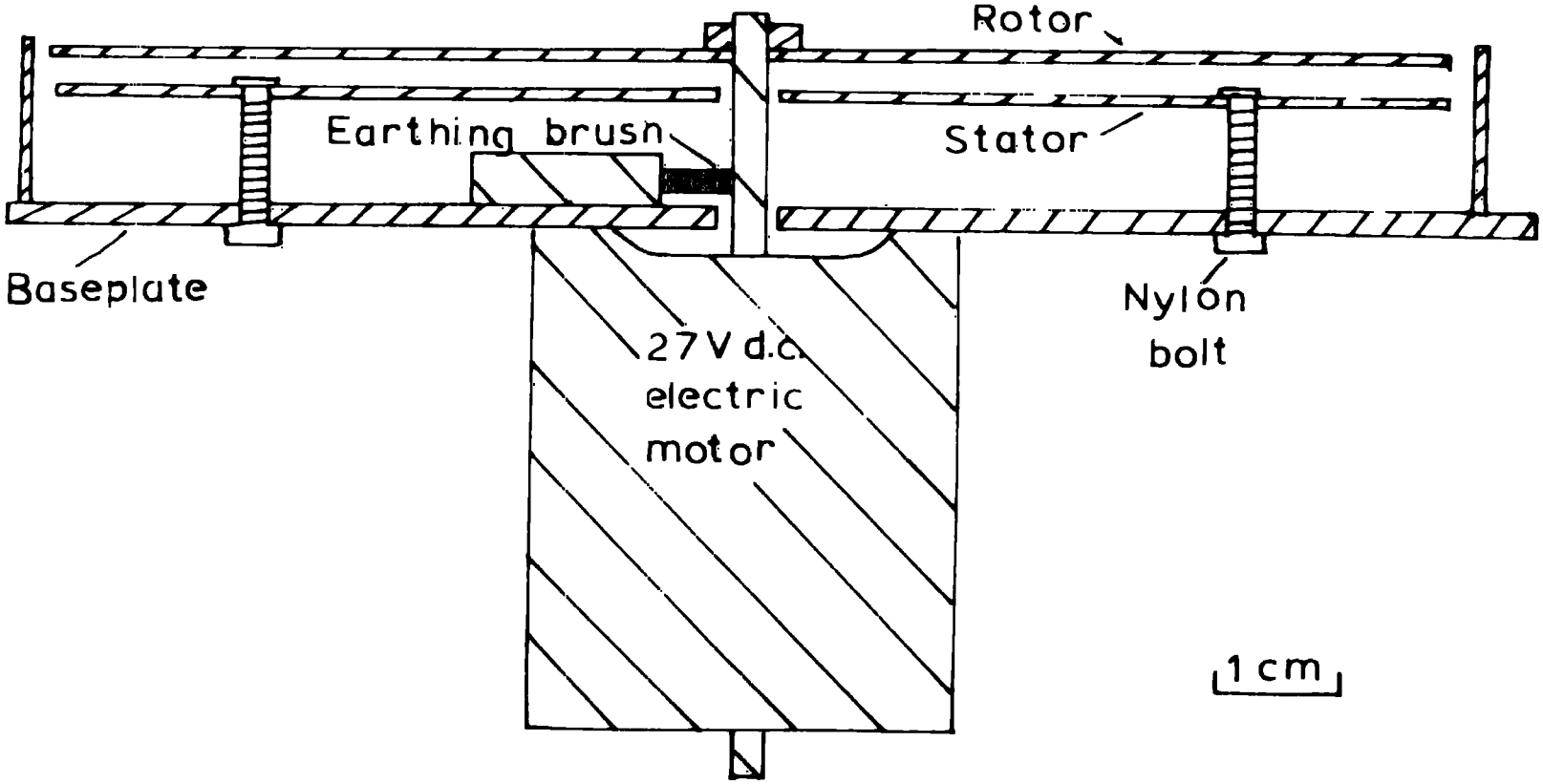

Fig. 4.4 Field mill construction.

Fig. 4.5. The Land-Rover field mill

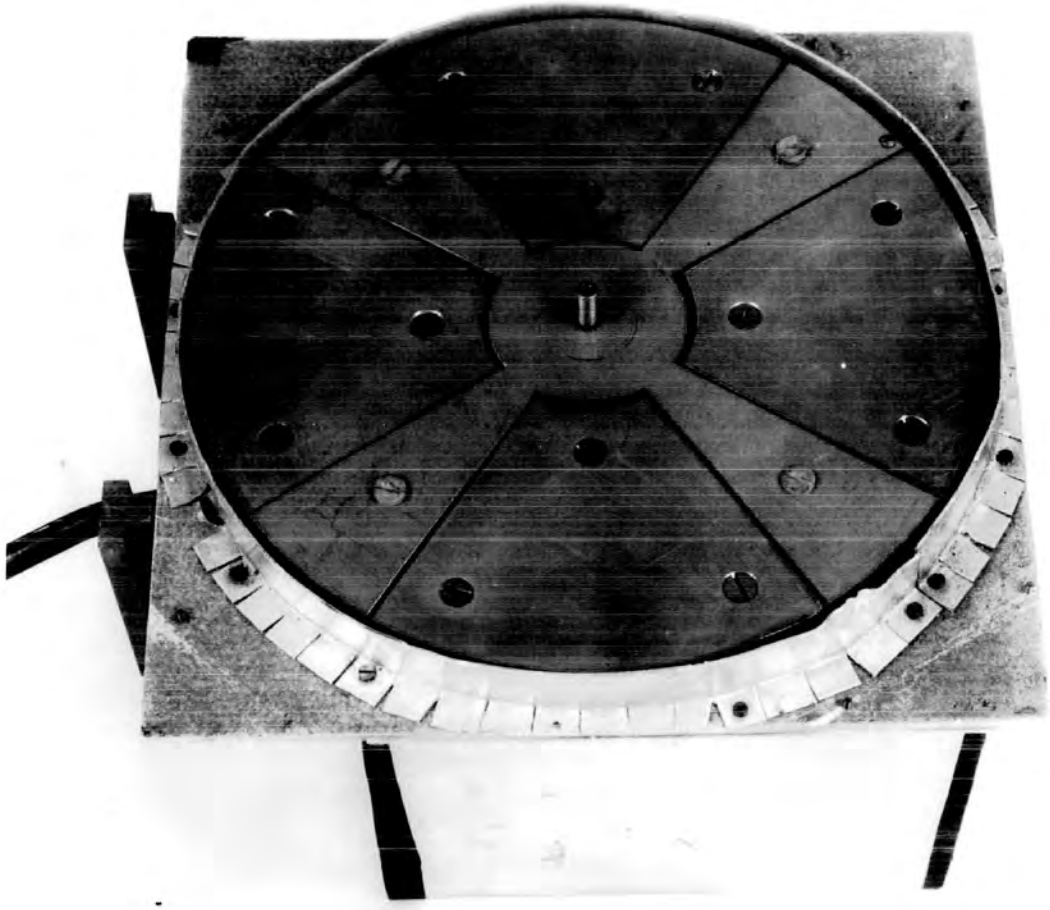

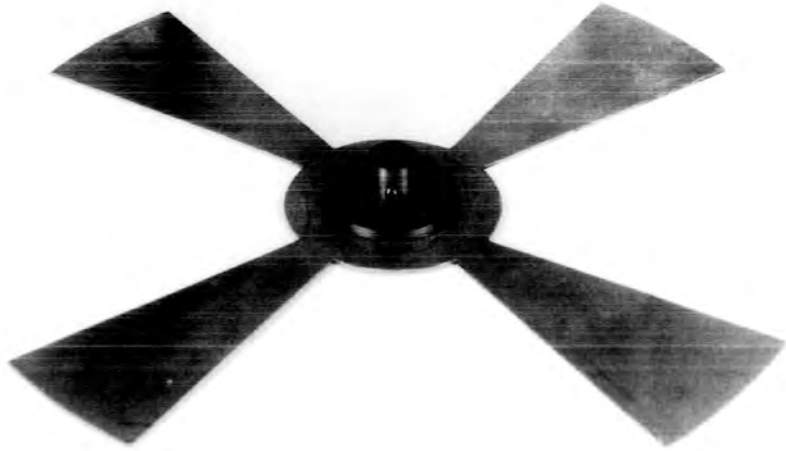

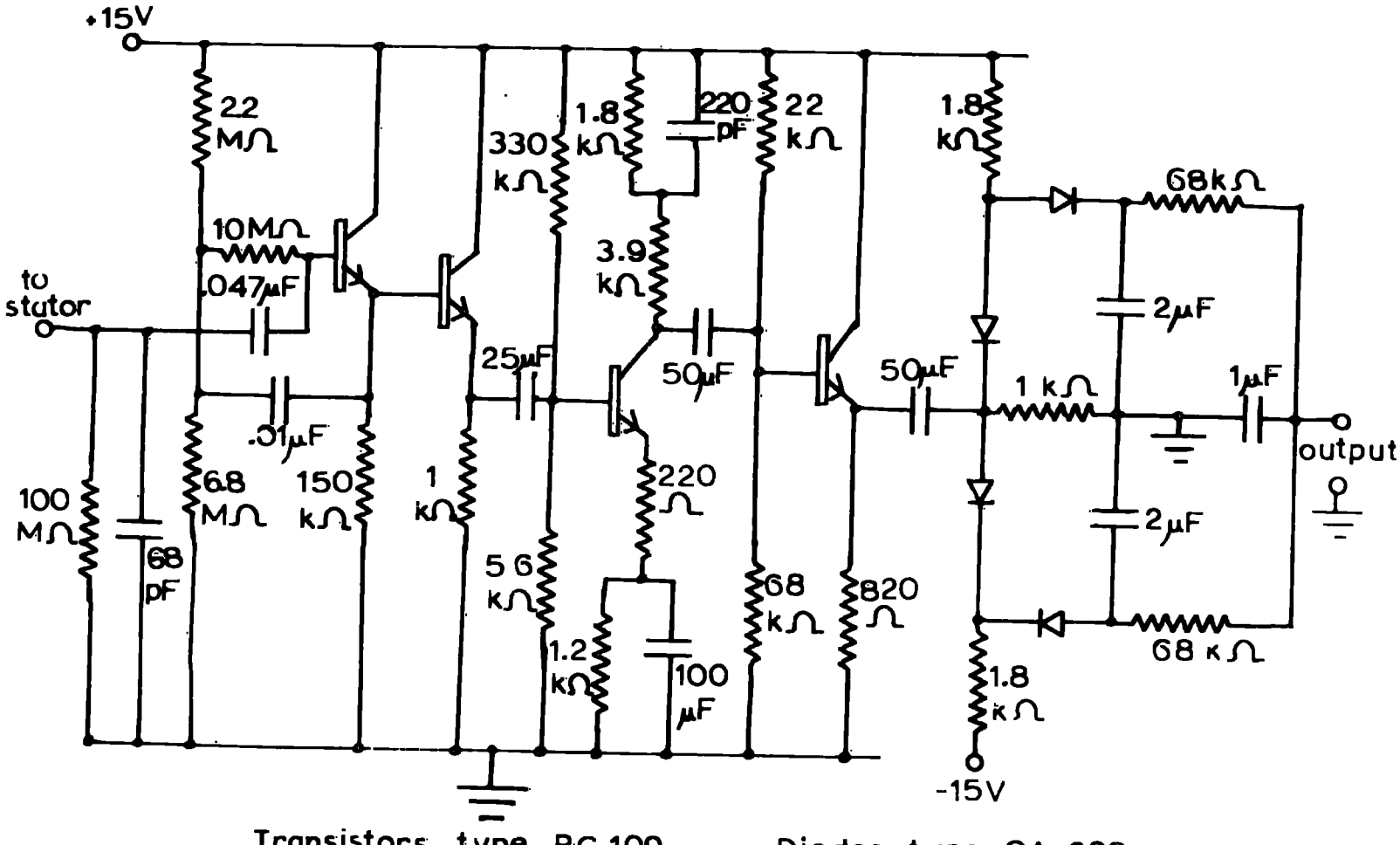

Fig. 4.6 Field mill amplifier and detector.

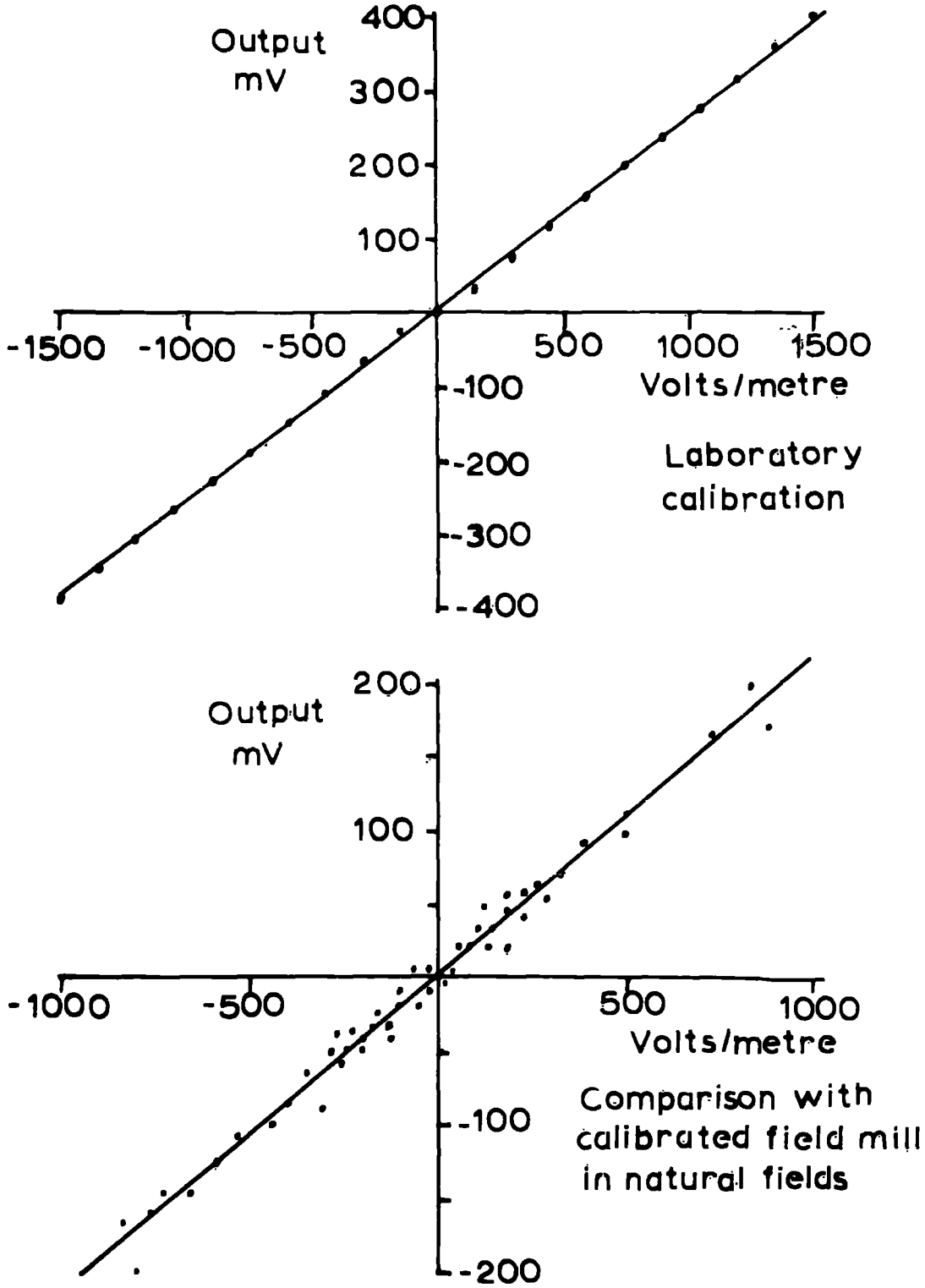

Fig. 4.7 Field mill calibration curves.

housing at Lanehead. Its amplifier and detector were enclosed in a small aluminium box inside the housing. The stabilised power supplies were brought from the field station through a twelve-way cable, and the detector output fed back through the same cable. The field mill was calibrated in the laboratory by applying known voltages to a fixed metal plate 10 cm above the field mill stator, and its exposure factor in situ was obtained by comparison with the calibrated field mill permanently operating at the field station (Fig. 4.7).

A similar field mill was constructed for use with the Land-Rover mobile station. The amplifier and detector were enclosed in the waterproof box surrounding the motor, and connected to the interior of the Land-Rover by a six-way cable and waterproof plug. The field mill was mounted on legs which enabled it to be easily slid into position on the side of the Land-Rover, or to be removed for travel. The calibration and determination of exposure factor were carried out in a similar manner to the original field mill.

4.3 The Anemometer

It was decided that a knowledge of the wind speed would be useful, particularly when evaluating the shielded collector

results. An anemometer is permanently mounted on a mast above the roof of the Lanehead field station, and in addition Mr. Aspinall recorded the wind speed at several heights near the ground during periods of precipitation. It was thought that these measurements at Lanehead would be adequate, and that an extra anemometer was required only for the Land-Rover.

For this purpose a Meteorological Office sensitive cup anemometer was mounted on a 2m long tubular steel mast which could easily be slid into a sleeve on the side of the Land-Rover. A pair of electrical contacts in the anemometer close twice every three revolutions, and so a pulse-rate counter was designed and constructed to provide a voltage output for the recording system (Fig. 4.8). The circuit comprises a monostable flip-flop to provide pulses of standard height and width from the anemometer contact pulses, an emitter follower buffer circuit, a transistor-diode pump circuit, and a Darlington pair output stage. Each contact of the anemometer gives a 3V positive pulse which is differentiated before the monostable input. The monostable pulses were chosen to have a width of about 100 ms and a height of 16V. The transistor-diode pump stage provides a d.c. voltage output which is proportional in magnitude to the pulse repetition frequency. Calibration was carried out by injecting pulses of known frequency, and by using the

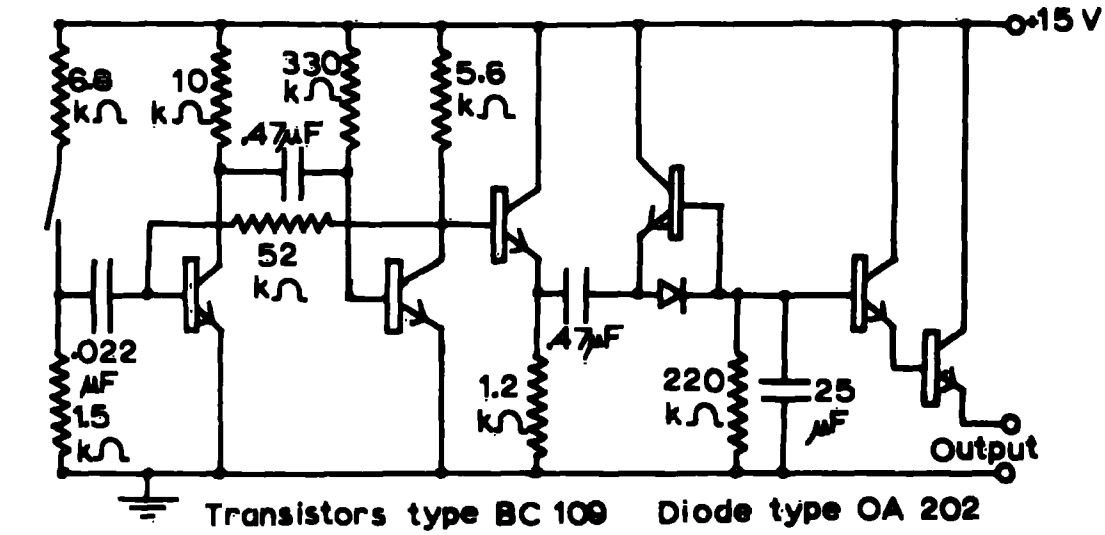

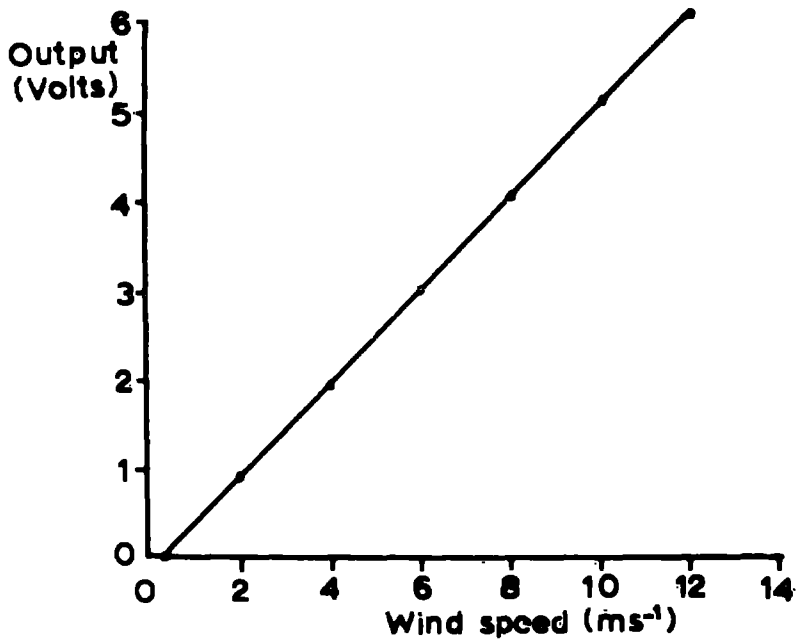

Fig. 4.8 Anemometer circuit diagram and calibration curve.

calibration of wind speed versus contact rate provided with the anemometer.

4.4 Rate of Rainfall Measurement

Although a knowledge of the rate of rainfall is not necessary for the evaluation of the precipitation current density measurements, as was discussed in Chapter 2, it was decided that this information might be useful. The experience of previous workers has shown that measuring rainfall rate over periods of the order of seconds is not easy because of the small volumes of water concerned.

Preliminary experiments showed that it would be feasible to arrange a small bucket to operate a sensitive microswitch when it filled with water, and that this could be achieved with less than 0.5 cm^3 of water. A bucket of capacity 1 cm^3 made of thin aluminium foil was attached by a No. 22 gauge wire of length 5 cm to the microswitch, and this arrangement was fastened to a bracket below the shielded collector bucket on the Land-Rover. The microswitch was wired to step on a 48-way uniselector which produced a steadily increasing voltage output by means of a resistor chain. This voltage was fed to an emitter-follower circuit, the output

of which was connected to one input of the automatic recording system (Fig. 4.9). Calibration in situ was carried out by introducing water at known flow rates into the collector. The result of this showed that, with a collecting area of 0.05 m^2, a rainfall rate of 1 mm hr^{-1} would produce a tip of the bucket every 35 seconds. The maximum expected rainfall rate of 6mm hr^{-1} would produce a tipping rate of one every 6s. The rate of rainfall could be calculated from the time between successive tips of the bucket.

In practice it was found that the device was very sensitive to the angle of tilt of the Land-Rover, which was difficult to level at nearly all of the recording sites used. These various angles produced erratic tipping of the bucket, rendering the measurements unreliable, and so use of this apparatus with the mobile equipment was discontinued.

At a later date, a Meteorological Office pattern recording rain gauge was loaned by the Department of Geography, and this was operated at the Lanehead station alongside the shielded collector. This apparatus produced a chart record of accumulated rainfall, the rate of rainfall being given by the slope of the graph.

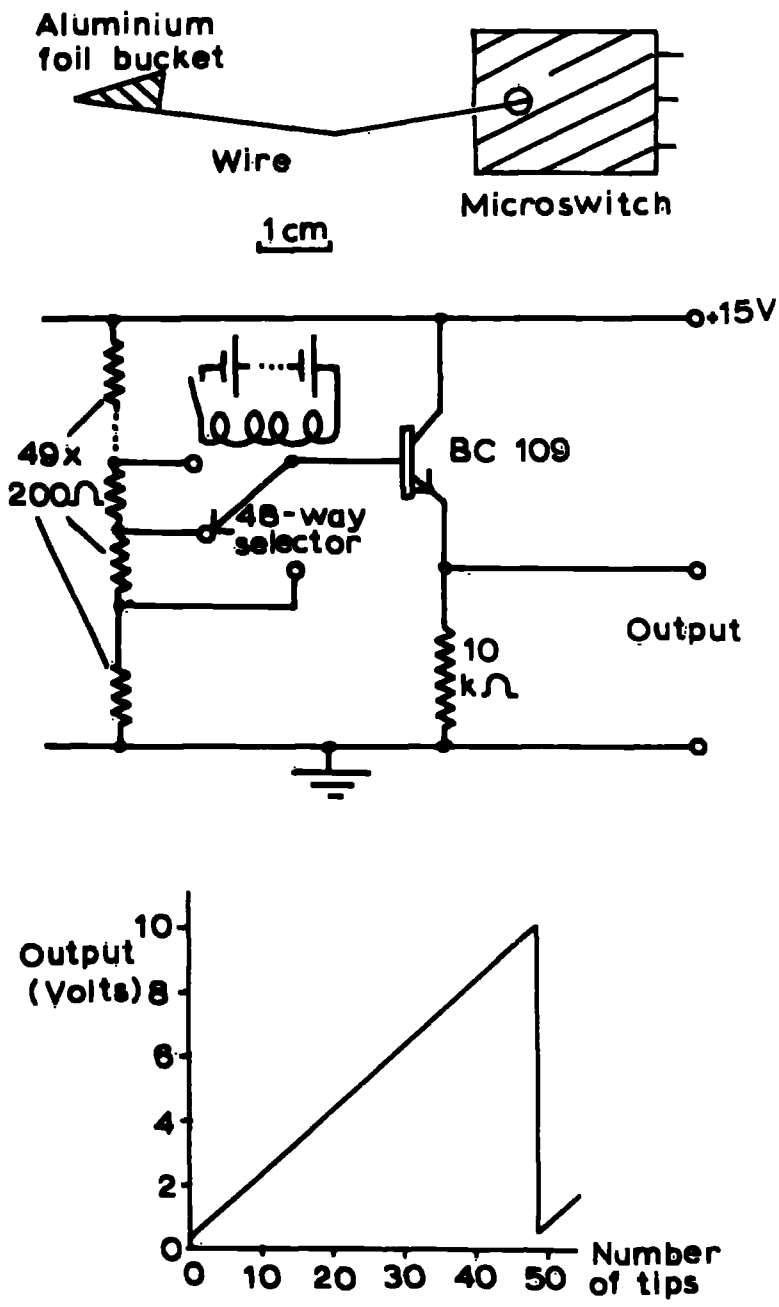

Fig. 4.9 Rainfall measurement apparatus.

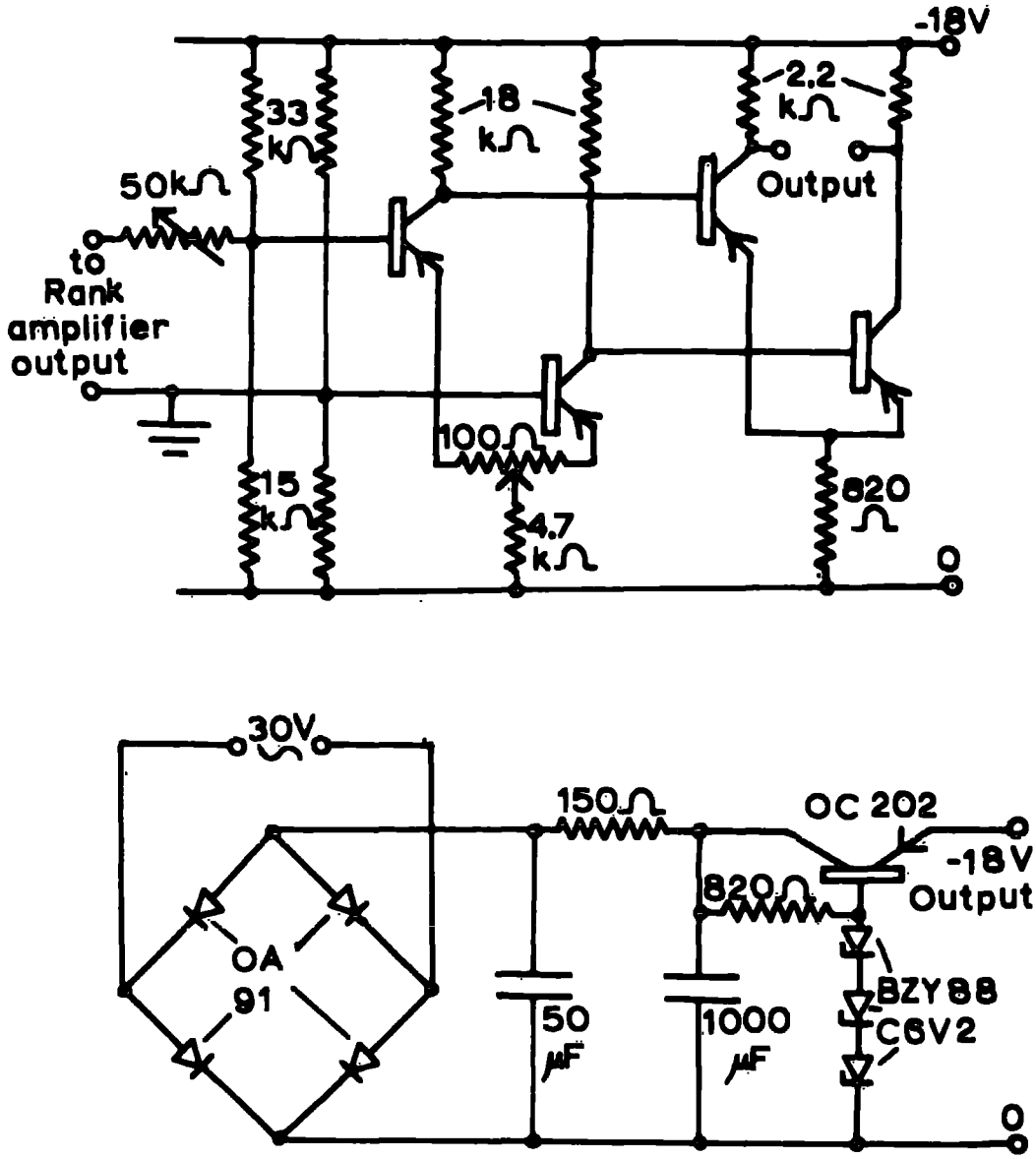

Fig. 4.10 The d.c. amplifier and power supply circuit diagrams.

4.5 The D.C. Amplifiers

The requirement of the automatic recording system input unit for 0 to 10V or ± 5V inputs meant that the outputs from the Rank Nucleonics amplifiers and the field mills needed further amplification. The Rank amplifiers produce an output of ± 1 mA full scale across 100 Ω, i.e. 100 mV, the signal thus requiring further amplification by a factor of 50. The field mill detectors produce a maximum output of ± 400 mV, and hence a further amplification of 12.5 is required.

When displacement current compensation by inverted test plate was being developed, a d.c. differential amplifier was designed and constructed (Section 3.3). As this amplifier had sufficient gain and output voltage for the recording system, it was decided to use similar amplifiers to amplify the Rank and field mill outputs. Two pairs of these amplifiers were constructed and each pair mounted on 19" panels, together with panel meters to display the input and output voltages of the amplifiers. A stabilised power supply was mounted on each panel to provide an 18V d.c. supply for the amplifiers (Fig. 4.10). Unfortunately, as these amplifiers are two-input-terminal devices, some difficulty was encountered

upon earthing them. Some of these difficulties were overcome, but it was found impossible to operate the Lanehead automatic recording system from these amplifiers because of the impossibility of earthing their output.

These amplifiers were thus rejected for use with the recording systems, and as an alternative, integrated circuits were considered. It was found that S.G.S. wide-band amplifiers, type μA 709C, had good characteristics for this application, and so six were obtained for the purpose. Four circuits were designed using these integrated circuits for operation at Lanehead, one for each of the two Rank amplifiers, one for the field mill, and one spare. Since these integrated circuits have such high open loop gain (about 45,000), the gain of the circuits used (Fig. 4.11) depends entirely upon the feedback network. The introduction of the capacitors in the circuits limits the frequency response of the amplifiers to about 100Hz. Two similar circuits for amplification of the Rank amplifier outputs in the Land-Rover were constructed and mounted on a 19" panel. Calibration was carried out by applying known input voltages and measuring both the output voltage and the count produced by the recording system. Since their installation, all of the circuits have performed satisfactorily and have not required attention.

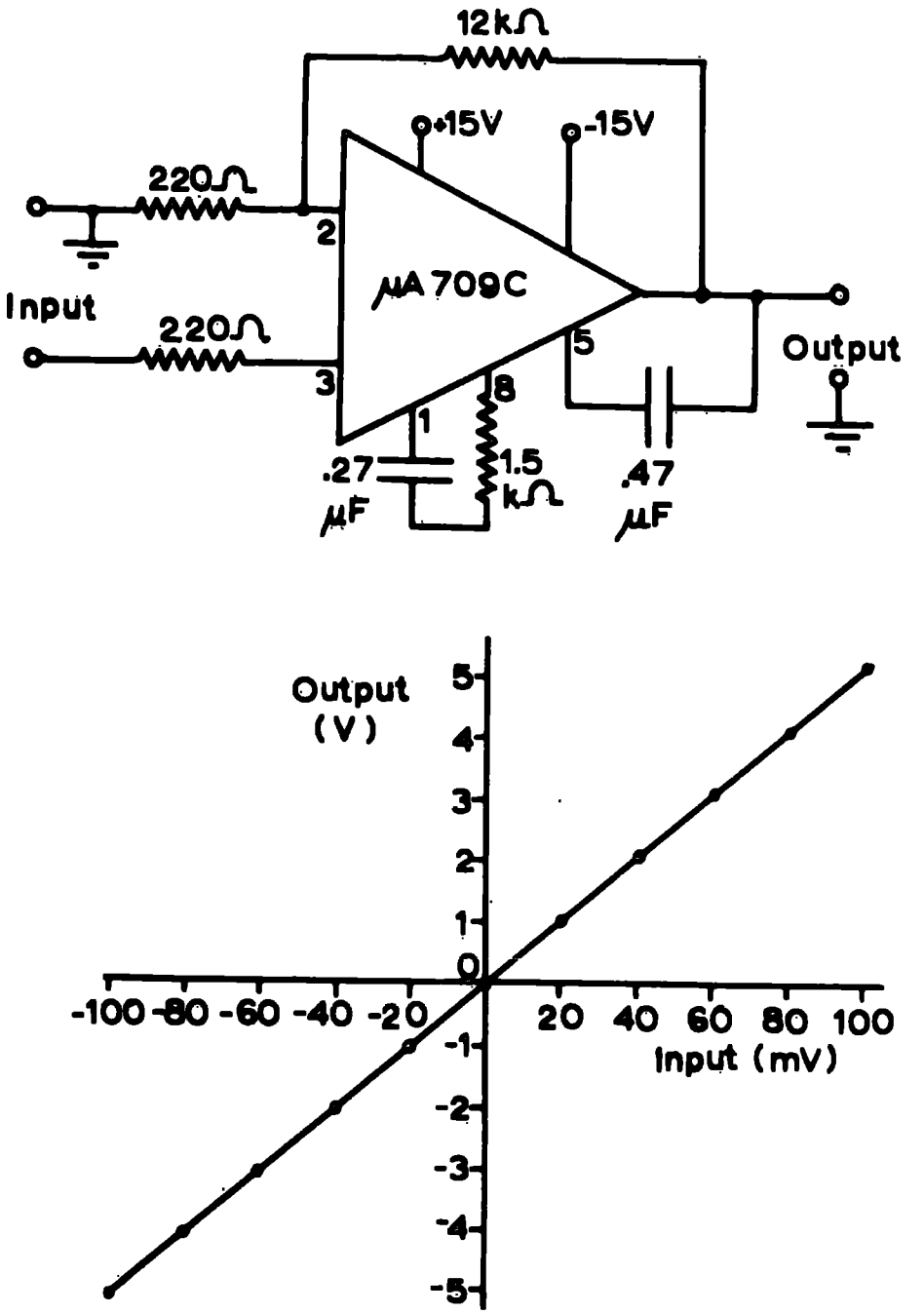

Fig. 4.11 The integrated-circuit d.c. amplifier and calibration curve.

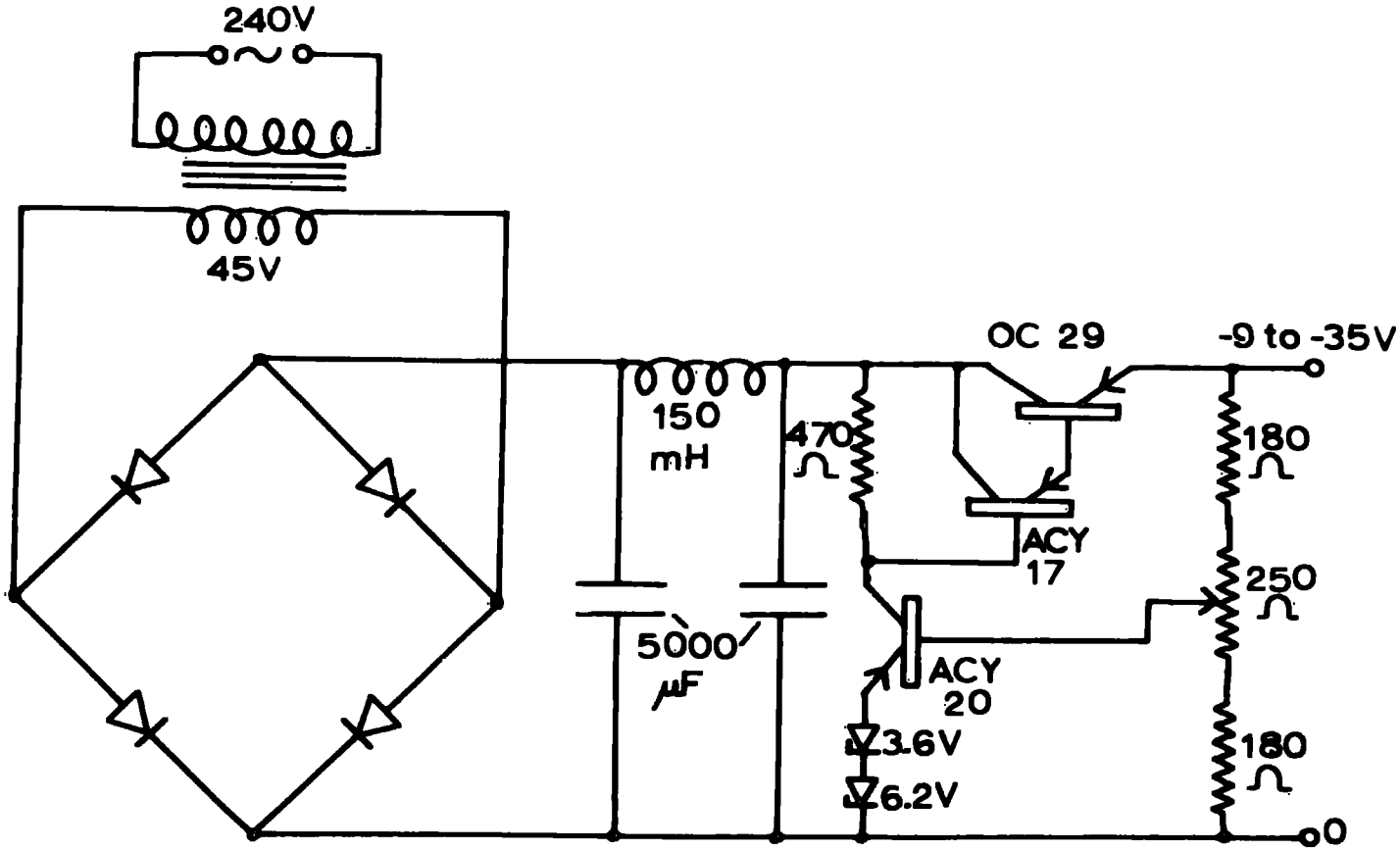

Fig. 4.12 Stabilised d.c. power supply circuit diagram.

4.6 The Power Supplies

The field mill amplifiers, the integrated circuits, the anemometer pulse counter circuit and the tipping bucket counter circuit all require d.c. power supplies of + 18V, -18V or both. Rather than use dry batteries or accumulators, it was decided to construct stabilised power supplies operated from the 240V mains supply at Lanehead or the 240V a.c. generator in the Land-Rover.

Two similar power supplies were designed and constructed on 19" panels for rack mounting (Fig. 4.12). Each supply comprises a mains voltage dropping transformer, silicon bridge rectifiers, capacitative-inductive smoothing circuits and transistor-controlled voltage stabilisation circuits. Each panel has a positive and negative supply, each of whose voltage can be varied from 9 to 30V. The supply currents are monitored by panel meters, and have a maximum value of 0.5A. The output voltages of the supplies were found to be stable to within 0.1V or better over long periods, and the mains ripple was less than 10mV. Apart from mechanical failure of two of the voltage-controlling potentiometers, no problems were encountered with the power supplies.

Unsmoothed d.c. power supplies were also constructed for

the Lanehead and Land-Rover field mill motors and exposed-collector insulator heaters. These supplies gave 27V d.c. with a maximum current output of 2.5A (Fig. 4.13).

4.7 The Nephoscope

It was originally intended to obtain cloud direction by visual alignment of the advancing or receding clouds with a prismatic compass. However, difficulties were encountered with this method and it did not prove sufficiently accurate for the purpose. It was then decided to construct a Meteorological Office pattern Besson comb nephoscope. This instrument consists of a vertical brass spindle mounted on bearings to allow rotation, and carries a horizontal cross-piece on its upper end. The cross-piece has seven vertical spikes mounted equidistantly along its length. The vertical spindle has a brass direction plate to indicate cloud direction.

A nephoscope of this type was constructed of brass rod, to Meteorological Office specifications, and mounted on a 5m long vertical wooden pole which was concreted in the field at Lanehead (Fig. 4.14). Cloud direction is obtained by standing at a distance of several metres from the nephoscope base and aligning a portion of the cloud with the central spike. The

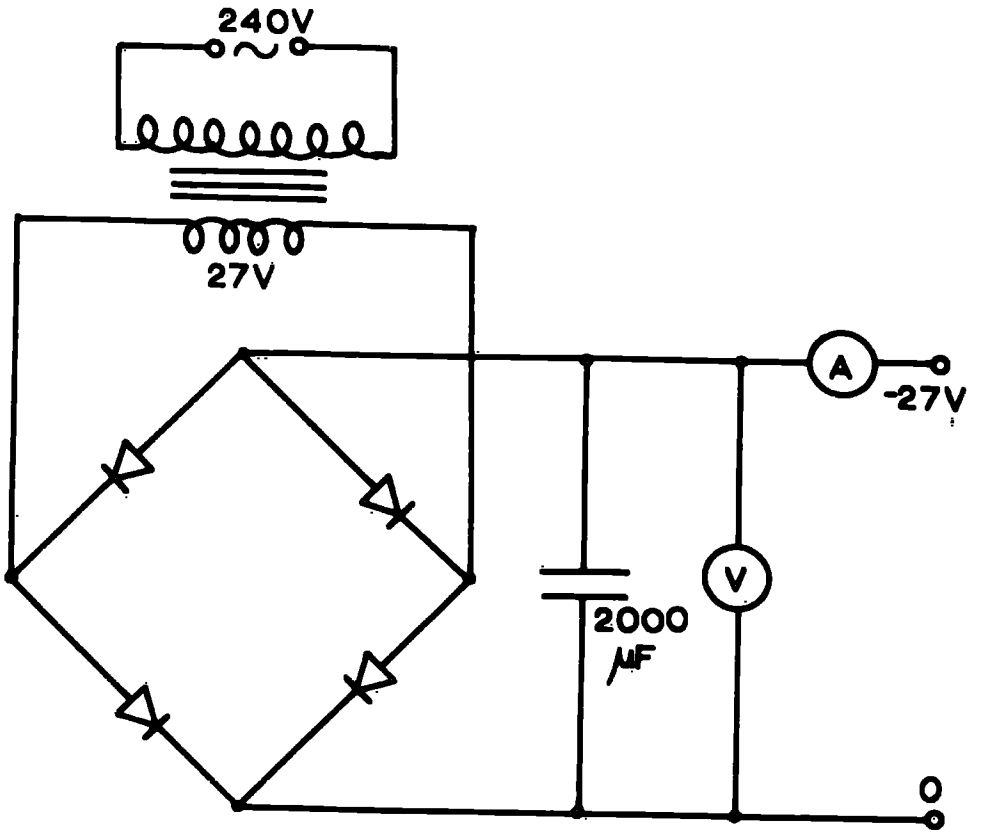

Fig. 4.13 27V d.c. power supply circuit diagram.

Fig. 4.14 The Nephoscope

Fig. 4.15 **The Lanehead field installations**

Fig. 4.16 **The Lanehead indoor installations and automatic recording system**

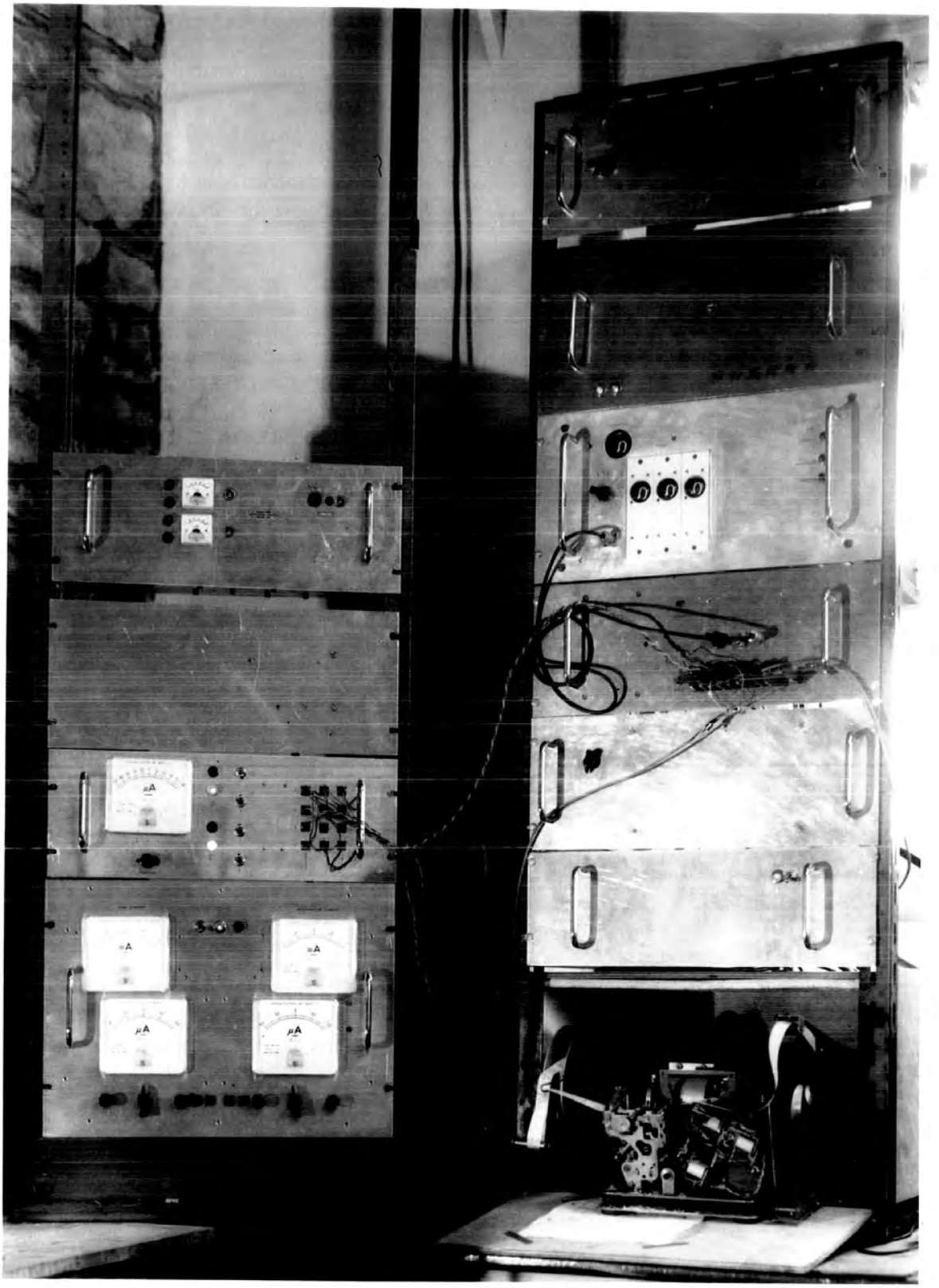
μA
μA
μA
μA

nephoscope is then rotated by using nylon cords attached to a small cross-piece on the spindle until the cloud appears to be moving along the spikes.

The cloud direction is then read off the direction plate directly. Angular cloud speed can be estimated by measuring the time of traverse of the cloud between spikes, and by the use of simple geometry. If the cloud height is known, its speed can be calculated.

4.8 The Lanehead and Land-Rover Installations

The final outdoor installations used at the Lanehead field station comprise the exposed collector raised to 2m above the ground, its mounting frame and equipment housing, the field mill with its amplifier and detector, and a short distance away the shielded rain collector, together with its Rank amplifier (Fig. 4.15). The indoor installations comprise the stabilised power supply, the Rank amplifiers output display meters, and the integrated circuit amplifiers. These were mounted on a 19" rack alongside the automatic recording system (Fig. 4.16). A 12-way cable was used to connect the power supply to the field mill amplifier, and to carry the outputs from the field mill and Rank amplifiers. A separate 3-way cable was used to carry mains supply to the Rank amplifiers and heater power supply in the field.

The Land-Rover installations comprise the shielded and exposed collectors, which were mounted on the roof, the field mill and anemometer, which were both mounted on brackets so they could be removed whilst travelling, and the Honda electric generator, which was placed 20m downwind whilst recording (Fig. 4.17). Inside the Land-Rover the Rank amplifiers, field mill amplifier and integrated circuit amplifiers, the anemometer and rainfall counter circuits, and the automatic recording unit were mounted on panels attached to three 19" racks situated along the nearside of the Land-Rover interior (Fig. 4.18). The tape recorder and recording system contact clock were situated underneath two of the racks during recording, and stowed in a protected compartment for travelling. In addition a fluorescent light was fitted to enable recordings to be made at night, and a 300W greenhouse heater was later added to prevent moisture from condensing on the instruments.

Fig. 4.17 The Land-Rover mobile station

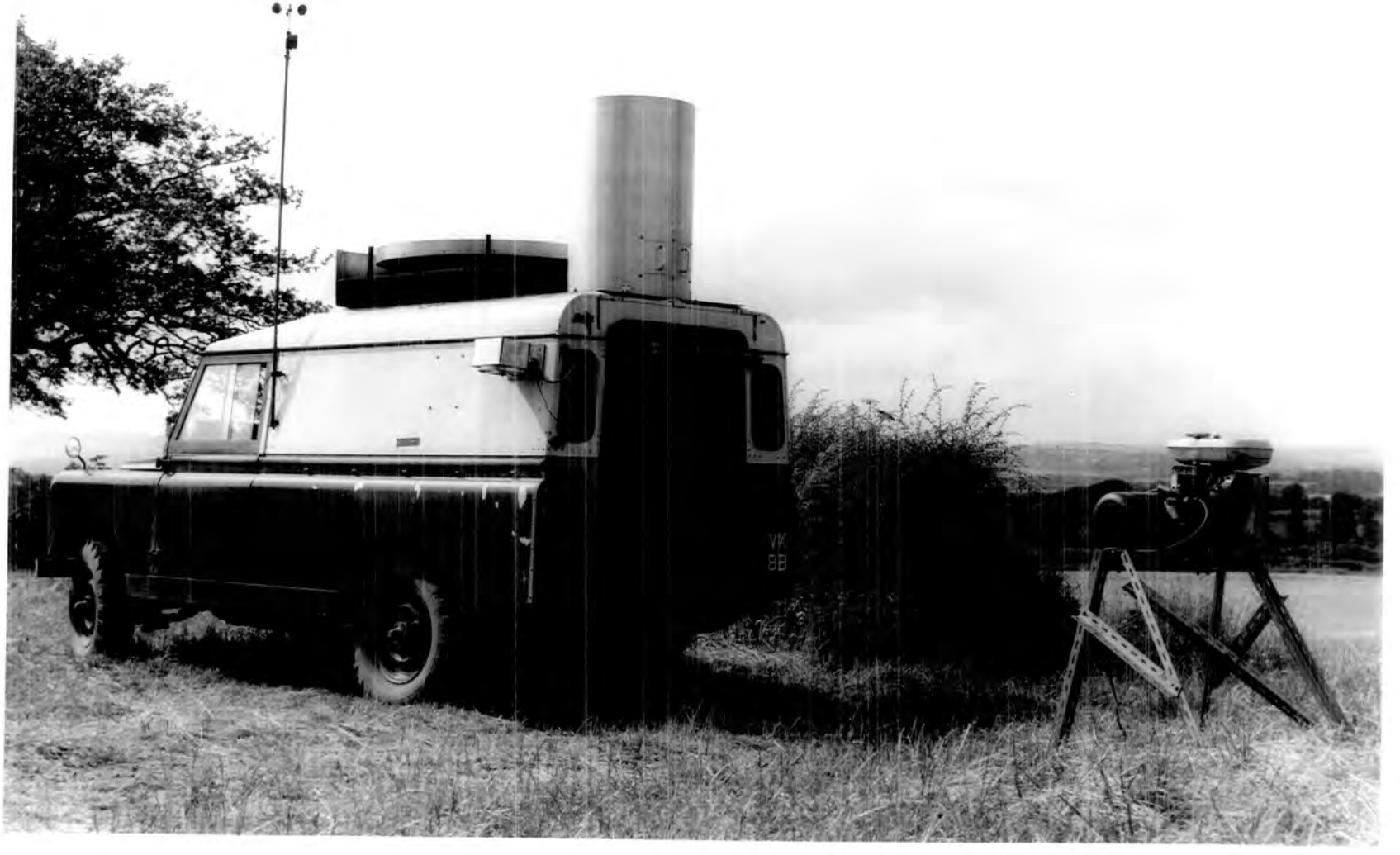

Fig. 4.18 **The Land-Rover interior**

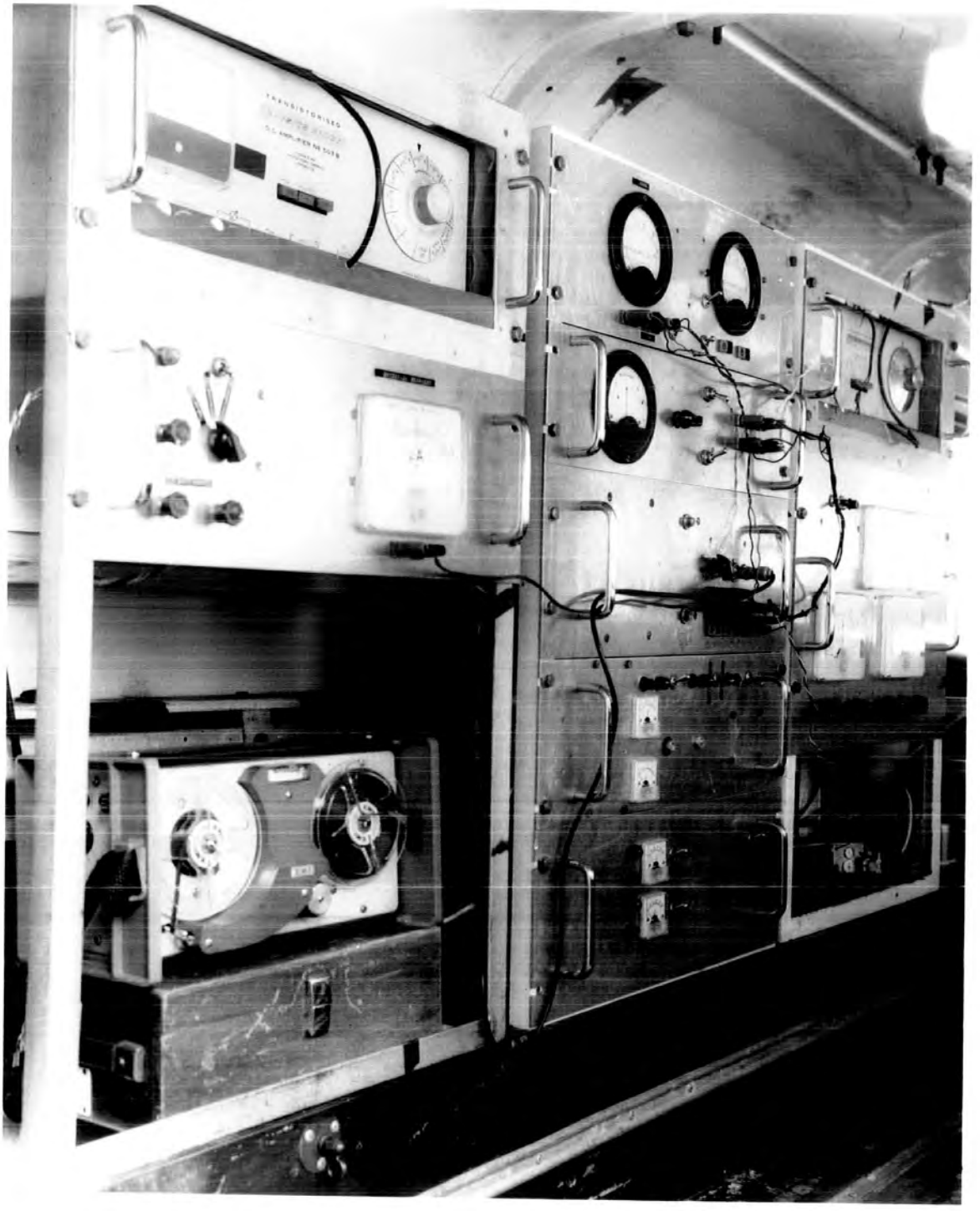

CHAPTER 5

EXPERIMENTAL TECHNIQUE

5.1 The Recording Sites

The Lanehead Field Centre, originally a school serving the small village of Lanehead, is situated on the side of the valley at the head of Weardale in the central Northern Pennines, at an altitude of 440m (1450 ft.). It is located on ground sloping gradually to the north, and is surrounded on the north and west by a plantation of conifers. The surrounding mountains reach about 700m (2300 ft.) in height. There are no large sources of pollution within 20km which might influence the atmospheric electric environment. A minor road runs past the station, but carries only very light traffic except on summer weekends. Analysis of the effect of the space charges in the exhaust gases of passing vehicles upon the Lanehead instruments has shown that any effects are small, if not negligible.

The research project required the mobile recording equipment to be located in a direction in the line of cloud movement from the fixed equipment. It was thought that a time of around 1000s for the clouds to travel between the two

sites would be adequate. This means a horizontal separation of the sites of 10 km with a cloud speed of 10 ms^{-1}. The network of minor moorland roads surrounding Lanehead provides numerous available recording sites at distances of up to 10km, principally between North-West and South-East. At most points along these roads it is possible to park a Land-Rover off the road to windward with the vehicle more-or-less level. The sites along these roads are nearly all very exposed compared with the relatively well-sheltered Lanehead site, and their altitude also varies between 300m and 675m. This was of course not desirable, but could not be helped. A map giving the main features of the area is shown in Fig. 5.1.

5.2 The Criteria for Recording

The criteria for the recording of data were of necessity very subjective. It was often found difficult to identify the meteorological conditions from observations made at the ground, and this was particularly so at the Lanehead station. In disturbed weather conditions the cloud base height was often close to or below that of the field station, and the proximity of the surrounding mountains made it possible to see only a small area of the sky. It was thus virtually impossible to identify nimbostratus clouds at the time of observation, and often impossible to distinguish them from any other clouds producing total sky cover. Well-developed warm-frontal systems could usually be fairly well identified with the aid of the Meteorological Office weather forecasts, which usually

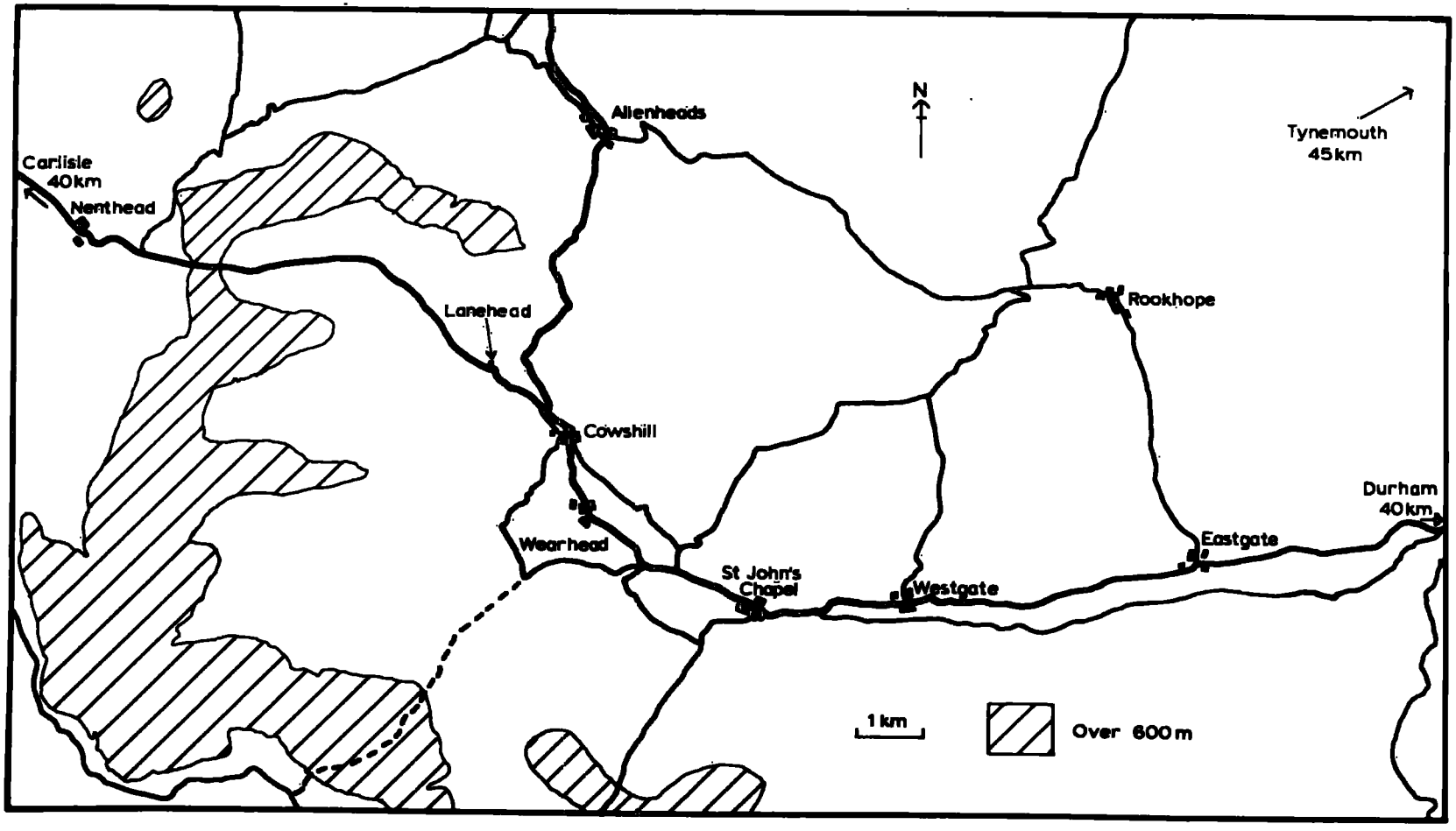

Fig. 5.1 Upper Weardale

predicted their time of arrival quite accurately. However, on many other occasions, steady continuous precipitation occurred which did not seem to be associated with any frontal systems, and on some of these occasions nimbostratus clouds were responsible.

As a result, mainly atmospheric electric criteria for data recording were used. Electrical measurements that had been made whilst the equipment was being developed had shown several qualitative factors. Firstly, the precipitation current density from stratiform clouds was found to be always negative for snow, except when blowing snow was present, and positive for rain. The only exceptions to this were currents less than 10 pAm^{-2}, which could not be measured with any great accuracy with the amplifiers on the range normally used. The precipitation current densities from these clouds rarely exceeded 200 $pA\ m^{-2}$, which represents full scale on the normal amplifier range, and they changed relatively slowly. The clouds were identified as stratiform from information taken from the Meteorological Office Daily Weather Report. Shower and non-stratiform clouds produced precipitation current densities which were basically different from

stratiform clouds. Rain currents were often negative, snow and graupel currents were often positive. Changes were frequent and rapid, and the magnitudes of precipitation current density were much higher, up to 10,000 pAm^{-2}.

Thus it was decided that for readings to be made in conditions of precipitation, the atmospheric electric criteria required that the precipitation should be continuous for an hour, and that the precipitation current should change slowly and be predominantly negative for snow, positive for rain. Any parts of records containing precipitation current densities in excess of 200 pAm^{-2} were to be rejected, unless very short in duration. As a precaution against the disturbance of point discharge, readings were only taken when the potential gradient at the ground was less than 1500 Vm^{-1}.

5.3 Cloud Observations

The cloud direction was ascertained by visual sighting with the aid of the nephoscope. Whenever possible, the cloud direction was measured at regular intervals before the onset of rain, in order that any systematic variations with time could be assessed. When higher clouds were also visible, it was

often noticeable that there was wind shear with height. It was thought that the higher clouds, being less affected by local topography, would be more representative of the cloud system. The cloud direction was then taken as the direction of the highest discernible cloud layer. The angular cloud speed was also measured using the nephoscope, except on the occasions when insufficient cloud detail was present, or when the cloud base was too low. The cloud height was estimated by eye, and the approximate cloud speed calculated.

A recording site was then chosen for the Land-Rover, taking into account the cloud direction and its systematic changes, and the cloud speed. It was possible to maintain the line joining the two recording sites within 3° of the cloud direction. This meant that a cloud passing over the upwind site would pass no more than 500m from the overhead position at the downwind site at a horizontal site separation of 10km. Any further cloud data, including cloud type, speed and height, were obtained later from the Daily Weather Report. The nearest weather stations to Lanehead are situated at Carlisle, Tynemouth and Leeming (Fig. 5.1).

5.4 Operation of the Apparatus

At the Lanehead Field Station, all of the recording equipment is running continuously and their outputs monitored on chart recorders. In addition, Mr. Aspinall has arranged his automatic recording system to integrate many of the parameters and sample them hourly. At the onset of rain, the one-hour automatic recording was manually disconnected and the sampling interval reduced to 3s. The channels to be recorded were connected to the recording system input, and the parameter switch set to the number of channels to be sampled. Usually only four or five channels were recorded in order to obtain good time resolution, and as a further improvement at a later date, only Mr. Aspinall's field mill was used, thus avoiding duplication of readings. Preparation of the field equipment before the onset of rain merely necessitated the checking and cleaning of insulators and heaters and zeroing the amplifiers when necessary. Spiders' webs proved to be the most persistent problem, but apart from this all the field equipment operated satisfactorily.

The Land-Rover equipment was checked each time before it was taken to a recording site. It was connected to the

mains supply at Lanehead, and the measuring and recording apparatus fully checked for satisfactory operation. Faults were often found to have arisen even after driving only short distances. Most of these faults were due to dry joints or broken wires produced as a result of vibration, and were easily remedied. A particularly severe cold spell which produced air temperatures of $-15^{\circ}C$ gave rise to faults in a wide range of equipment. These were attributed to physical changes in the solder, which occur to a significant degree at temperatures below $-5^{\circ}C$. The only other two severe equipment failures were due to damage to a Rank amplifier electrometer valve and the breakage of a reed relay in the Land-Rover automatic recording system. The exposed and shielded collector insulators required more frequent attention due to their increased exposure to dust and moisture, and they were usually cleaned twice monthly.

On arrival at a recording site, the Honda a.c. supply generator was set up on its stand and started. The Land-Rover was then driven a further 10-20m upwind and positioned as level as possible facing into the wind. The mains supply cable was plugged in, and the generator voltage adjusted to 240V by varying the motor speed. Whilst the electronic

measuring equipment was warming up, the field mill was slid on to its bracket and plugged in, and the anemometer mounted in position on its mast. The tape recorder was connected to the recording system, the recording system contact clock started, and the system checked for satisfactory operation. Data recording was usually begun at the onset of appreciable precipitation currents, that is in excess of about $5pAm^{-2}$. Data logging then proceeded automatically, but a constant check was maintained in case of faults or deflections in excess of full scale. The input pulses to the tape recorder were monitored continuously on its loudspeaker so that any failure would be immediately noticed. The magnetic tapes required changing every 48 minutes, but the process only takes about 30s so that little loss of information was experienced. After 2 or 3 hours of continous recording, the tape recorder battery was exchanged for a freshly charged one, a process which could be carried out without interrupting recording, and the generator petrol supply was replenished. At the end of the recording period, which was a maximum of 5 hours, the zero settings of the amplifiers were checked for drift, and all the apparatus checked for faults.

CHAPTER 6

THE ANALYSIS AND HANDLING OF THE DATA

6.1 The Statistical Analysis of the Data

The outputs of the equipment recording atmospheric electric and meteorological parameters are in the form of continuously varying analogue voltages. These outputs are sampled at periodic intervals by the automatic recording units to produce time series consisting of discrete numbers separated by a constant time interval. Each measurement of a parameter made at either of the two recording stations can be regarded as a valid estimate of that parameter. However, as with all experimentally obtained data, the measured values are subject to errors. Some of these errors may depend on factors which can be determined, such as the reduction in collecting efficiency of a rain gauge due to wind, and which can therefore to some extent be compensated by previously obtained data. This is not possible with accidental or random errors, and the effects of these can only be estimated from the experimental data by an application of statistics. Consequently, in order to obtain the maximum amount of information from the data, statistical methods have been employed throughout.

For all of the statistical computations it has been assumed that the time series of each parameter forms stationary random data. That is, the means, standard deviations and all of the higher moments are assumed to be time invariant. Whereas this was almost certainly not rigorously true for all the experimental data obtained, it was found that the time series of precipitation current density and potential gradient were weakly stationary. Weak stationarity is implied when the means and standard deviations of a parameter do not vary significantly between statistical samples of the parameter, and this was found to be true of the data recorded independently at the two recording sites. Weak stationarity is a sufficient condition for the application of the normal statistical analysis techniques used for random data.

For each time series of experimental data, the mean and standard deviations were calculated, and no further explanation of these is thought necessary. As a measure of the dependence of one parameter upon another, cross-correlation analyses have been used. Cross-correlation allows the degree of linear correspondence between parameters to be estimated. In addition, since most time series exhibit persistence,

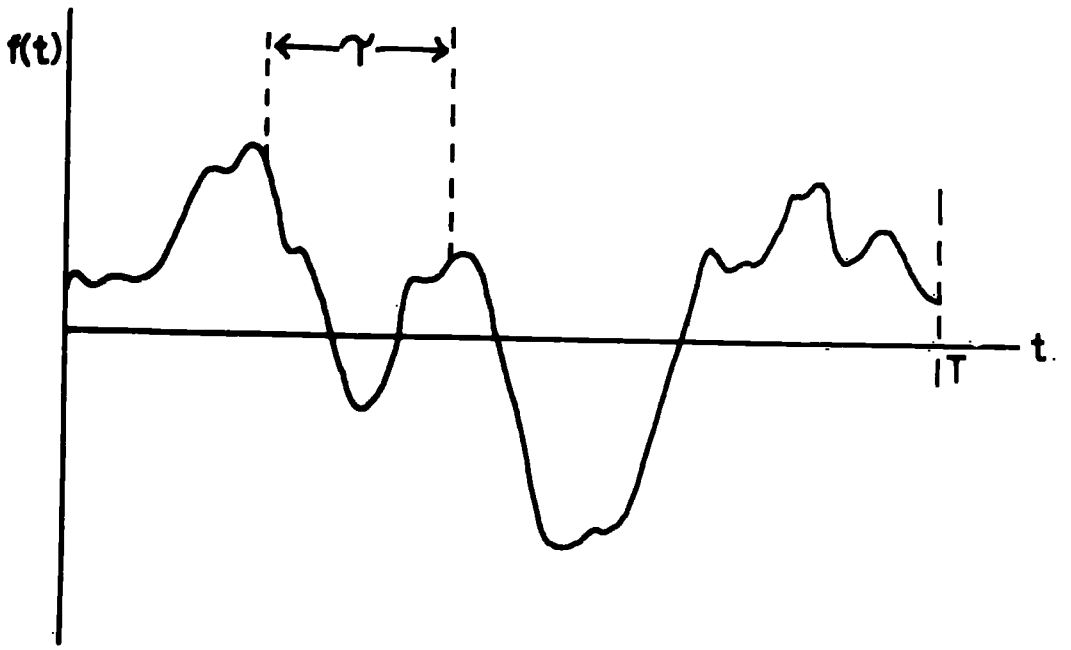

Fig. 6.1 Autocorrelation measurement.

autocorrelation tests have also been used. These tests find the degree of linear correspondence of a time series with itself at a different time, and give a measure of the persistence of the series. Since the results of these analyses rarely give conclusive results, significance tests must be applied to see whether or not the results might have arisen by chance. These will be discussed in greater detail in the following sections.

6.2 The Autocorrelation Tests

The autocorrelation function for random data describes the general dependence of the values of the data at one time upon the values at another time. For data consisting of time series comprising discrete measurements, autocorrelation analysis is usually carried out by comparing all pairs of measurements of a parameter which are separated by a fixed time lag τ in a particular portion of length T of the time series (Fig. 6.1). If we have a time series f(t) whose mean value μ does not vary with time (t), the variance (var) of the time series for the sample length T will be given by

$$\text{var}\,(f(t)) = \frac{1}{T}\sum_{t=0}^{T}(f(t)-\mu)^2 \quad \ldots\ldots (1)$$

An autocovariance function can be defined in a similar manner to the variance, in terms of the sum of the products of the

differences from the mean of values separated by a time τ. Thus the autocovariance A (τ) for a time lag τ averaged over the interval T will be given by

$$A(\tau) = \frac{1}{T}\sum_{t=0}^{T}(f(t) - \mu)(f(t+\tau) - \mu) \quad \ldots (2)$$

If the data is composed of discrete measurements recorded at a sampling interval of t_o, and the sample length T comprises N measurements, then the autocovariance for a lag τ is given by

$$A(\tau) = \frac{1}{N t_o}\sum_{t=0}^{N t_o}(f(t) - \mu)(f(t+\tau) - \mu) \quad \ldots (3)$$

In this case τ will be an integer multiple of t_o.

An autocorrelation coefficient r (τ) can be defined as the ratio of the autocovariance for a lag τ and the variance, so that r (τ) is given by

$$r(\tau) = \frac{A(\tau)}{\text{var}(f(t))} \quad \ldots\ldots (4)$$

From equation (2) it can be seen that

$$A(o) = \frac{1}{T}\sum_{t=0}^{T}(f(t) - \mu)^2 = \text{var}(f(t)) \quad \ldots (5)$$

Thus r(o) for all functions is equal to unity. A plot of r (τ) or A(τ) against τ is known as an autocorrelogram. Some typical autocorrelograms for random and non-random data are shown in Fig. 6.2.

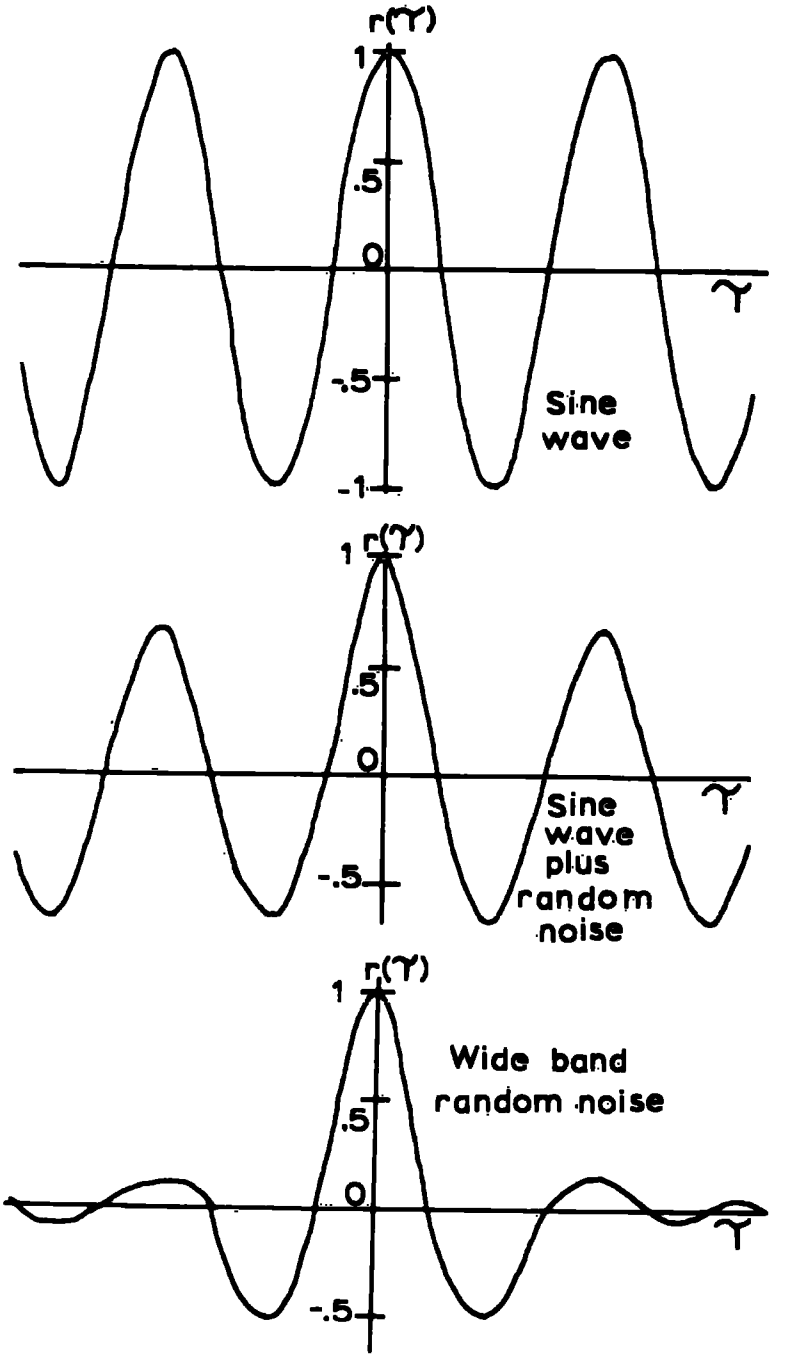

Fig. 6.2 Typical autocorrelograms.

Atmospheric electric parameters occasionally exhibit sinusoidal or quasi-sinusoidal variations with time. When this happens, the data can no longer be regarded as random, but become deterministic, and the normal statistical procedures cannot be used. However, the autocorrelation function of a sinusoid is also sinusoidal, so that an autocorrelogram provides a reliable method of retrieving perhaps hidden sinusoidal variations. As standard procedure, autocorrelograms were plotted for all the time series analysed in order that periodic variations could be identified.

Autocorrelation functions are also used as a measure of persistence of the value of a given parameter. The result of a finite autocorrelation or persistence will be to render observations of an autocorrelated parameter redundant if they are made at too frequent intervals. This also means that subsequent measurements of a parameter will no longer be independent of each other, which will lead to an overestimate of the number of independent observations and consequently to an underestimate of the possible errors. AWE (1964) has shown that an autocorrelation interval L can be defined which represents the time within which members of a series may be considered as being autocorrelated. He has

shown analytically that L is equal to the integral of the squares of the autocorrelation coefficients for all time lags, so that L is given by

$$L = \int_{-\infty}^{\infty} r^2 (\tau)\, d\tau \qquad \ldots\ldots (6)$$

He has also shown that a good estimate of L may be obtained by integrating $r^2 (\tau)$ over only the central maximum of the autocorrelogram. The normal statistical tests can be assumed to be valid for an autocorrelated series, but the effective number of independent observations N is smaller than the actual number of observations n. If the sampling interval of the parameter is t_o, and the length of the time series T, then L, N and n are related as follows:-

$$N = T/L = nt_o/L \qquad \ldots\ldots\ldots (7)$$

The use of N instead of n is particularly important when applying tests of significance, since if $L > t_o$, $N < n$, and the number of independent observations is less than the actual number.

Collin, Groom and Higazi (1965) have shown that the reciprocal of the autocorrelation interval of the conductivity of the air near the ground varies linearly with wind speed. For atmospheric electric parameters it therefore seems that

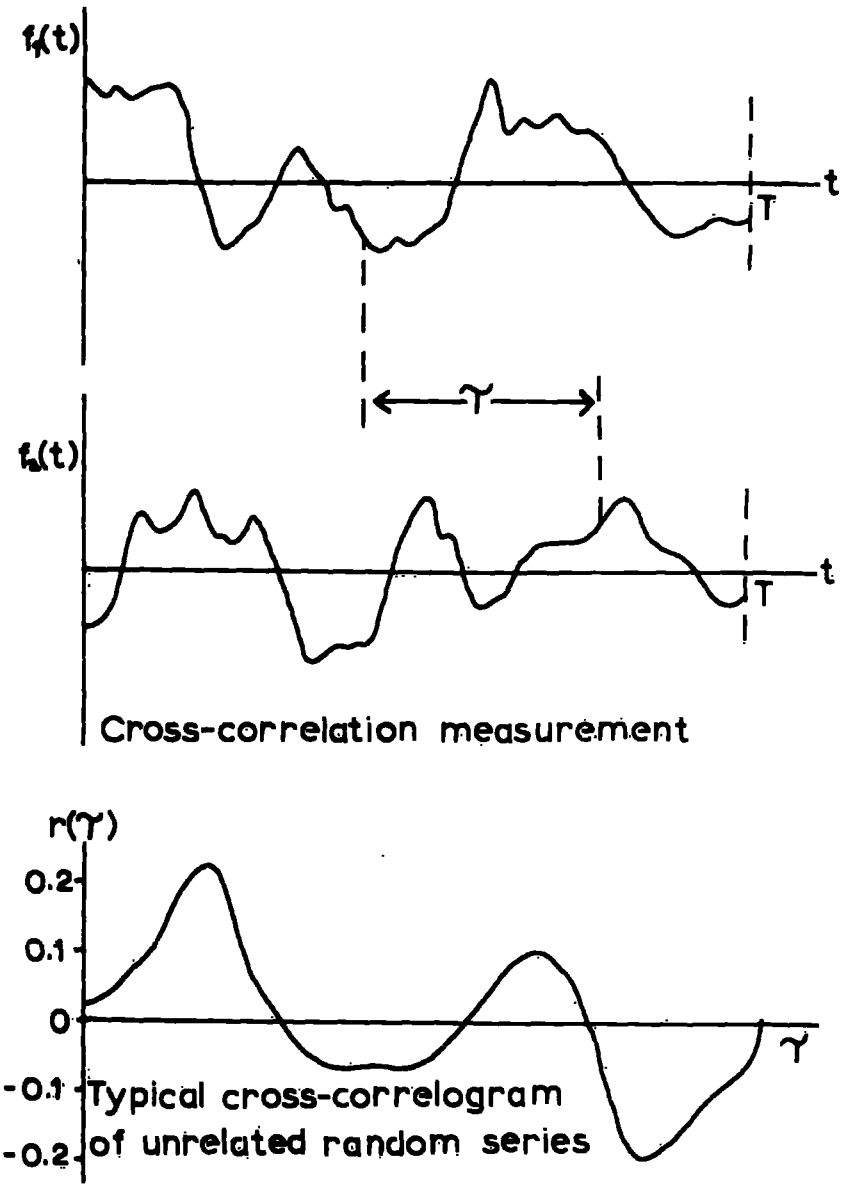

Fig: 6.3 Cross-correlation measurement and correlogram of unrelated series.

the autocorrelation interval is dependent more on wind speed than on electrical effects, mechanical replacement and mixing being relatively more important than electrical relaxation.

6.3 The Cross-Correlation Tests

The cross-correlation function between the random data of two time series is a measure of the interdependence between the two series. More exactly, it is a measure of the linear correlation between the two series. The cross-covariance between two time series is defined in a similar way to the autocovariance of a single series (Fig. 6.3). For two time series $f_1(t)$ and $f_2(t)$, whose respective mean values are μ_1 and μ_2, the cross-covariance $C(\gamma)$ for a time lag γ between the series, averaged over a length T of the series, is given by

$$C(\gamma) = \frac{1}{T} \sum_{t=0}^{T} (f_1(t) - \mu_1)(f_2(t+\gamma) - \mu_2) \quad \ldots\ldots (8)$$

Similarly the cross-correlation coefficient $r(\gamma)$ between the two series for a lag of γ is given by

$$r(\gamma) = \frac{C(\gamma)}{[\mathrm{var}(f_1(t)).\ \mathrm{var}(f_2(t))]^{\frac{1}{2}}} \quad \ldots\ldots (9)$$

The cross-correlation coefficient for series related linearly is

+1 for directly related series, -1 for inversely related series. Totally unrelated series will have a coefficient of zero for all τ. However, random time series which are not infinite in length frequently exhibit cross-correlation coefficients different from zero even when the series are totally unrelated (Fig. 6.3). Different sampling of the cross-correlation coefficient of unrelated series will give rise to different values. The average of these values will be zero, and their distribution about this value will be predictable if the original series are truly random. To assess whether or not a given correlation coefficient obtained from experimental data is meaningful, significance tests must be applied to see if the result could occur by chance out of statistical sampling.

Cross-correlation analysis and the plotting of cross-correlograms are very useful for the comparison at different points in time of a signal subject to random variations. In this case, cross-correlation analyses were carried out between the data of precipitation current density and potential gradient recorded at the Lanehead and Land-Rover stations. Peaks in the cross-correlogram occur at times of maximum linear correlation, and were expected for lags equal to the time of passage of cloud from one recording site to the other.

6.4 Significance Tests

It can be shown that for time series which are not infinite in length, spurious values of correlation coefficients may arise. A non-zero correlation coefficient does not necessarily indicate that there is a real correlation between two series, in fact unrelated random series very rarely give correlation coefficients which are exactly zero. Therefore to obtain some idea of the reliance that it is possible to place upon the values of computed correlation coefficients, tests of significance must be carried out. The result of a significance test will be to indicate the probability of a given value arising by chance out of random data. A correlation coefficient is usually regarded as significant if the probability of it arising by chance from random data is less than 0.05. That is a correlation coefficient of that particular value will on average occur only 5 times out of 100 trials. Thus if the value is significant at the 95% confidence level, it will on average arise on 95 out of 100 occasions other than by chance. Those values which are significant at the 99% confidence level, that is those which would arise accidentally on average only once in 100 trials, are usually considered to be highly significant.

If the random data of the time series are distributed according to the normal distribution, the correlation coefficients calculated in a number of samples of a given series will be similarly distributed.

If the expected distribution of correlation coefficients from unrelated series can thus be assumed, the probability of a value of a coefficient arising by chance can be estimated from the probability distribution by the Student t-test. For a correlation coefficient of r obtained from two time series, each containing N independent pairs of data, a coefficient t is defined by

$$t = \frac{r\sqrt{N-2}}{\sqrt{1-r^2}}$$

Computed statistical tables are available giving the values of t corresponding to different values of r which might arise from uncorrelated data at various levels of significance

6.5 The Processing and Analysis of Data

The recorded parameters at the Lanehead field station were obtained in the form of a series of three-digit numbers punched on five-hole paper tape. Before the data were analysed, a print-out of the tapes was obtained by means of a Creed line printer. The recording system output unit also punches spaces and carriage control characters for the line printer so that each data set is tabulated in columns. A visual check of the data was then carried out in order to find any errors that had arisen from incorrect punching of the tape or other malfunction. Errors, mainly due to

occasional mis-punching of the tape punch, were often found. These were remedied either by removing the portion of tape containing the error and splicing in a fresh piece, or by duplicating the whole of the data tape using the Creed printer and correcting the mistakes manually by use of the keyboard.

The readings obtained at the Land-Rover mobile station recorded on magnetic tape were later converted onto paper tape by using the automatic recording system output unit located at Lanehead. Each Land-Rover station record consisted of a number of magnetic tapes, and these were converted to an equal number of paper tapes. All of the paper tapes from a particular recording period were joined together, after the errors had been removed, to form a single continuous paper tape. The data that had been lost during changing of magnetic tapes whilst recording was inserted by hand, the values having been interpolated linearly. The time lost due to changing tapes usually amounted to less than 1% of the length of the record, so that interpolation did not introduce any serious errors, whilst maintaining continuity.

The paper tapes were then fed into the paper tape reader at the computer terminal in Durham and the recorded data transferred onto a magnetic disc storage unit of the N.U.M.A.C. I.B.M. 360 digital electronic computer situated at Newcastle-upon-Tyne. Although it

would have been quite simple using the computer to convert the raw data from the three-digit numbers into actual values of the measured parameters, it was decided to carry out all of the statistical tests on the raw data. Since all of the calibration curves of the recording equipment were almost exactly linear, the raw data were perfectly representative of the actual parameters. Programs were written in Fortran IV language to compute the arithmetic means, the standard deviations, the autocorrelation coefficients for various time lags, and the autocorrelation interval for the time series of each parameter. Since all of the records obtained at Lanehead were longer than those obtained at the Land-Rover, the corresponding periods were selected from the Lanehead records and analysed, in addition to the whole of the Lanehead records. Cross-correlation analysis was first carried out between precipitation current and potential gradient recorded at the two sites for various time lags, using time series covering the same period at each site. The time of maximum correlation was found by inspection of the results, and further cross-correlation analyses carried out with one time series shifted so as to give maximum cross-correlation for zero time lag. This was done because with records of finite length, errors may occur when correlation analyses are carried out with time lags in excess of about 15% of the record length. Theoretically, we might expect that the two records obtained by such shifting represent independent measurements of the same portions of cloud at different intervals in

time. The average values of the parameters at the two stations for these equivalent periods were compared, as were the standard deviations and the autocorrelation intervals. The average values of the raw data were converted into actual values of the parameter by reference to the calibration curves.

In addition to the computation of statistical data, the computer was also used to provide a visual indication of the time series. A program was written which produced a simulated chart record for the parameters recorded at the two stations for comparable periods in time. Although chart records were made at Lanehead, none were available for the Land-Rover data. It often happens that visual inspection of records gives rise to information not obvious from the numerical data. The two simulated charts could be laid side by side and visual correlations carried out. In some cases the time lag for maximum correlation could be determined by eye, and the number of computations was thus reduced.

As well as the comparisons between the data simultaneously recorded at the two stations, single station data were analysed in greater detail. The Land-Rover sites, nearly all of which were very exposed, made dependence of the parameters with wind speed more apparent, and comparisons were carried out to determine any effects of wind. Also, the data from Lanehead were analysed in greater detail. Some of the records were very long, and most covered all

of the significantly charged precipitation that fell during the period concerned. With these long records, short-term variations were eliminated by taking 5-minute averages of all of the parameters. It was thought that this smoothing would tend to minimize local effects and effects due to mechanical separation of the cloud and its precipitation. Cross-correlation analyses were carried out on the smoothed data between potential gradient and precipitation current density, potential gradient and space charge density, and precipitation current density and space charge density. Comparisons of parameters with rainfall rate were made in a limited number of cases, and the variation of autocorrelation interval with wind speed was studied.

Chapter 7

THE ANALYSIS OF THE TWO-STATION OBSERVATIONS

7.1 Introduction

The preliminary trials with the precipitation current measuring equipment and displacement current compensation systems at Durham University Observatory took place from September 1966 to May 1967, after which the apparatus was transferred to Lanehead. This apparatus and the Lanehead field installations were completed by July 1968, with the exception of the shielded collector which was installed three months later. The automatic recording system was installed in the school by Mr. Aspinall during the summer of 1968, although electronic interface problems prevented its use with the rain collector amplifiers until December 1968 when the modifications were carried out. The Land-Rover, which was made available for this project in October 1967, had to be completely re-equipped. The rain collectors, field mill, the associated electronics and controls were installed in their final form by November 1968, and the automatic recording unit was brought into operation in early January 1969. In early February 1969, the Land-Rover exposed-collector's Rank amplifier was put out of action by the failure of its electrometer valve, and in March the shielded collector amplifier failed when a switch assembly broke. Since it was considered more important for the project to obtain

good time-resolution precipitation current records, the exposed-collector amplifier from Lanehead was transferred to the Land-Rover for use with the shielded collector. The number of parameters recorded at each station was then reduced to four, giving a sampling interval for each parameter of 12s.

From the beginning of January 1969 to the end of July it had been hoped to record on every possible occasion of quiet precipitation. However, the weather conditions throughout the whole period were far from satisfactory. On several occasions snowfalls blocked the moorland roads around Lanehead, rendering operation of the mobile station impossible. One such period lasted from early March to mid-April, cut off Lanehead itself for several days, and rendered all equipment inoperative for several weeks. Even when the roads had been cleared, a strong or gale force easterly wind prevailed for many weeks. In conditions of snow, blowing snow near the ground produced strong electrical effects, masking any effects attributable to the cloud. In addition to these adverse conditions the period was, as a whole, fairly dry, and nimbostratus conditions were relatively rare.

During the three-month period from mid-January to mid-April, two-station observations were only made on two occasions. Between mid-April and the end of June, a further seven two-station results were obtained, giving a total of 16 hours of simultaneous

records in quiet precipitation. On three of the nine occasions the observations had to be rejected, two because of instrumental failures at Lanehead which were discovered only on analysis of the data, and one because of a large wind shift during the recording period. Of the remaining six records, four comprised simultaneous records of both potential gradient and precipitation current density, one comprised a simultaneous record of potential gradient only, and the other, precipitation current density only. In addition a simultaneous record was obtained on a further occasion with the Land-Rover situated at Lanehead, 10 metres from the field equipment there.

7.2 Comparison between the fixed and mobile stations

Before analysing the simultaneous records obtained with large horizontal separations between the stations, it will be profitable to consider whether or not the two stations measure the same parameters reasonably accurately. This can be assessed from the simultaneous record obtained with the mobile station operated at Lanehead alongside the fixed apparatus.

The period comprising the comparison run is a 33 minute period commencing just before 22.00 G.M.T. on 2nd June 1969. Heavy continuous rain had been falling for nine hours at that time, and a 4-hour simultaneous two-station record had been made. The Land-Rover was positioned 10 metres upwind of the

Lanehead equipment, the wind speed being about 1 ms^{-1}. The variations of precipitation current density and potential gradient during part of the period as indicated by the two stations are shown in Fig. 7.1. These curves have been plotted by hand from the numerical data. As can be seen, general agreement between the two sets of instruments is good, although there are differences in detail. The average values over the whole period, the standard deviations and autocorrelation intervals are given in Table 7.1. The average values are in excellent agreement, although the standard deviations and autocorrelation intervals do exhibit some differences. The cross-correlation coefficient between the precipitation current density records is 0.87, which is significant at the 99% level, and the correlation coefficient between the potential gradient records is 0.98, which is significant at a level higher than the 99.9% level. The autocorrelograms of the four parameters are given in Fig. 7.2. The general shape of the autocorrelograms of precipitation current density and potential gradient is the same for the two stations, although the Land-Rover parameters display a faster decline, which is reflected in the lower autocorrelation intervals. The cross-correlograms are shown in Fig. 7.3. The large width of the cross-correlograms is due to the persistence of the correlated parameters, and this is borne out by the fact

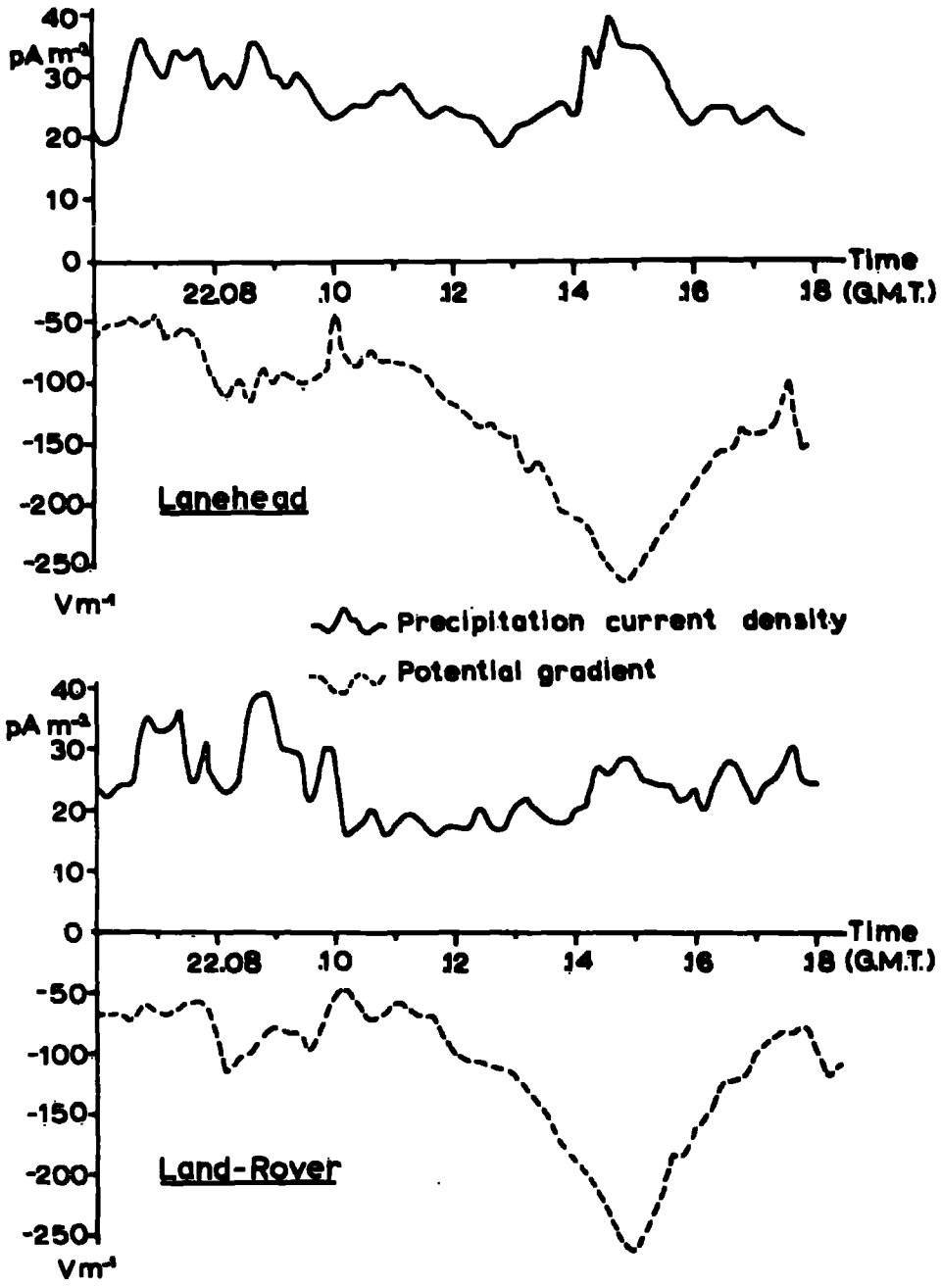

Fig. 7.1 Simultaneous two-station comparison record, 2nd June 1969.

TABLE 7.1

SIMULTANEOUS TWO-STATION RECORD 2ND JUNE 1969

	POTENTIAL GRADIENT (Vm^{-1})		PRECIPITATION CURRENT DENSITY (pAm^{-2})	
	Lanehead	Land-Rover	Lanehead	Land-Rover
AVERAGE	-108	-104	17.5	18.0
STANDARD DEVIATION	52	68	22	31
AUTOCORRELATION INTERVAL (s)	212	147	286	180

Time of simultaneous record	21.52 to 22.25 G.M.T.
Wind Speed	1.2 ms^{-1}
Air Temperature	9°C
Horizontal separation of sites	10m
Maximum precipitation current cross-correlation	0.87
Time lag for maximum correlation	0($\pm$ 6s)

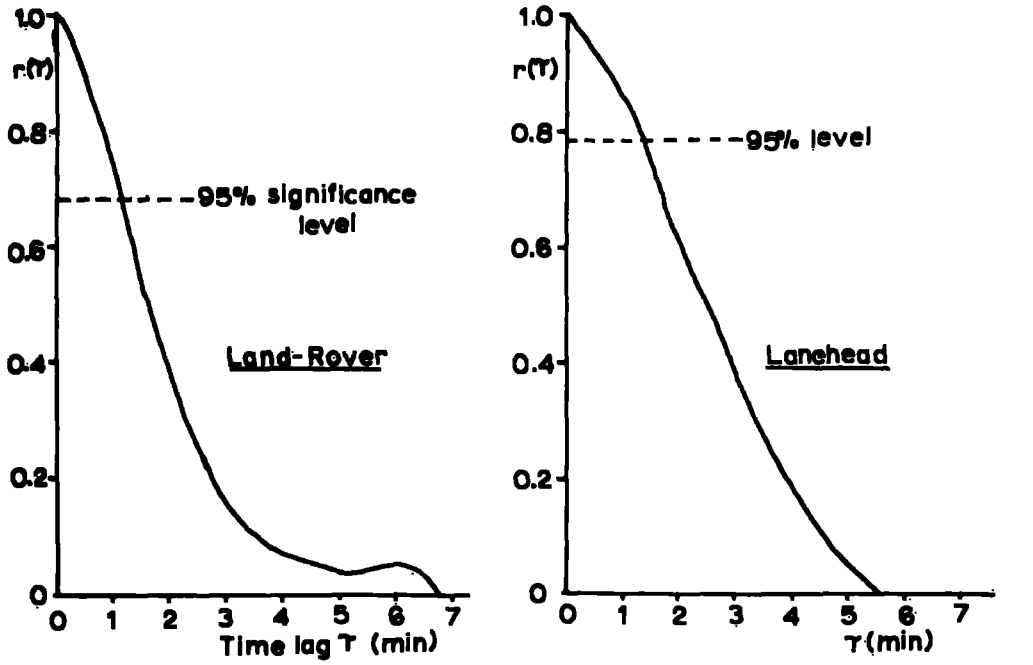

Potential gradient autocorrelograms

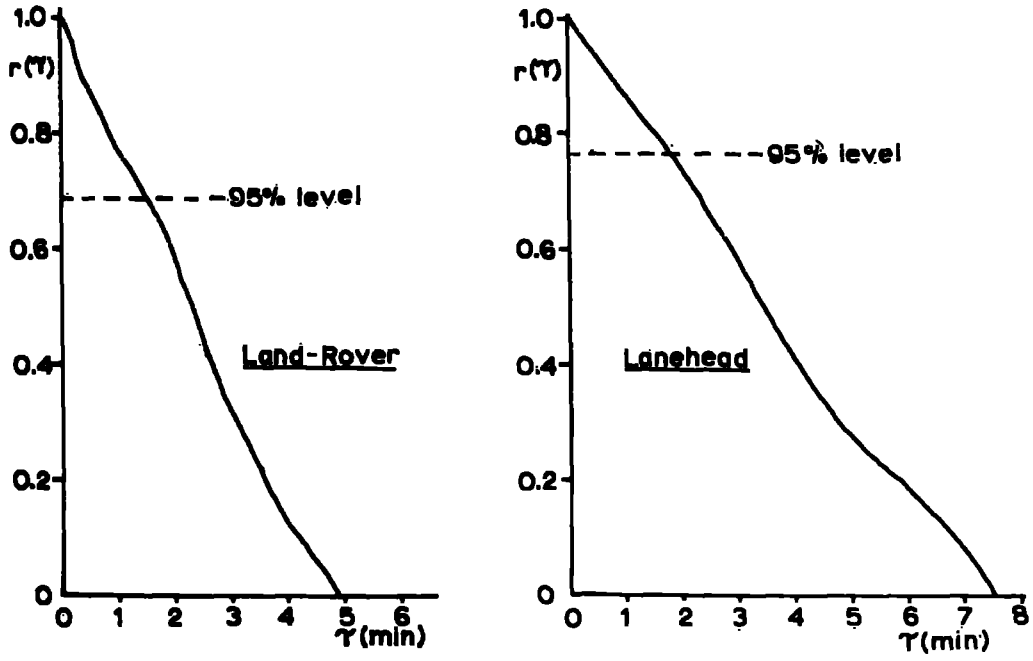

Precipitation current autocorrelograms

Fig. 7.2 Autocorrelograms of 2nd June comparison records.

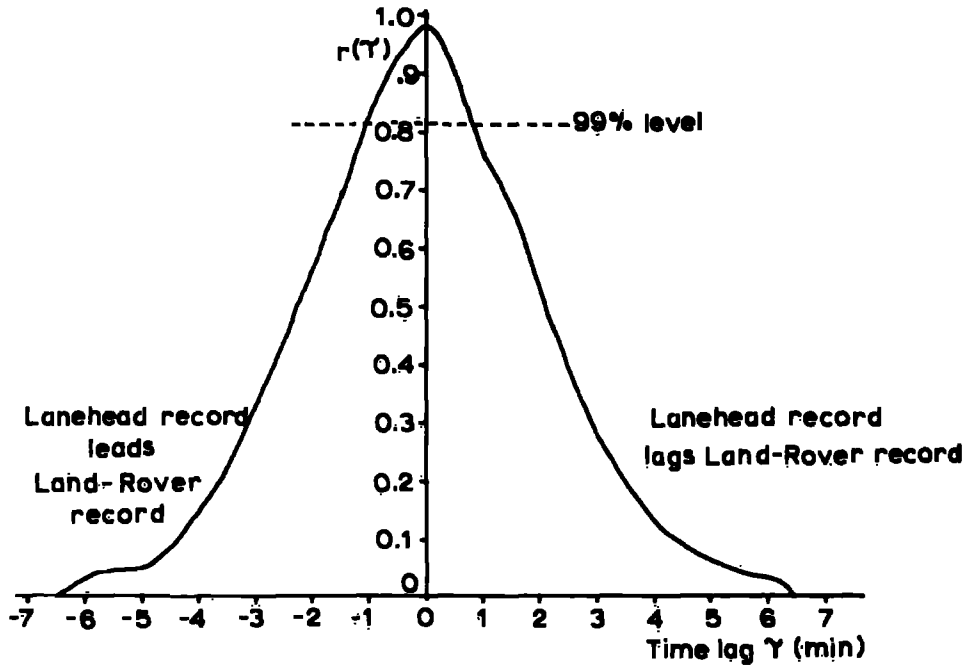

Potential gradient cross-correlogram

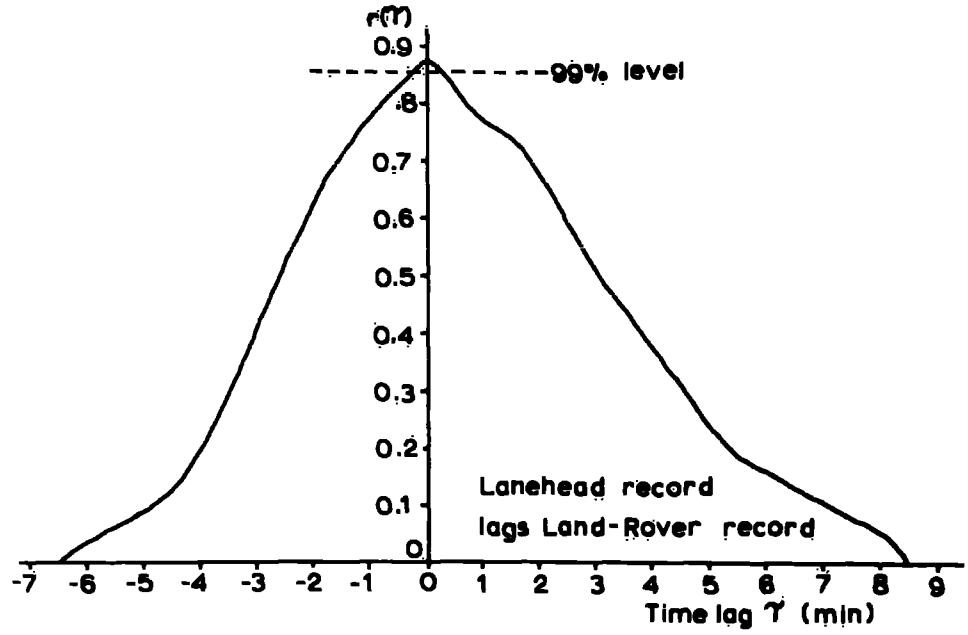

Precipitation current cross-correlogram

Fig. 7.3 Cross-correlograms of 2nd June comparison records.

the width of the cross-correlogram is almost identical to twice the width of the corresponding autocorrelogram. The lower cross-correlation for precipitation current than potential gradient is understandable. Each rain collector collects a different sample of rain, and we assume that it will be representative of the rain falling in a larger area. However, the field mills effectively 'see' the same charges, and a greater correspondence is to be expected.

The greater variance of the parameters recorded at the Land-Rover station may be a result of the different height above the ground of the apparatus. The shielded collector is at a height of 2m compared with ground level and the field mill $1\frac{1}{2}$ m compared with 1m. The extra height of the Land-Rover rain collector will introduce larger errors due to wind, and drop-splashing from the shield rim may be more important because of its greater exposure factor. Nevertheless the correspondence between the two stations is good, and the experimental error seems to be much lower than had originally been anticipated.

7.3 The Two-Station Records

A brief description of the meteorological conditions prevailing during each of the recording periods will be given, followed by a description of the records obtained at the two stations. The average values of the parameters, the standard

deviations, autocorrelation intervals, the autocorrelograms and cross-correlograms will be given, together with a brief description. The two-station results as a whole will be discussed in Section 7.4.

RECORD 1 12th February 1969

A depression situated over the North Sea produced strong easterly winds over much of the British Isles. There were periods of snow or snow showers in many districts. At Lanehead, moderate snow began falling from total cloud cover at about 05.00 G.M.T. and continued until about 13.00 when breaks in the cloud developed and a more showery activity was apparent.

After some faults had been cleared, the Lanehead equipment commenced automatic recording at 09.22. Cloud direction was obtained, and the cloud speed estimated. The Land-Rover was taken to a recording site near Rookhope village, 7.95 km upwind at an altitude of 350m (1150 ft). A power cable fault rendered the field mill and automatic recording system inoperative, so that recording of precipitation current density and wind speed was carried out by hand. Readings were noted every 12 seconds for a continuous period of 67 minutes, at which point the snow ceased temporarily and the record was terminated.

The results of the record and a summary of the prevailing conditions are given in Table 7.2. It can be seen that the Land-Rover collector gave a smaller average current over the

TABLE 7.2

SIMULTANEOUS TWO-STATION RECORD

12th February 1969

	PRECIPITATION CURRENT DENSITY (pAm^{-2})	
	Lanehead	Land-Rover
AVERAGE	-15.2	-10.1
STANDARD DEVIATION	27	14
AUTOCORRELATION INTERVAL(s)	117	121
EFFECTIVE NUMBER OF INDEPENDENT OBSERVATIONS	35	34

Time of simultaneous record		11.34 to 12.41 G.M.T.
Wind Speed	Lanehead	2.5 ms^{-1}
	Land-Rover	7.2 ms^{-1}
Air Temperature		$-2^{\circ}C$
Cloud Direction		85°
Cloud Speed		10ms^{-1}
Horizontal separation of sites		7.95 km
Vertical Separation of sites		98 m
Maximum current cross-correlation		0.69
Time lag for maximum correlation		11.5 min
Cloud speed from maximum correlation		11.5 ms^{-1}

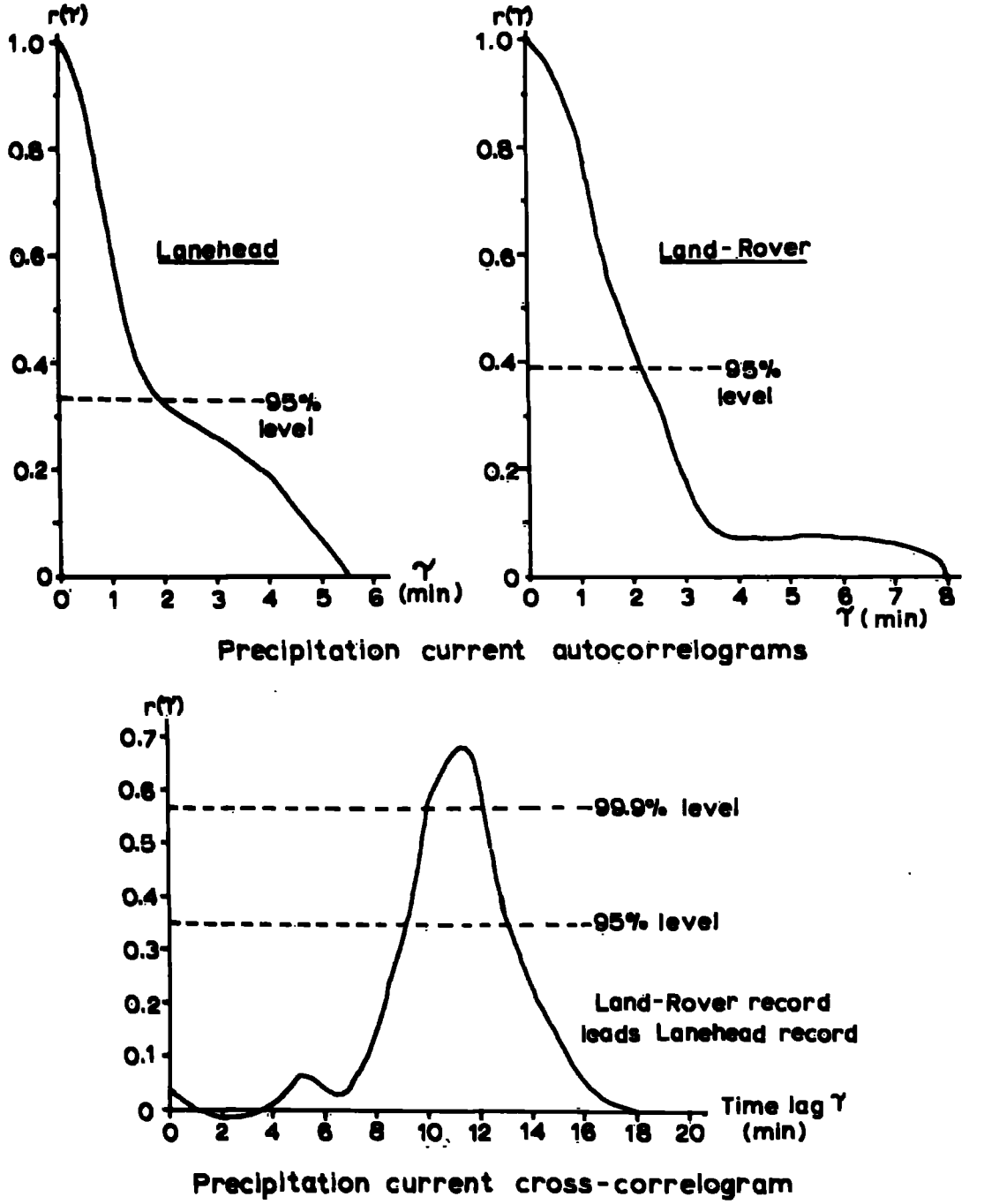

Fig. 7.4 Autocorrelograms and cross-correlogram of 12th February records.

period despite the good correlation between the records at the two sites. The autocorrelograms and cross-correlogram of precipitation current density are shown in Fig. 7.4. The autocorrelograms are basically similar and there is no significant departure from the autocorrelogram of random data in either case. The cross-correlogram reaches a relatively sharp peak of 0.69 for a lag of 11½ minutes of the Lanehead record upon the Land-Rover record. This corresponds to a cloud speed of 11.5 ms^{-1}. The 99.9% significance level is 0.57 and so the peak value is very highly significant. The width of the cross-correlogram peak at the 95% significance level is similar to the width of the autocorrelograms and we therefore conclude that the spread about the peak is a consequence of the persistence of precipitation current.

RECORD 2 14th April 1969

A warm-frontal system associated with a depression over Iceland moved eastwards throughout the 14th April producing periods of light or moderate rain over the British Isles. At Lanehead the rain became continuous and steady about midday and continued until about 18.30 G.M.T.

The Lanehead equipment recorded from 12.20 to 18.30 G.M.T. The Land-Rover was stationed downwind at a horizontal separation of 5.75 km at an altitude of 440m (1450 ft.). The Land-Rover record began at 15.20 and continued until 16.23 when the electric generator failed. Throughout the whole recording period the wind

was strong and gusty at both recording sites, although Lanehead was a little more sheltered. The records for comparable periods are summarised in Table 7.3. A part of the records obtained is shown in Fig. 7.5, the diagram having been taken from the computer - simulated chart. The similarities and differences can be seen from this section. The autocorrelograms and cross-correlograms for precipitation current and potential gradient are shown in Figs. 7.6 and 7.7. The autocorrelograms have the same general shape, but those of the Land-Rover parameters slope more steeply suggesting a lesser persistence. The current cross-correlogram reaches a peak value of 0.64 for a lag of 9 minutes of the Land-Rover upon the Lanehead record, which corresponds to a cloud speed of 10.8 ms^{-1}. The 99.9% significance level is 0.56, so that the result is very highly significant. A statistically significant correlation exists from -2 minutes up to 15 minutes lag. There is no significant correlation between the potential gradient records.

The Land-Rover station results gave markedly different values from the Lanehead station. The average precipitation current density was nearly four times as large, and the potential gradient nearly double. The standard deviations of potential gradient are not significantly different, although the autocorrelation intervals differ. The standard deviation of precipitation current density is higher at the Land-Rover and the autocorrelation interval shorter.

TABLE 7.3

SIMULTANEOUS TWO-STATION RECORD

14th April 1969

	POTENTIAL GRADIENT (Vm^{-1})		PRECIPITATION CURRENT DENSITY (pAm^{-2})	
	Lanehead	Land-Rover	Lanehead	Land-Rover
AVERAGE	-605	-1007	9.0	34.5
STANDARD DEVIATION	225	235	6	15
AUTOCORRELATION INTERVAL(s)	577	104	385	134
EFFECTIVE NUMBER OF INDEPENDENT OBSERVATIONS	7	36	10	28

Time of simultaneous record	15.20 to 16.23 G.M.T.
Wind Speed	Lanehead 6.0 ms^{-1}
	Land-Rover 8.1 ms^{-1}
Air Temperature	$5^{\circ}C$
Cloud Speed	12 ms^{-1}
Cloud Direction	244°
Horizontal separation of sites	5.75 km
Vertical separation of sites	0
Maximum precipitation current cross-correlation	0.64
Time lag for maximum correlation	9.0 min
Cloud Speed from maximum correlation	10.8 ms^{-1}

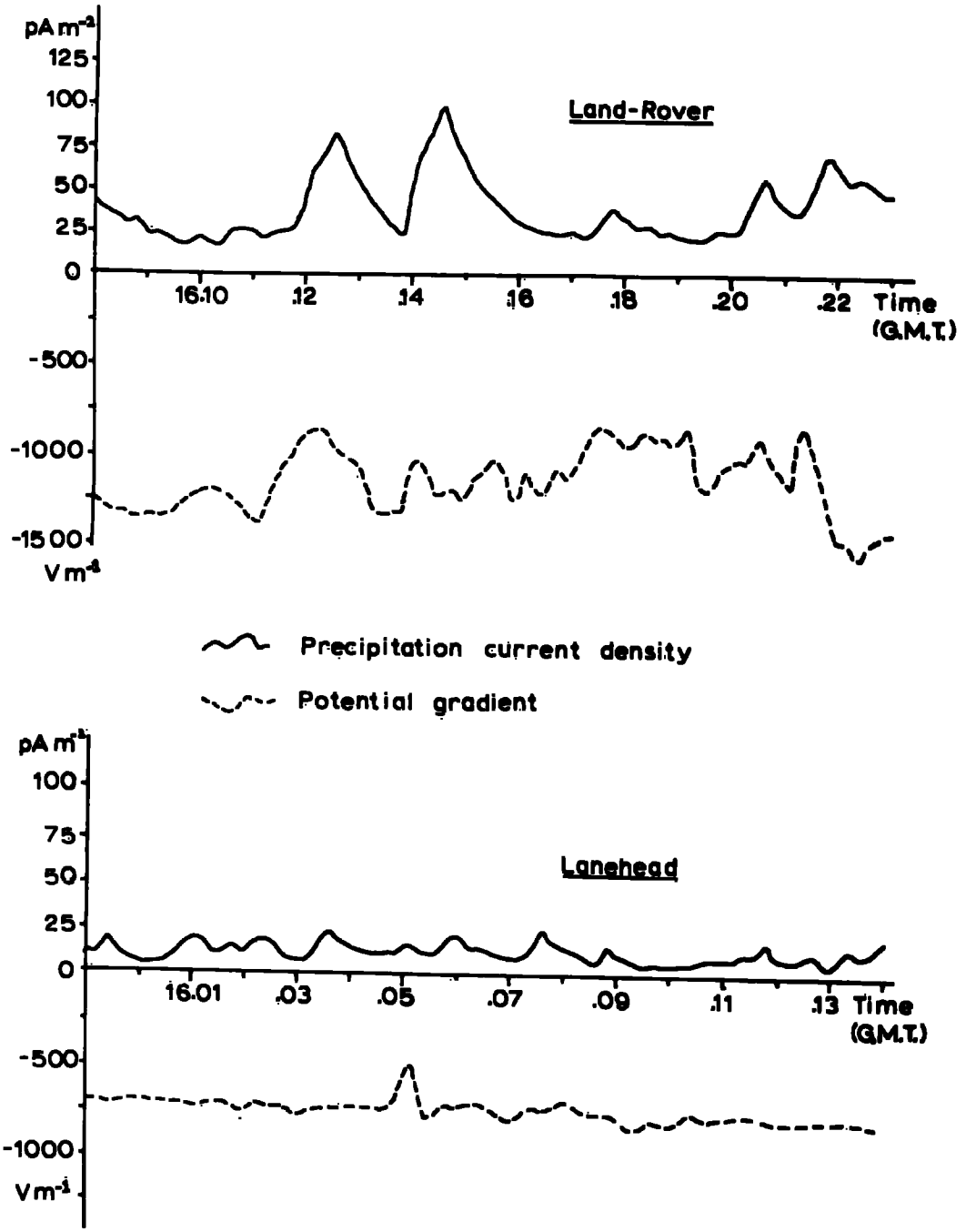

Fig. 7.5 Comparable sections of 14th April two-station records.

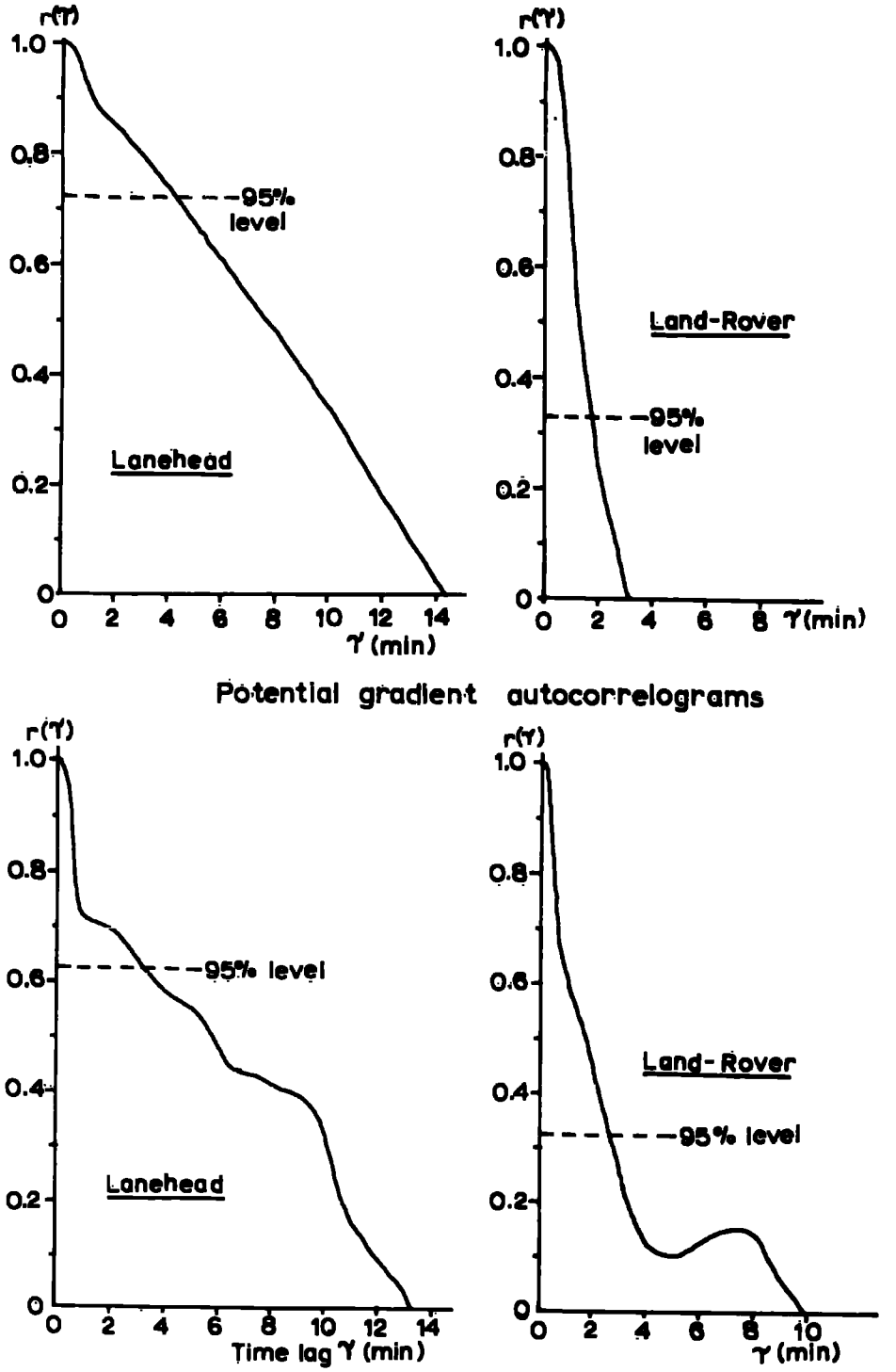

Fig. 7.6 Autocorrelograms of 14th April records.

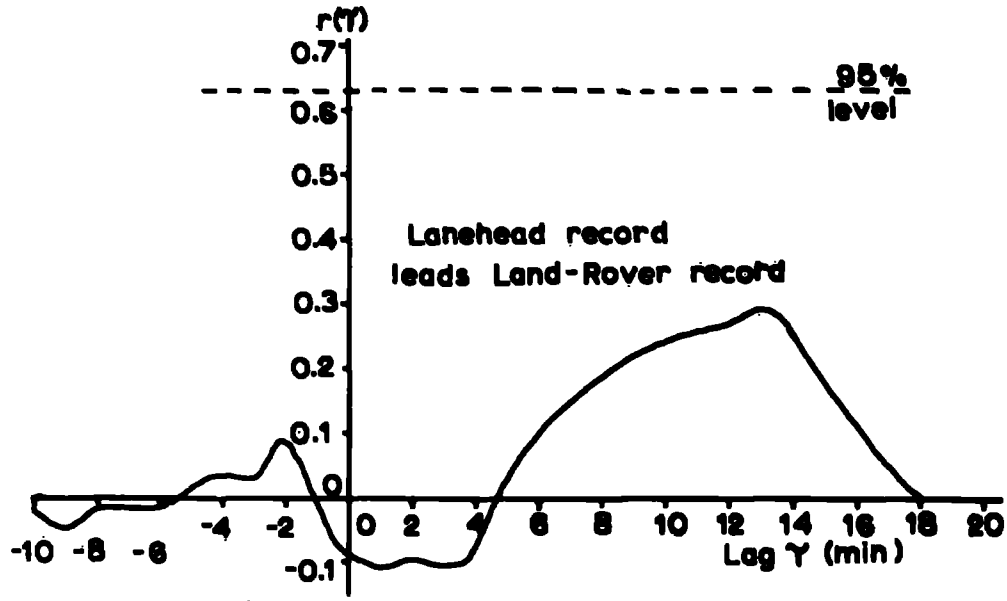

Potential gradient cross-correlogram

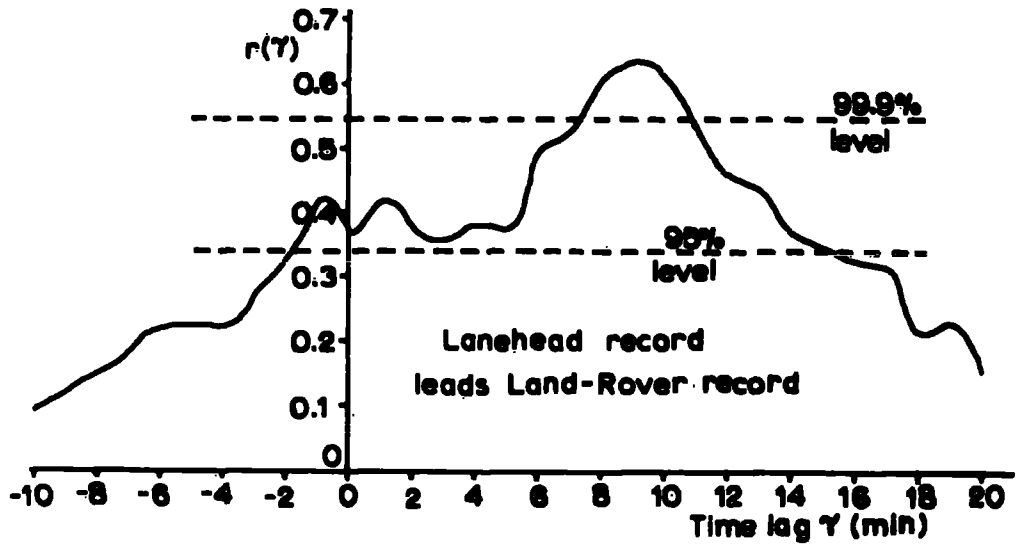

Precipitation current cross-correlogram

Fig. 7.7 Cross-correlograms of 14th April records.

TABLE 7.4

SIMULTANEOUS TWO-STATION RECORD

6th May 1969

	POTENTIAL GRADIENT (Vm^{-1})		PRECIPITATION CURRENT DENSITY (pAm^{-2})	
	Lanehead	Land-Rover	Lanehead	Land-Rover
AVERAGE	-138	-746	15.4	37.1
STANDARD DEVIATION	55	410	13.6	34.2
AUTOCORRELATION INTERVAL(s)	747	181	549	225
EFFECTIVE NUMBER OF INDEPENDENT OBSERVATIONS	8	32	11	26

Time of simultaneous record			14.45 to 16.22 G.M.T.
Wind Speed	Lanehead 2ms^{-1}	Land-Rover	3.4 ms^{-1}
Air Temperature			4°C
Cloud Speed			-
Cloud Direction			70°
Horizontal separation of sites			6.0 km
Vertical separation of sites			15m
Maximum precipitation current cross-correlation			0.64
Time lag for maximum current cross-correlation			29.2 min
Cloud speed from maximum correlation			3.4 ms^{-1}

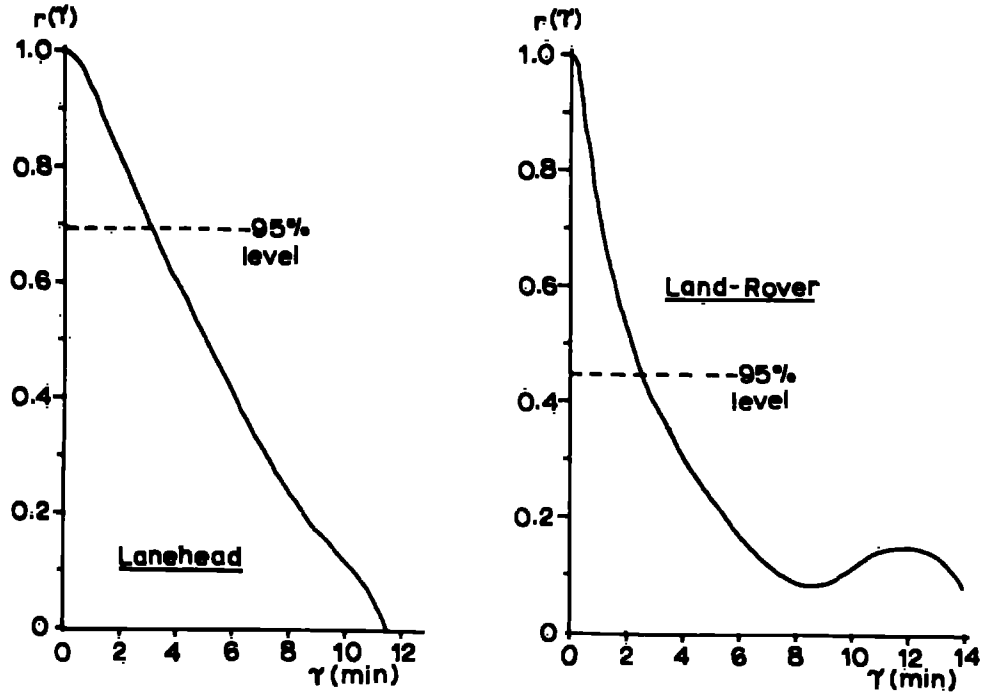

Potential gradient autocorrelograms

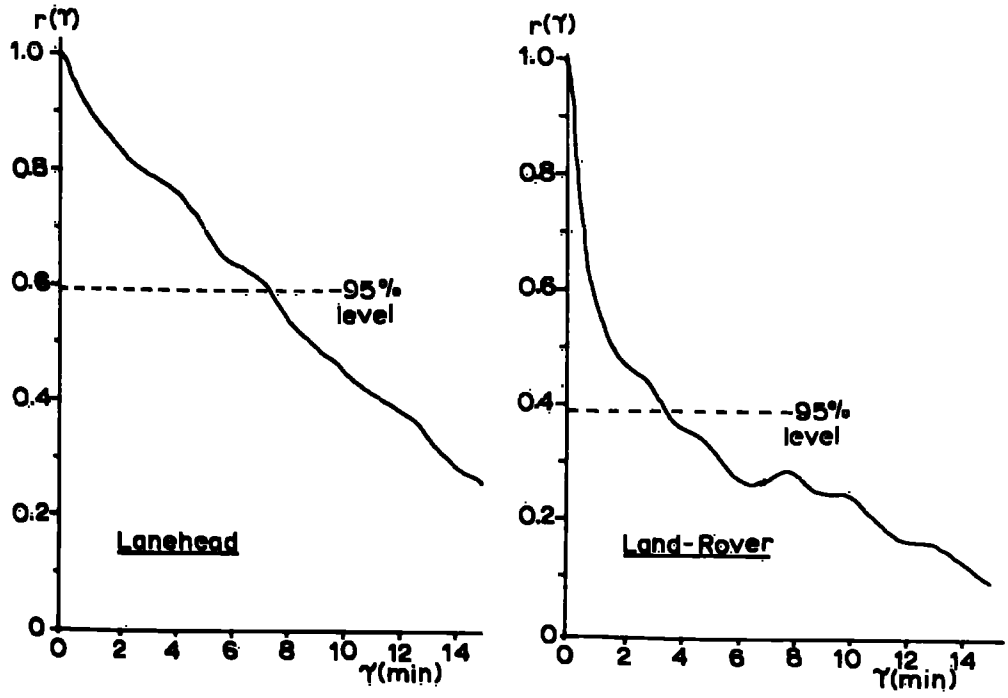

Precipitation current autocorrelograms

Fig. 7.8 Autocorrelograms of 6th May records.

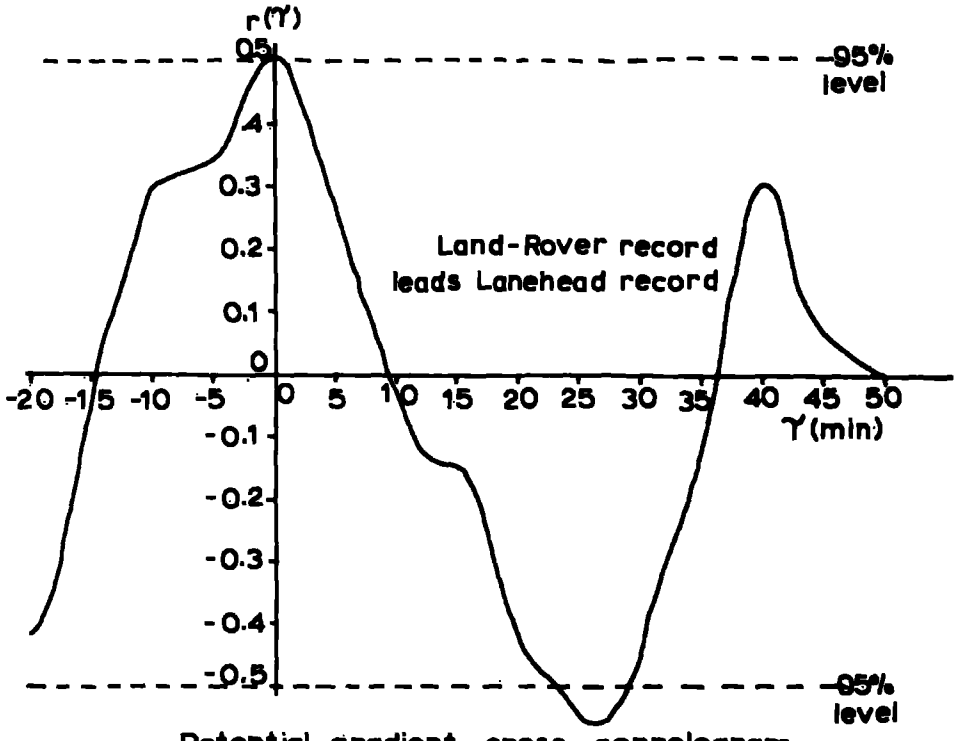

Potential gradient cross-correlogram

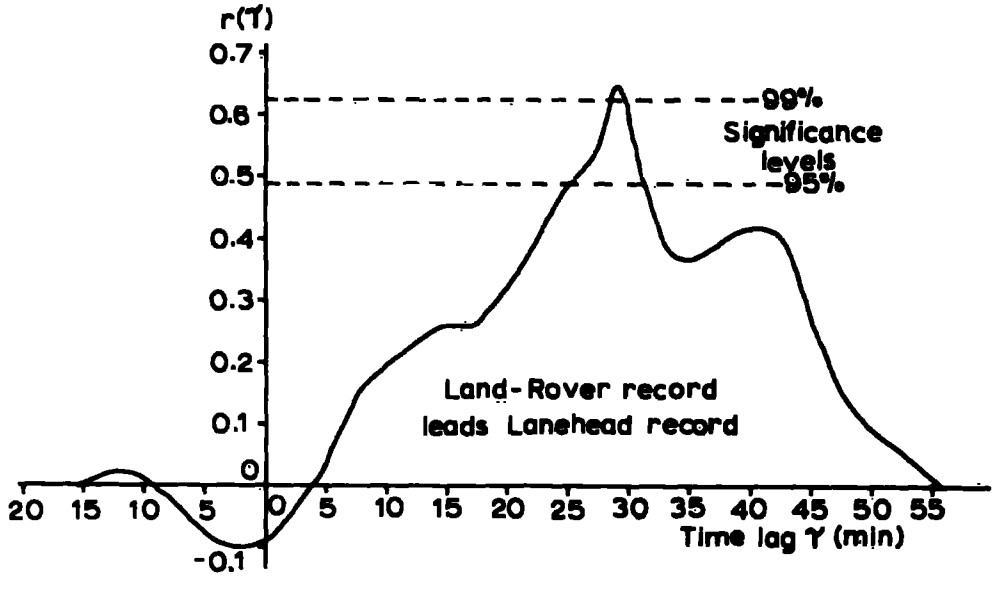

Precipitation current cross-correlogram

Fig. 7.9 Cross-correlograms of 6th May records.

RECORD 3 6th May 1969

A complex area of low pressure extending from Southern Italy across Germany and the British Isles, together with a northwards moving trough gave rise to rain over much of the British Isles. At Lanehead, continuous rain commenced about noon and by 13.00 was moderate. The automatic recording system was started at 13.15 G.M.T. and a continuous record obtained till 16.52. The Land-Rover was taken to a position 6.0 km upwind at an altitude of 425 m (1400 ft). A record was obtained from 14.45 to 16.22, at which time the rain began to ease. The wind speed was light throughout the record at both of the recording sites. A summary of the two equivalent records is given in Table 7.4.

The Land-Rover station gave higher values of precipitation current density and potential gradient, and these parameters also showed a much greater variance as displayed by the higher standard deviations and lower autocorrelation intervals. Despite this, the maximum cross-correlation coefficient between the potential gradient records was 0.5, and between the precipitation current density records 0.64. The autocorrelograms of the parameters are shown in Fig. 7.8. Generally the shapes are similar and correspond to random data, although the slopes of the mobile station parameter curves are steeper, showing a lesser persistence. The cross-correlograms are shown in Fig. 7.9. The precipitation current correlogram displays a very broad maximum,

but with a fairly well-defined peak for a lag of 29 min. of the Lanehead upon the Land-Rover record. The peak value is significant at the 99% level. The potential gradient records exhibit a cross-correlation coefficient of 0.5 for zero lag, which is significant at the 99% level, and a correlation coefficient of -0.55 for a lag of 27 minutes. The simultaneous correlation of 0.5 probably means that the two field mills were under the influence of the same charges at the same time, which is quite feasible for charges at cloud height.

RECORD 4 2nd June, 1969

A slowly moving frontal system approached the British Isles from the West during the 2nd June, the system comprising a warm front to the South, an occluded front to the north, with the point of occlusion situated around the Scottish border. After midnight and during 3rd June, the front became stationary before moving south-west. Rain fell in most regions throughout the 2nd and the morning of the 3rd. At Lanehead a long period of drizzle turned into continuous rain about 01.00, but this ceased briefly about 15.00. From 15.15 on 2nd June until 01.15 on 3rd June there was moderate or heavy continuous rain.

The Land-Rover mobile station was positioned downwind of Lanehead at a horizontal separation of 5.2 km and at an altitude of 475m (1550 ft). A continuous record was obtained at this point from 16.25 to 20.23 G.M.T. The wind speed was very low during the whole record at both stations. A comparable section of each record from

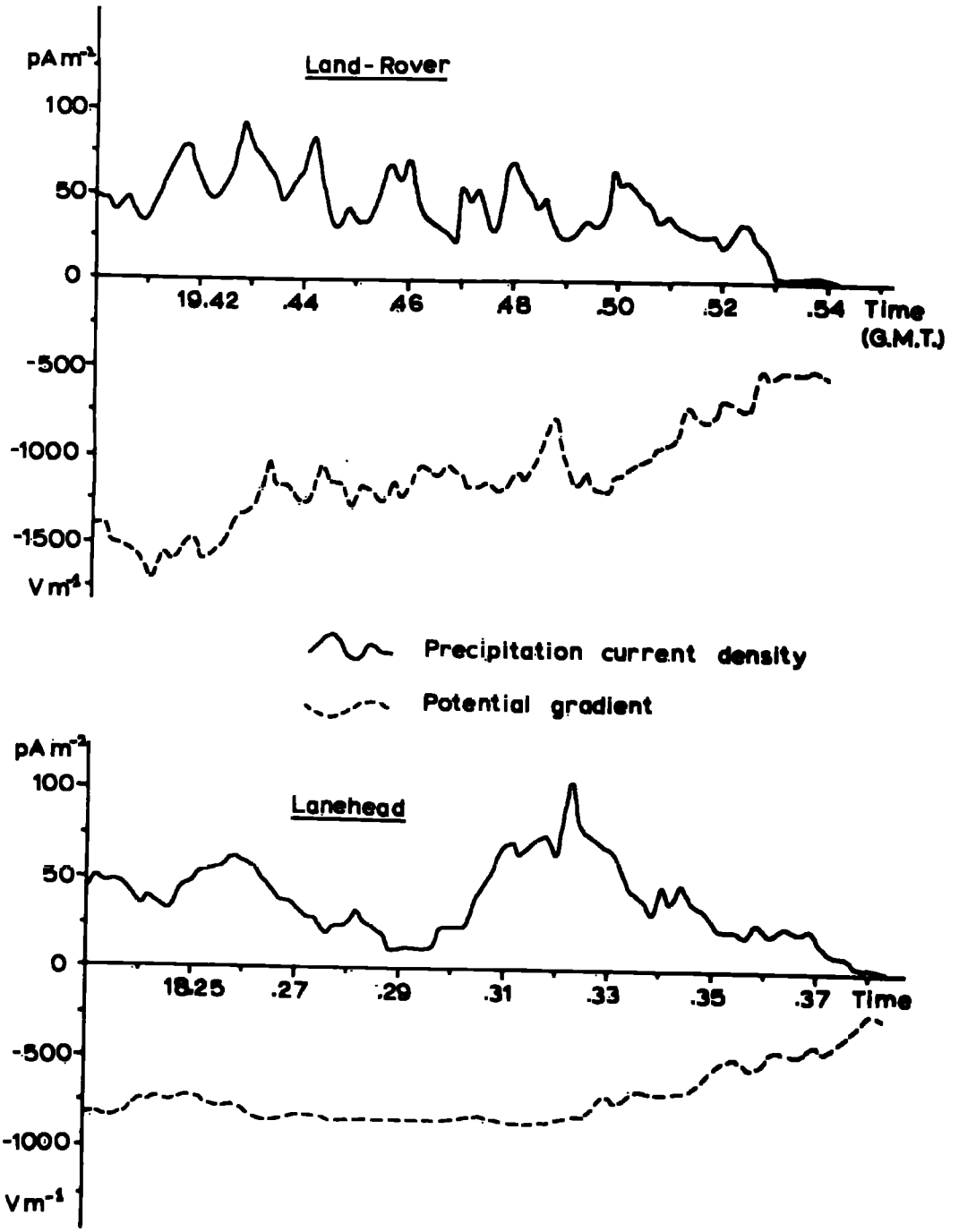

Fig. 7.10 Comparable sections of 2nd June two-station records.

TABLE 7.5

SIMULTANEOUS TWO-STATION RECORD

2nd June 1969

	POTENTIAL GRADIENT (Vm^{-1})		PRECIPITATION CURRENT DENSITY(pAm^{-2})	
	Lanehead	Land-Rover	Lanehead	Land-Rover
AVERAGE	-99	-235	6.3	6.1
STANDARD DEVIATION	245	430	13.6	20.8
AUTOCORRELATION INTERVAL(s)	968	596	626	327
EFFECTIVE NUMBER OF INDEPENDENT OBSERVATIONS	15	24	23	44

Time of simultaneous record	16.25 to 20.23 G.M.T.
Wind Speed	Lanehead - , Land-Rover 1.4 ms^{-1}
Air Temperature	$10^{o}C$
Cloud Speed	4 ms^{-1}
Cloud Direction	240^{o}
Horizontal Separation of Sites	5.2 km
Vertical separation of sites	35 m
Maximum precipitation current cross-correlation	0.50
Time lag for maximum current cross-correlation	77 min
Cloud speed from maximum correlation	1.1 ms^{-1}

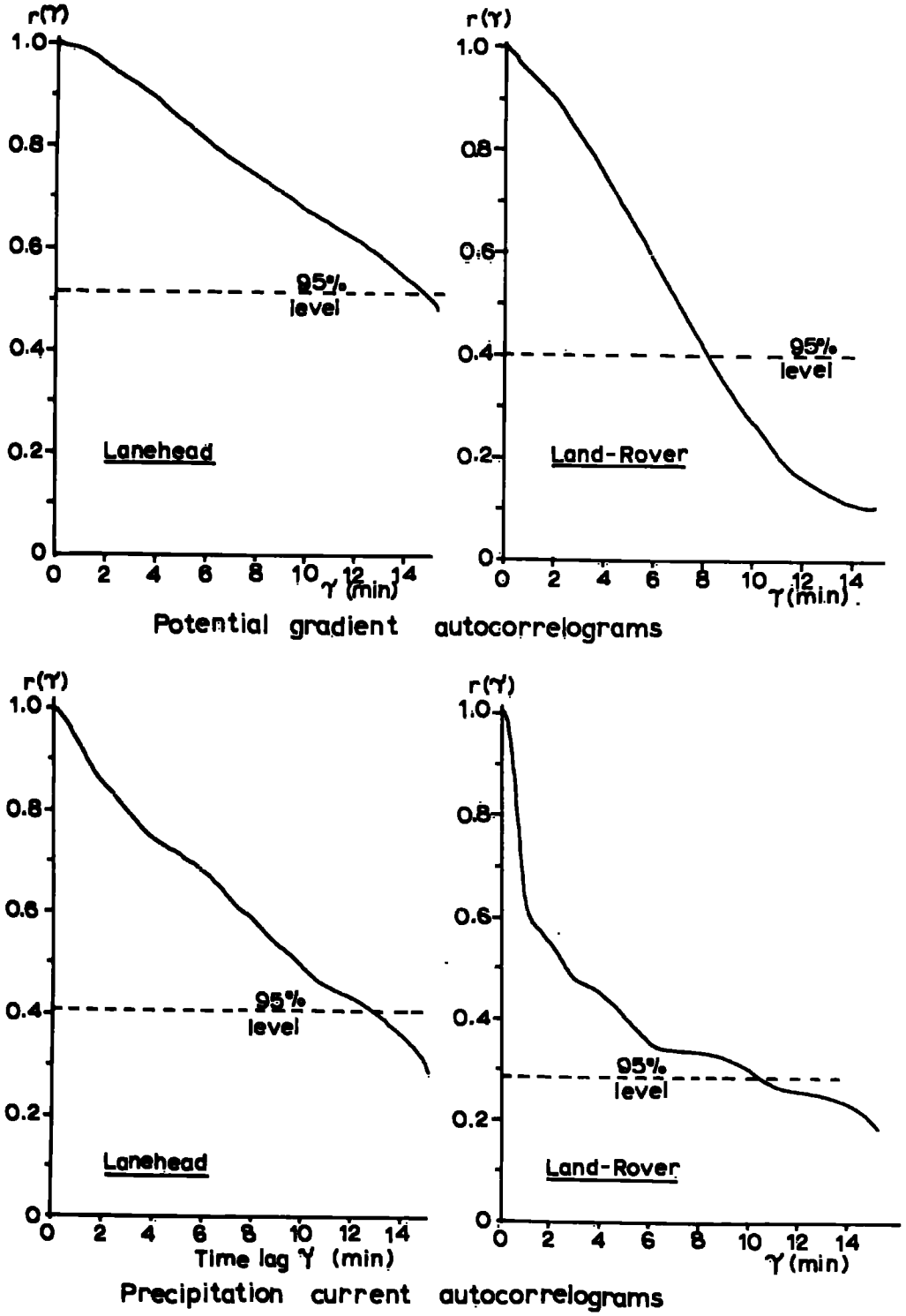

Fig. 7.11 Autocorrelograms of 2nd June records.

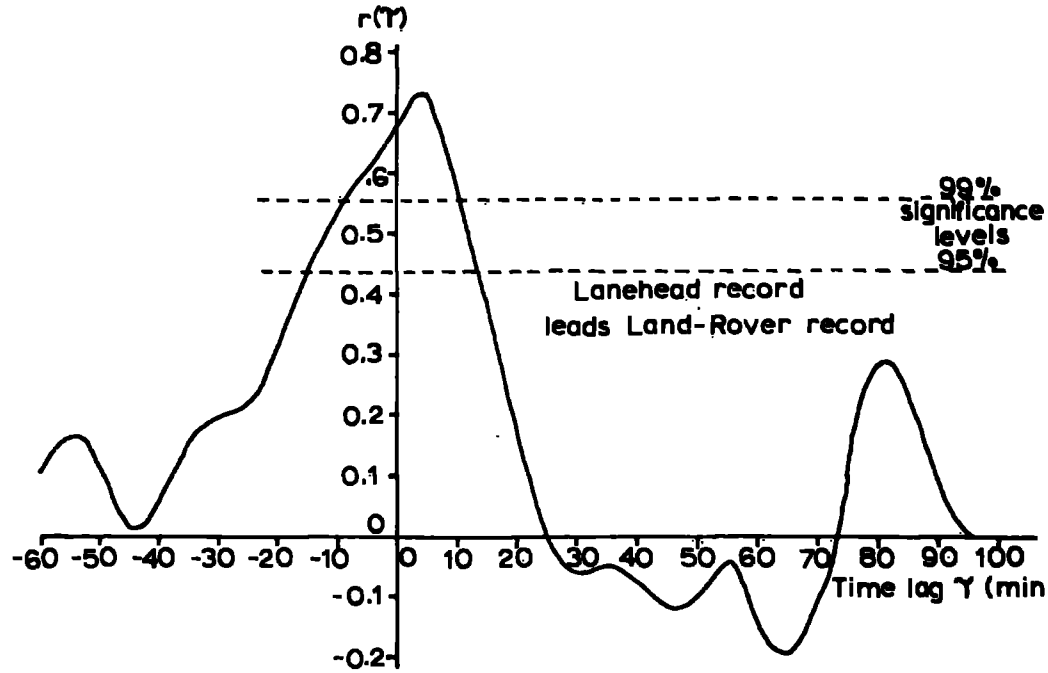

Potential gradient cross-correlogram

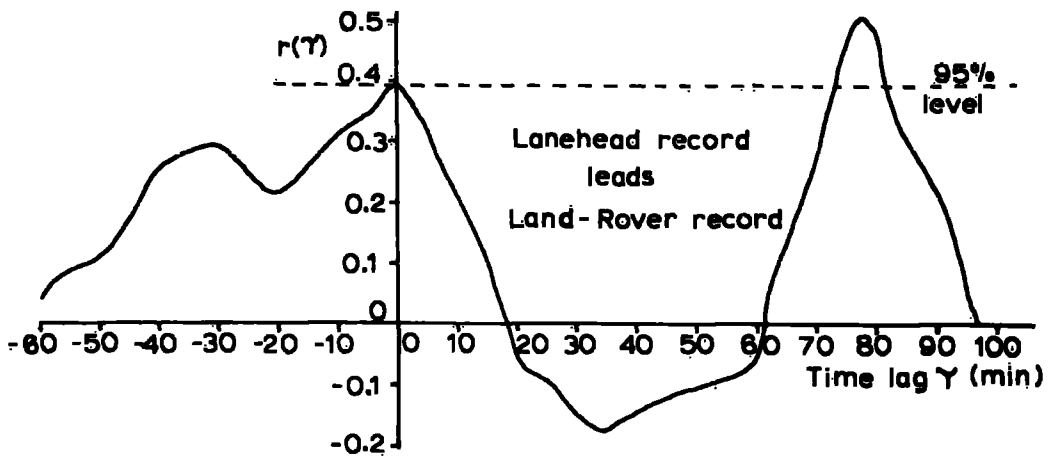

Precipitation current cross-correlogram

Fig. 7.12 Cross-correlograms of 2nd June records.

the two stations is shown in Fig. 7.10. The whole of the simultaneous records are summarised in Table 7.5.

The averages of precipitation current density recorded at the two stations are in excellent agreement, especially considering the very low currents throughout the period, the large separation of the sites and slow movement of the clouds. The Land-Rover site parameters showed more variance and less persistence than those at the Lanehead site, and the potential gradient was also higher at the mobile station. The autocorrelograms of the parameters are shown in Fig. 7.11. They do not differ markedly from each other, but again the parameters recorded at the Land-Rover exhibit a lesser persistence than the same parameters recorded at Lanehead. The cross-correlograms are given in Fig. 7.12. The notable points are the relatively sharp peak in the current correlogram for a time lag of 77 minutes of the Land-Rover upon the Lanehead record and the significant correlation for zero time lag. The potential gradient correlogram shows a very notable peak at about zero time lag, and a peak at 80 minutes time lag. Although the latter peak is statistically insignificant, in view of the current correlogram peak for an almost identical time lag, it is very probably physically significant. The strong correlation for zero time lag can probably be explained by the two field mills being affected by the same charge systems simultaneously.

RECORD 5 20th June 1969

A depression situated to the North of Ireland and an associated occluded front produced rain over the British Isles during the early part of the day. At Lanehead, light continuous rain commenced about 06.00 G.M.T. and continued till about 12.00. The mobile station was positioned downwind at a horizontal separation of 5.0 km and an altitutude of 565m (1850 ft). A continuous record was obtained at this site from 08.04 to 09.17 when the rain became very light. Throughout the recording period the wind was very strong and gusty at the Land-Rover site but only moderate at Lanehead. The record is summarised in Table 7.6. The differences between the stations on this occasion were very great, particularly with respect to the precipitation current records. At Lanehead the precipitation showed very little electrical activity with a peak value of about 7.0 pA m^{-2}. At the Land-Rover site however there was notable electrical activity, and a maximum precipitation current of over 200 pA m^{-2} was measured. The potential gradient at the mobile site was higher, as it had been on previous occasions. The autocorrelation intervals however, were smaller at Lanehead than at the Land-Rover, and this had never occurred before, even on windless occasions. The autocorrelograms (Fig. 7.13) are not unusual, showing the characteristics of random data. The cross-correlograms, however (Fig. 7.14), do not show any marked features, and in neither case was there any significant correlation.

TABLE 7.6

SIMULTANEOUS TWO-STATION RECORD

20th June 1969

	POTENTIAL GRADIENT (Vm^{-1})		PRECIPITATION CURRENT DENSITY(pAm^{-2})	
	Lanehead	Land-Rover	Lanehead	Land-Rover
AVERAGE	-201	-518	1.7	11.0
STANDARD DEVIATION	86	475	1.75	41.0
AUTOCORRELATION INTERVAL(s)	441	726	205	387
EFFECTIVE NUMBER OF INDEPENDENT OBSERVATIONS	10	6	21	11

Time of simultaneous record	08.04 to 09.17 G.M.T.	
Wind Speed	Lanehead 4 ms^{-1}	Land-Rover 8.1 ms^{-1}
Air Temperature		$10^{o}C$
Cloud Speed		12 ms^{-1}
Cloud Direction		138^{o}
Horizontal separation of sites		5.0 km
Vertical separation of sites		125 m
Maximum precipitation current cross-correlation		0.33
Time lag for maximum cross-correlation		18 min
Cloud speed from maximum correlation		4.6 ms^{-1}

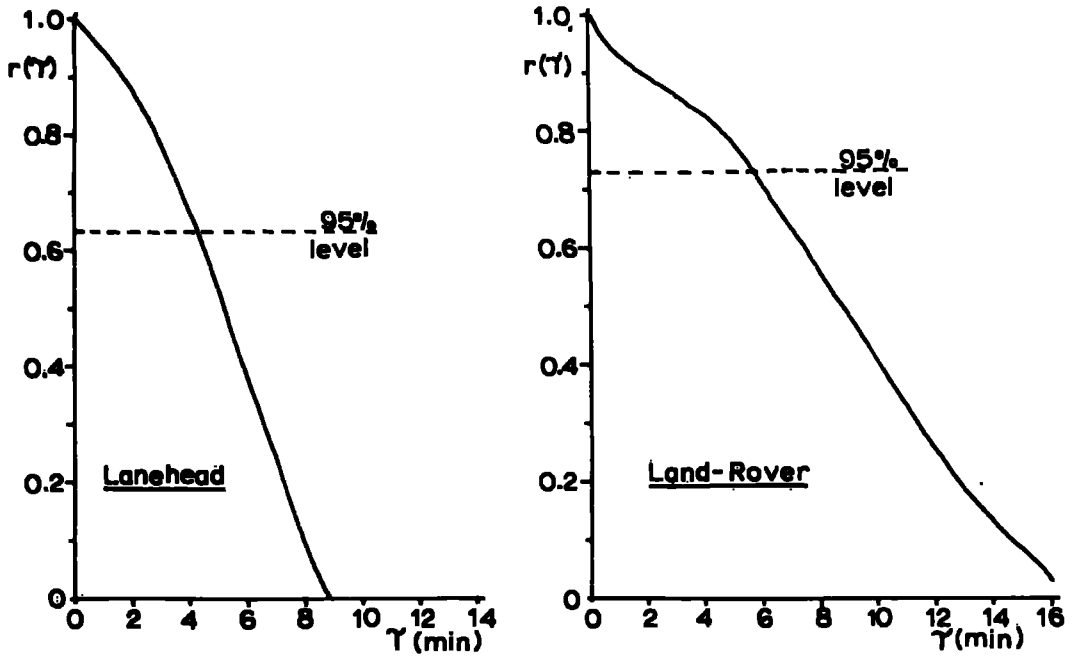

Potential gradient autocorrelograms

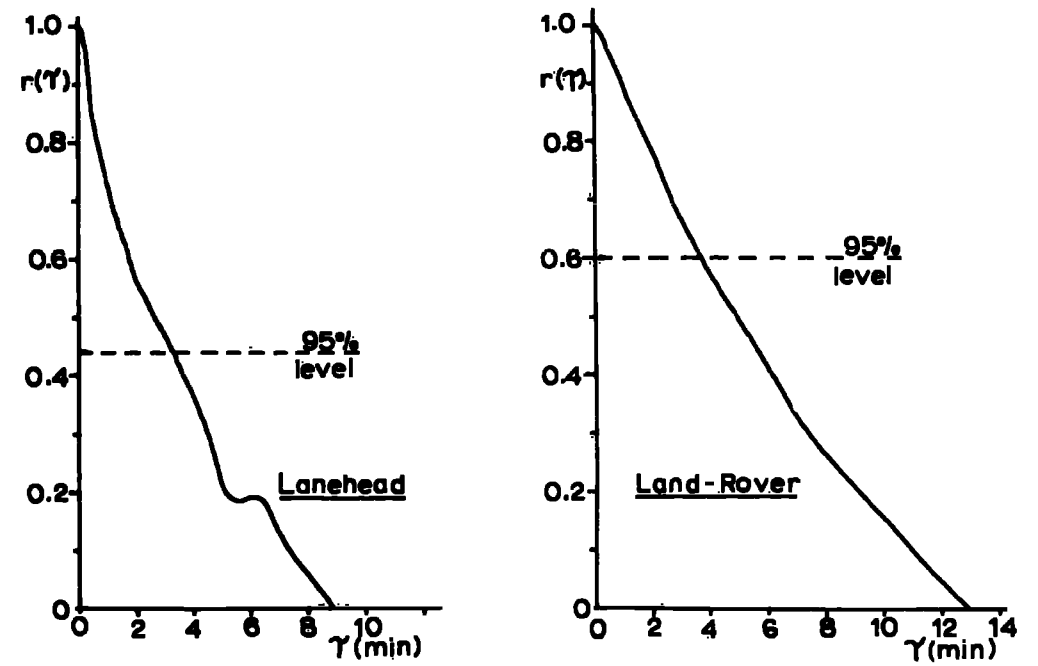

Precipitation current autocorrelograms

Fig. 7.13 Autocorrelograms of 20th June records.

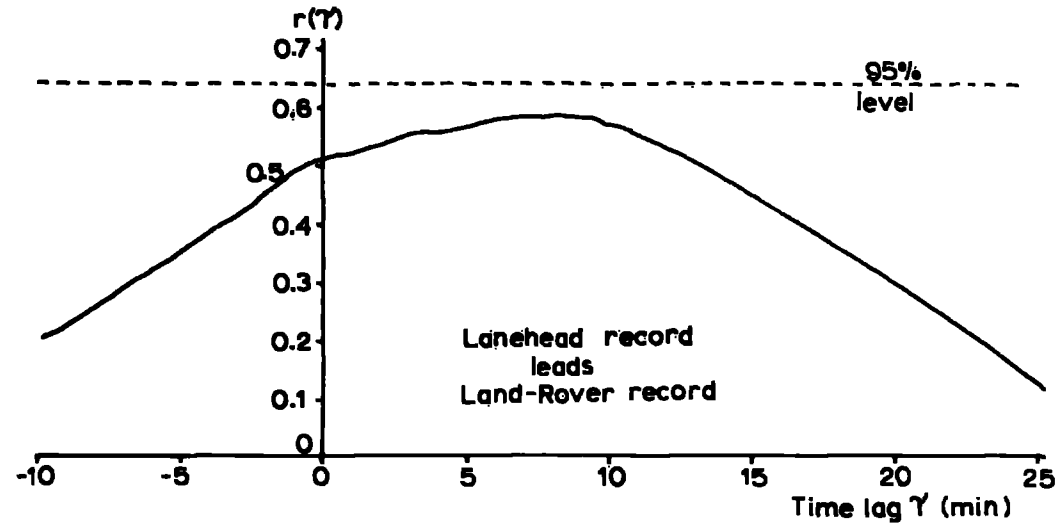

Potential gradient cross-correlogram

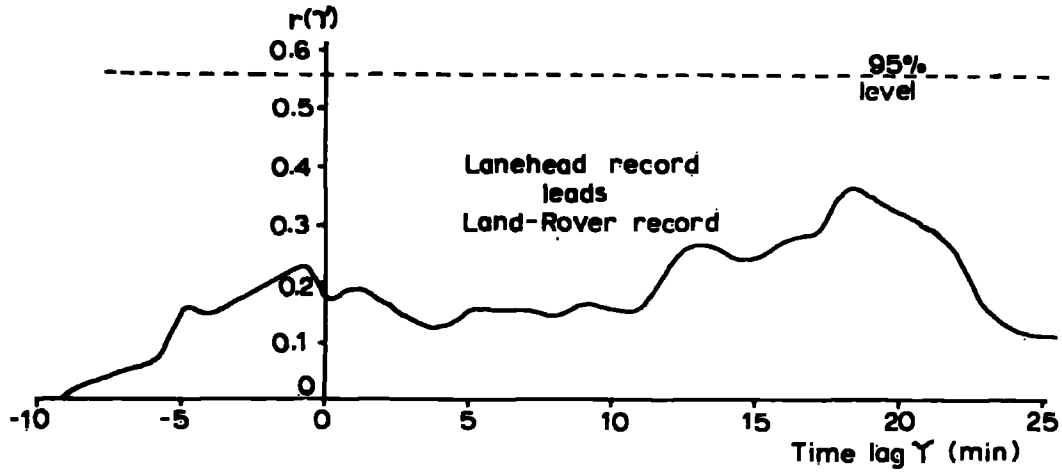

Precipitation current cross-correlogram

Fig. 7.14 Cross-correlograms of 20th June records.

TABLE 7.7

SIMULTANEOUS TWO-STATION RECORD

26th JUNE 1969

	POTENTIAL GRADIENT (Vm^{-1})	
	Lanehead	Land-Rover
AVERAGE	-64	-166
STANDARD DEVIATION	100	87
AUTOCORRELATION INTERVAL(s)	290	123
EFFECTIVE NUMBER OF INDEPENDENT OBSERVATIONS	10	23

Time of simultaneous record		19.21 to 20.09 G.M.T.
Wind Speed	Lanehead 6 ms^{-1}	Land-Rover 14 ms^{-1}
Air Temperature		15°C
Cloud Speed		16 ms^{-1}
Cloud Direction		202°
Horizontal separation of sites		6.0 km
Vertical separation of sites		235 m

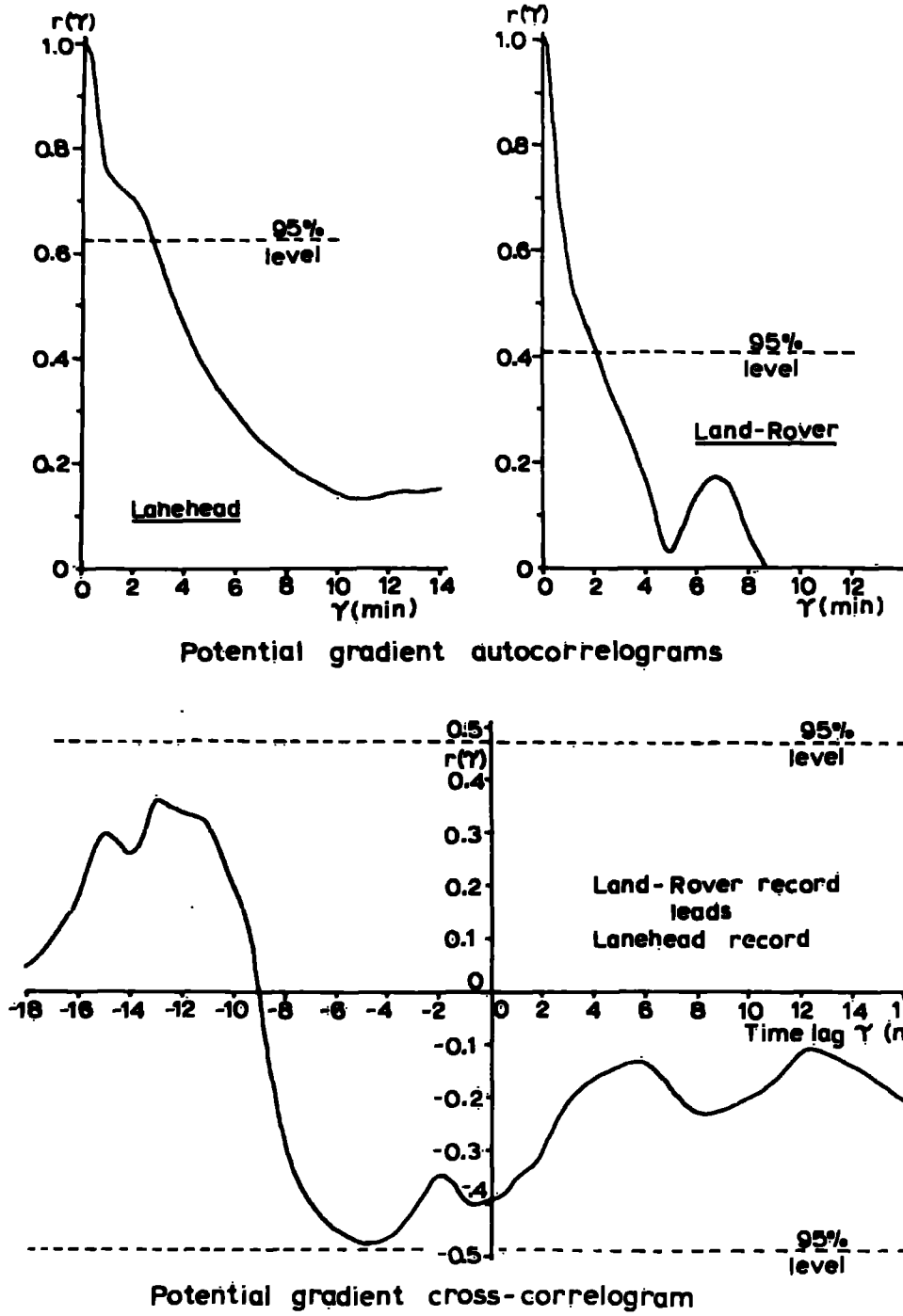

Fig. 7.15 Autocorrelograms and cross-correlogram of 26th June records.

RECORD 6 26th June 1969

A depression west of Scotland and its associated frontal system moved steadily westwards over the British Isles giving light rain and drizzle in many areas. At Lanehead intermittent light drizzle during the late afternoon became heavier and continuous about 18.00. The Land-Rover was taken to a recording site upwind of Lanehead at a horizontal separation of 6 km and an altitude of 675 m. The wind speed at this site was 16 ms^{-1} which prevented the use of the shielded collector as it did not collect any precipitation. A record of potential gradient only was made from 19.21 to 20.09 at this site. During the whole period the mobile station remained above cloud base which was at an altitude of approximately 550 m. The records are summarised in Table 7.7. The Land-Rover potential gradient was higher than that at Lanehead, although its standard deviation was smaller. The autocorrelation interval of the potential gradient recorded in the cloud was less than half that of the potential gradient recorded at Lanehead, which is in accordance with expectations. The autocorrelograms show a slight tendency to sinusoidal variations, but it does not appear to be statistically significant. The cross-correlogram (Fig. 7.15) does not show any statistically significant correlation, although there is a fairly high negative correlation between lags of zero and eight minutes which corresponds to a period in which the cloud was between the two stations, and the maximum negative correlation corresponds well with the time of travel of the clouds between the stations.

7.4 DISCUSSION OF THE TWO-STATION RESULTS

(a) The cross-correlation results

Of the six occasions that simultaneous two-station observations were obtained, four produced statistically significant correlation between precipitation current density, and three between potential gradient, at the two stations. In the four cases, the maximum cross-correlation coefficient occurred for a lag of the downwind station record on the upwind record, and at a time consistent with the disturbance travelling with the cloud in the direction of its motion. This suggests that the primary cause of the time variation of the electrical parameters is due to movement of the cloud rather than its electrical development. If these four maximum correlation coefficients are plotted against the time of travel of the cloud between the stations (Fig. 7.16), it can be seen that there is a decrease with time. This decrease is very much slower than that exhibited by the precipitation current autocorrelograms, which indicate a maximum persistence of about 20 minutes. The diagram perhaps indicates the true autocorrelation length of a nimbostratus cloud, and indicates that it might be as long as several hours.

In addition, on two of the occasions, a statistically significant precipitation current correlation was found between the stations for zero time lag, that is simultaneous records. The first of these on the 14th April (Fig. 7.7) may not be physically significant because

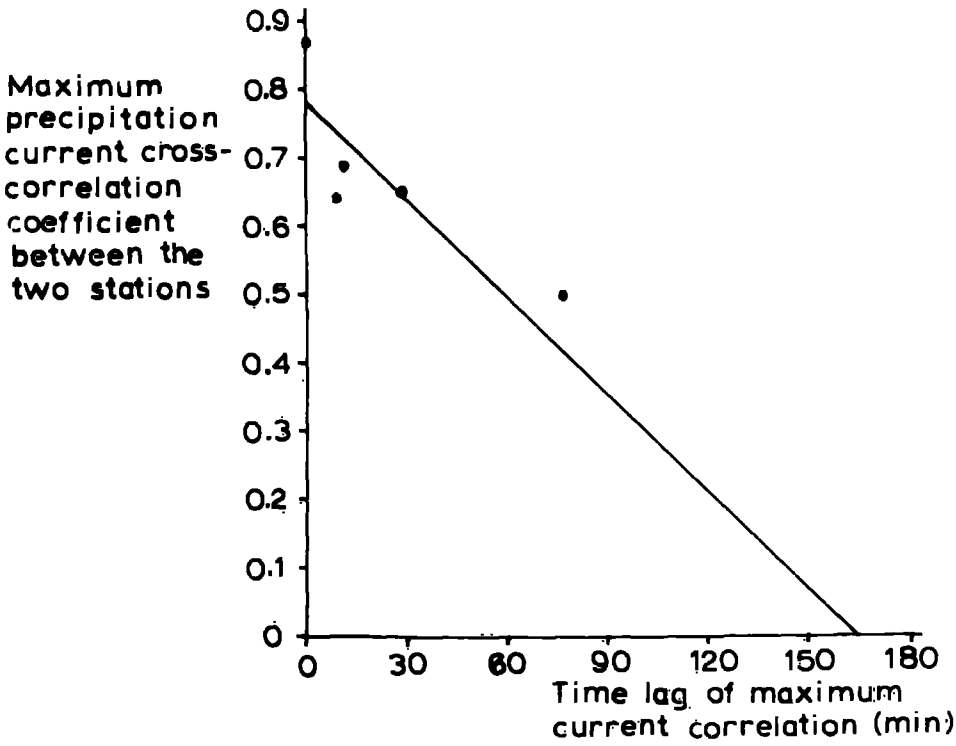

Fig. 7.16 Dependence of maximum precipitation current correlation on time lag between the two stations.

the correlation extends from time lags of -2 min up to +15 min, and might therefore be due to persistence across the cloud. The time lag for maximum current correlation (9 mins) is not far different from the precipitation current correlation interval ($6\frac{1}{2}$ mins), which seems to support this. On the other occasion, however, the 2nd June (Fig. 7.12), there is a significant correlation peak at zero time lag as well as at a time lag corresponding to the cloud travel time and these peaks are separated by a long period where there is no correlation. It appears on this occasion that the precipitation currents at the two sites varied at least partly simultaneously, or at least, that part of the variations at the two sites were controlled by effects operating over a large area of the cloud. This effect was certainly not due to persistence as the time of travel of the cloud (77 mins) between the sites was much longer than the current autocorrelation interval ($10\frac{1}{2}$ mins).

The potential gradient correlograms for the 6th May (Fig. 7.9) and 2nd June show a well-defined positive correlation for a time lag of about zero. As remarked earlier, this is almost certainly due to the field mills at the two stations being influenced by the same charges at the same time, and that the existence of large-scale phenomena cannot be inferred. However, these results are important from another point of view. On both of these occasions the Land-Rover site was at about the same altitude as the Lanehead site, but

separated by a mountain ridge about 200m higher. Thus the charges which were simultaneously influencing the two stations could not have been near to the ground, but must at least have been at cloud base height several hundred metres above the stations. Hence it is inferred that charge separation does take place within the cloud, and not wholly near the ground as suggested by some workers.

(b) The Station Differences

Despite the high correlations obtained with large separation of the stations on certain occasions, the two stations did show wide differences. The comparison run of the two stations alongside each other showed that the average values would be expected to be similar, but that the parameters recorded at the mobile site would exhibit greater variance and lesser persistence. This was found to be so on nearly all of the recording periods, but the differences were greater than would be expected from purely instrumental differences. In addition, in all of the recorded periods the potential gradient at the mobile site was much higher than at Lanehead, and on many occasions of rain the precipitation current density was much higher too.

The occasions of excess rain currents at the mobile site coincide with the recording periods when there was a strong wind. There does not seem to be any effect due to the difference in height of the stations, which was very small. The first consideration is therefore whether or not the exposed collector on the Land-Rover

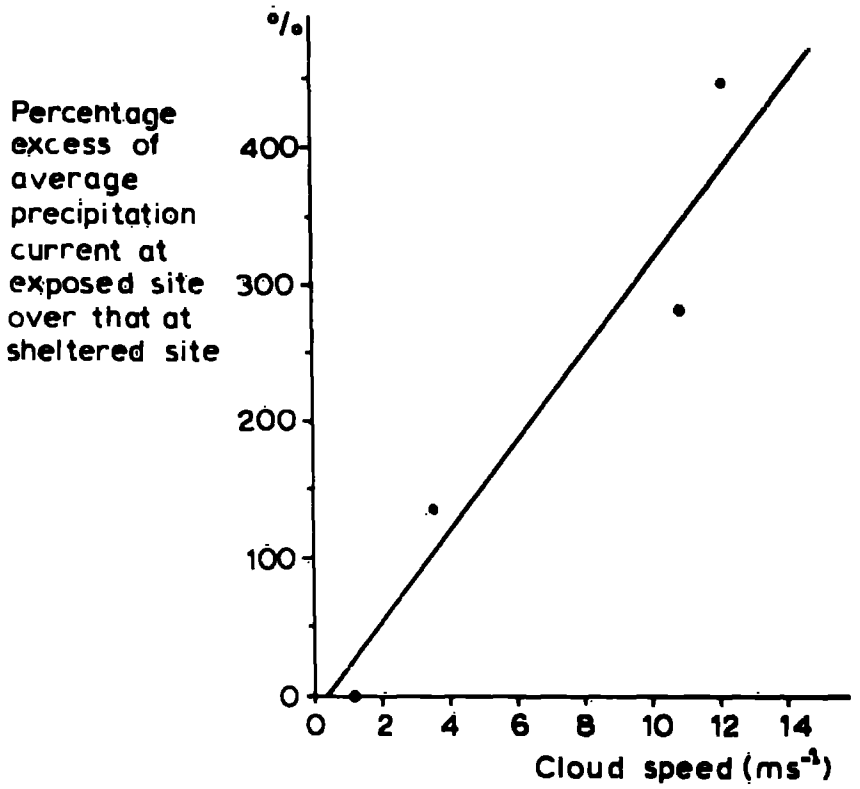

Fig. 7.17 Dependence of precipitation current density upon exposure of recording site.

will give rise to spurious currents in high winds. It will be expected that drops hitting the outer shield and splashing off will carry a sign opposite to the potential gradient, that is, usually positive. The amount of charge carried will be proportional to the potential gradient, which will be enhanced by the elevation of the collector. Several estimates have been made of the magnitude of this effect (e.g. Collin and Raisbeck (1964)), and it seems that in the most unfavourable conditions, with a rainfall rate of 5 mm hr^{-1} and a potential gradient of 1000 vm^{-1}, the measured current may be in error by as much as 10 pA m^{-2}. As the records show, the average currents over the recording periods differed by more than this amount on several occasions, whilst the peak currents often differed by more than ten times this value. It therefore seems that there may be a real difference in the parameters recorded at the two stations, and that this difference is in some way dependent upon the wind speed (Fig. 7.17).

The difference in the values of potential gradient recorded at the two sites may, at least in part, be due to the difference in exposure of the two sites. In its sheltered position, Lanehead may be shielded from the effects of some cloud charges. However, the difference is very great in some cases and may be due to a real difference between the sites. If this is so, this becomes consistent with the excess of precipitation current density at the mobile site on

certain occasions, and perhaps suggests that there is a local charge separation effect near the ground which depends on local topography, as well as effects on a wider scale attributable to the cloud. Drop-shattering in turbulence near the ground will satisfy these conditions and explain some of the discrepancies between the stations. A further analysis of the effect of wind is made in the following Chapter, as well as analyses of the long Lanehead records. A complete discussion of all the results will follow in Chapter 9.

CHAPTER 8

THE ANALYSIS OF THE SINGLE-STATION OBSERVATIONS

8.1 The Effects of Wind Speed

It has been suggested in the previous chapter that, although there may be discrepancies due to instrumental errors, the more exposed sites are subject to enhanced rain electrification, and this effect may be attributable to the increased wind speed and associated turbulence at those sites. Since the effects were most noticeable with the Land-Rover situated at exposed sites, it was decided to carry out an analysis of the effects of wind speed on a shorter time scale upon the measurements of precipitation current density and potential gradient obtained at the mobile station.

On all four of the occasions of rain when precipitation current density was measured simultaneously at the two stations, a continuous record of wind speed was also obtained at the Land-Rover. Computer programs were written to calculate the correlation coefficients for various time lags between wind speed and precipitation current density and between the square of wind speed and precipitation current density. Similar calculations were made for potential gradient also. In none of the four periods analysed was there any significant correlation between potential gradient and wind speed, but on three of the four occasions there was significant correlation between precipitation current density and wind speed and the square of wind speed.

The record obtained on 2nd June, from 16.25 to 20.23 G.M.T., had the lowest average wind speed of 1.4 ms^{-1}. On this occasion the maximum cross-correlation coefficient between precipitation current density and wind speed, for the whole record, was -0.3 for zero time lag, and this value is not quite significant at the 95% level. However, this result is probably meaningful as it suggests that an increase of wind speed reduces the recorded precipitation current density, and this is just what we expect of the shielded collector. It suggests also that there are no effects attributable to the wind other than a reduction in collection efficiency of the instrument.

The other three records produced a positive correlation between precipitation current density and wind speed. The record obtained on the 14th April from 15.20 to 16.23 G.M.T., when the average wind speed was 8.1 ms^{-1}, gave a maximum cross-correlation coefficient of 0.42, which is significant at the 95% level. The record of the 6th May, from 14.45 to 16.22 G.M.T., when the average wind speed was 3.4 ms^{-1}, gave a maximum cross-correlation coefficient of 0.58, which is significant at the 99.9% level. The record of 20th June, from 08.04 to 09.17, when the average wind speed was 8.1 ms^{-1}, gave a maximum cross-correlation coefficient of 0.26, which is just significant at the 95% level. All these maximum correlations are for zero time lag, that is simultaneous correlation. The cross-

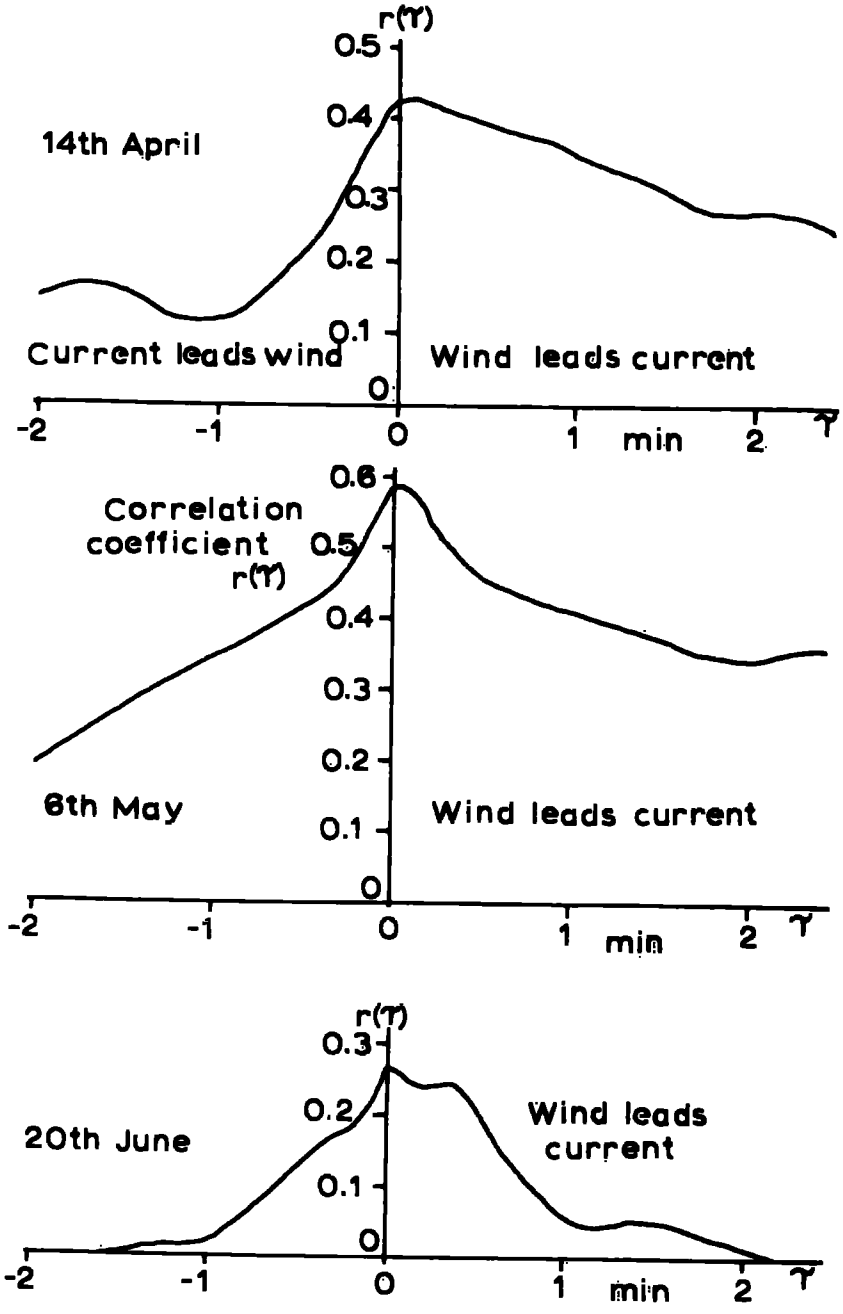

Fig. 8.1 Wind speed - precipitation current cross-correlograms.

correlograms for these three cases are shown in Fig. 8.1. The most notable feature of these correlograms is their asymmetry. All three show a higher cross-correlation for a given time lag for wind speed leading the precipitation current density than for it lagging. Although the effect of the persistence of the parameters is to spread the maximum of a correlogram, it should produce a spread which is symmetric about the maximum. It appears, therefore, that the difference in correlation may be real.

The physical meaning of this is that an increase in wind speed will produce a corresponding increase in precipitation current density, but that the effect also persists after the wind subsides. This suggests that the wind produces effects some distance above the ground, and the correlation for non-zero time lags represents the time of fall of the raindrops affected by the wind. From Fig. 8.1 it can be seen that the time lag is of the order of 1 min, which represents a fall height of 250m for 1 mm diameter raindrops. It seems very unlikely that an effect such as charging arising from splashing at the rim of the collector could give rise to the observed asymmetric correlations, and drop—shattering in the air above the ground offers a plausible explanation.

It might be thought that drop-shattering would be dependent more on the square of wind speed than on wind speed, as this perhaps

better represents the wind force acting on the drops. The record of the 6th May, when the wind speed was very low and which gave an insignificant negative correlation between precipitation current density and wind speed, gave no significant correlation with the square of wind speed, as expected. The other three records, which gave significant positive correlation with wind speed, also gave significant positive correlation between precipitation current density and the square of wind speed. The records of 14th April, 6th May and 20th June gave maximum cross-correlation coefficients of 0.39, 0.34 and 0.30 respectively. All are for zero time lag, and are significant at the 95% level. The corresponding cross-correlograms are shown in Fig. 8.2, and all demonstrate the asymmetry shown previously.

The above analyses clearly suggest that there is some effect of wind speed upon rain electrification. The results imply that there is a charge separation process which operates close to the ground, but which may extend upwards for several hundred metres. It is to be expected that any charge separation process such as drop-shattering will be dependent upon other factors, such as local topography and the presence of large raindrops, in addition to wind speed. This may explain why the observed correlation coefficients are not higher.

8.2 The Autocorrelation Intervals

The analyses of the two-station results in the previous chapter showed that the autocorrelation intervals of the atmospheric

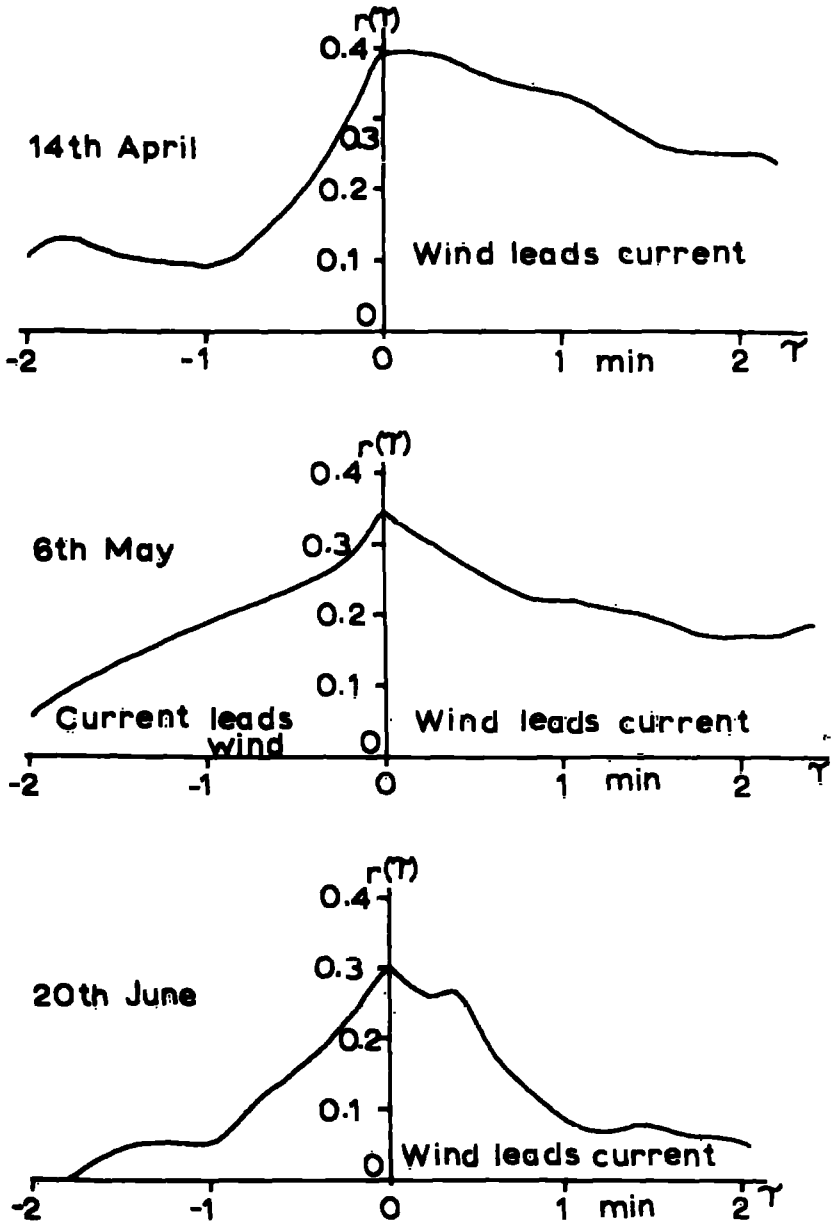

Fig. 8.2 Square of wind speed-precipitation current cross-correlograms.

electric parameters depend upon wind speed. Collin, Groom and Higasi (1966) have shown that the inverse of the autocorrelation interval of the conductivity of the air is proportional to the wind speed, which suggests that mechanical replacement and mixing are more important than electrical relaxation. Similar plots were therefore made of the inverse of the autocorrelation intervals of precipitation current density and potential gradient from the data recorded at Lanehead. The five records available from the occasions when simultaneous records were obtained were used for the purpose. It was thought that cloud speed might be more meaningful, and the results are shown in Fig. 8.3.

As can be seen, a similar relationship holds in these cases. The correlation coefficients are 0.74 and 0.78 respectively for the precipitation current density and potential gradient autocorrelation intervals. The 95% significance level is 0.79, and so it is extremely likely that the results are meaningful. The relationship between autocorrelation interval L and wind speed v can be written $L^{-1} = av + c$, where a and c are constants. When $v = o$, $C^{-1} = L$, and C^{-1} therefore represents the autocorrelation interval for a stationary cloud. The values obtained statistically from the two graphs are $C^{-1} = 42$ min for precipitation current density and $C^{-1} = 18$ min for potential gradient. The electrical relaxation time of the atmosphere at the ground at Lanehead during quiet precipitation is of the order of

15 min, which is not greatly different from the autocorrelation interval of potential gradient obtained for a stationary cloud, and this result may be significant.

The relationship between autocorrelation interval and wind speed may be rewritten $L^{-1} = v/W + C$, where $W = {}^{1}/a$. If L is expressed in s and v in ms^{-1}, it can be seen that the constant W has the dimensions of length in metres. It may be considered therefore that W represents an 'autocorrelation width' of the cloud, that is the horizontal dimensions of the cloud across which finite autocorrelation exists at a given point in time. From the two graphs of the experimental data, W is found to be 3.4 km for the precipitation current autocorrelation intervals and to be 10.5 km for the potential gradient autocorrelation intervals. The potential gradient autocorrelation width might be expected to be greater as a field mill is influenced by charges over a large area of cloud.

As the autocorrelation widths of the nimbostratus clouds investigated are very similar, it is possible that, if the autocorrelation widths of convective clouds are very different from stratiform clouds, the autocorrelation width might offer a means of identifying cloud type without the necessity of human judgement. Although no investigation has yet been carried out, it seems that the autocorrelation widths of convective clouds are much smaller than those of stratiform clouds, and the proposed method of cloud

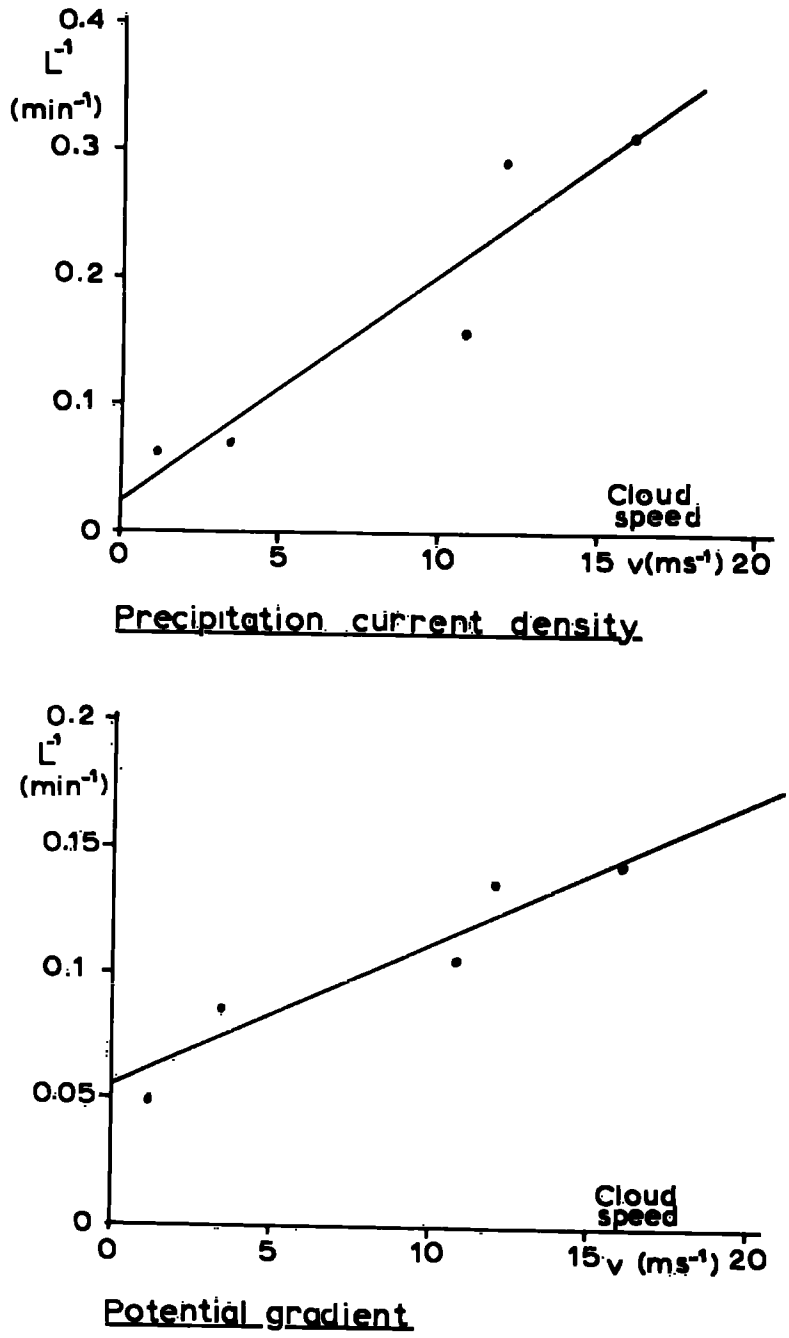

Fig. 8.3 Dependence of autocorrelation interval on cloud speed.

identification may be feasible. Autocorrelation measurement can be carried out automatically by relatively cheap and simple electronics without the necessity of any calculations being made. A knowledge of cloud speed would be needed, but at many sites this can be determined by the wind speed at the ground.

8.3 Cross-Correlation Analysis of Smoothed Data

When the two-station observations were made, the automatic recording equipment at Lanehead was run for the whole of the period when rain was falling continuously. On five of the six occasions it proved possible to analyse these long records obtained at Lanehead in greater detail. These records were obtained in the periods described in the previous chapter, the record of the 12th February being unsuitable for analysis since the field mill was inoperative.

Instead of the small-scale time variations investigated in the previous sections, relatively long-term effects were thought to be of most interest, in particular the relationship between potential gradient and precipitation current density and its application to test the model proposed in chapter 2. The parameters recorded at Lanehead which were analysed were precipitation current density, potential gradient, space charge density and rainfall rate. The space charge density was measured by means of a filtration apparatus which was being used in conjunction with Mr. Aspinall's experiment. However, it was thought that the results would be of interest in this case also.

As a simple method of smoothing the parameters to remove short-term variations, 5-minute averages were calculated. Computer programs were written to do this and to perform the cross-correlation analyses for various time lags between precipitation current density and potential gradient, precipitation current density and space charge density, and space charge density and potential gradient. On three occasions, rainfall accumulation was measured using a Meteorological Office pattern recording rain gauge. The best resolution possible for rate of rainfall was 12 min, and so 12-min averages of the atmospheric electric parameters were computed also. Correlation analyses were then carried out between rainfall rate and the atmospheric electric parameters. A brief description and summary of the records will be followed by a discussion of the results.

14th April 1969

The record commenced at 12.20 G.M.T. and finished at 18.30, during the whole period the space charge collector was inoperative. The record is summarized in Table 8.1. There was no significant correlation between any of the atmospheric electric parameters, although the correlation between potential gradient and precipitation current density was negative. The lack of correlation is also borne out in a plot of the time variations of the smoothed parameters (Fig. 8.4).

TABLE 8.1

LANKHEAD SINGLE-STATION RECORD

14th April 1969

	Potential Gradient (Vm^{-1})	Precipitation Current Density ($pA\ m^{-2}$)
AVERAGE	-430	5.7
STANDARD DEVIATION	290	13
MAXIMUM	130	44
MINIMUM	-900	-11

Time of record 12.20 to 18.30 G.M.T.

Total precipitation charge brought to earth 0.13 μCm^{-2}

Correlated Parameters	Maximum Cross-Correlation Coefficient	Time Lag for Maximum Correlation
Potential gradient-precipitation current	-0.3	15 min, potential gradient leads precipitation current
Potential gradient-space charge density	0.1	15 min, potential gradient leads space charge
Precipitation current-space charge density	-0.28	0

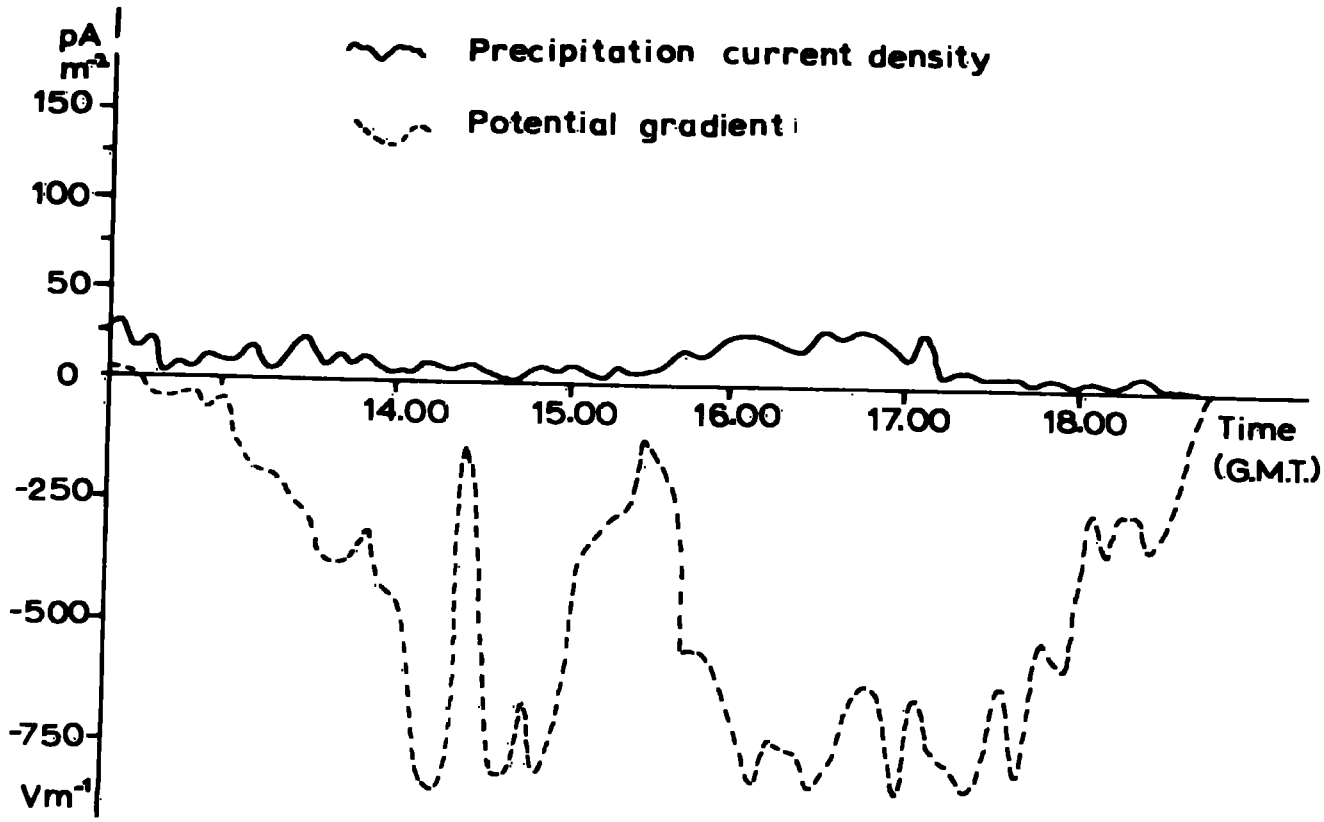

Fig. 8.4 Record of smoothed parameters, 14th April 1969.

TABLE 8.2

LANKHEAD SINGLE-STATION RECORD

6th May 1969

	Potential Gradient (Vm^{-1})	Precipitation Current Density ($pA\ m^{-2}$)	Space Charge Density(pCm^{-3})
AVERAGE	-140	32	50
STANDARD DEVIATION	75	35	84
MAXIMUM	-3	180	415
MINIMUM	-370	-20	7

Time of record 13.15 to 16.52 G.M.T.
Total precipitation charge carried to earth = $0.42\ \mu Cm^{-2}$

Correlated Parameters	Maximum Cross-Correlation Coefficient	Time Lag for Maximum Correlation
Potential gradient-precipitation current	-0.32	5 min, Potential gradient leads current
Potential gradient-space charge density	-0.62	10min, Potential gradient leads space charge
Precipitation current-space charge density	-	-

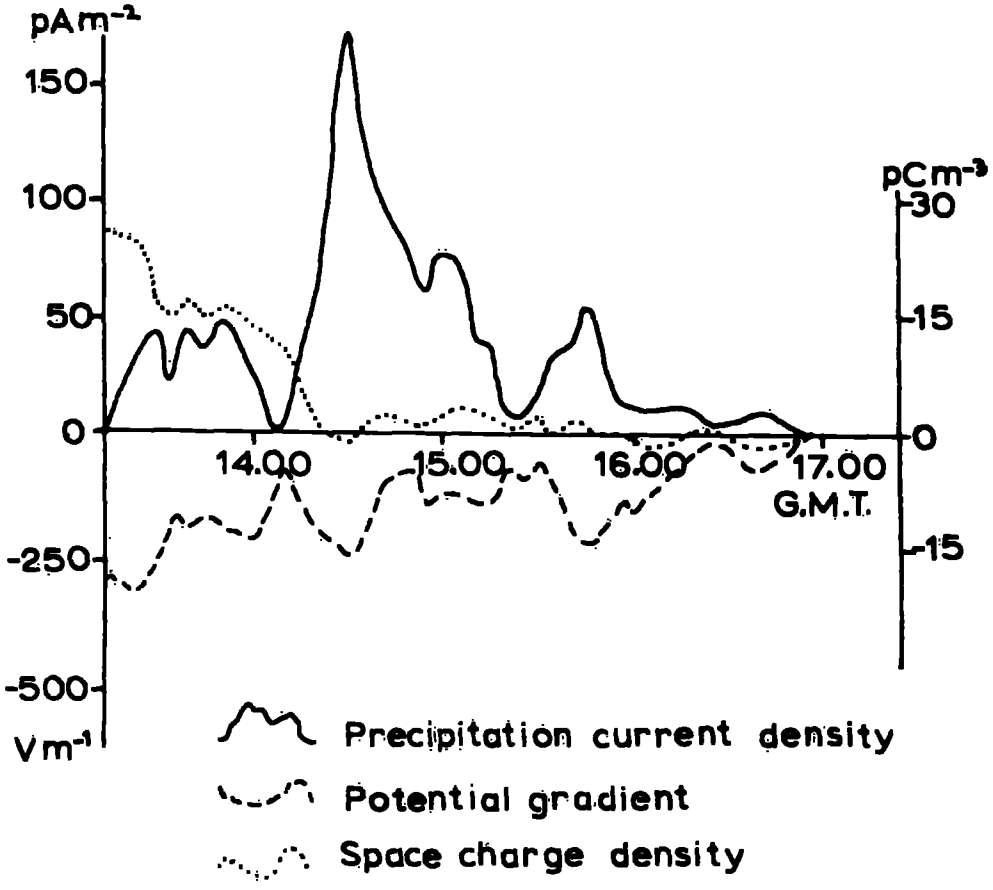

Fig. 8.5 Record of smoothed parameters, 6th May 1969.

TABLE 8.3

LANKHEAD SINGLE-STATION RECORD

2nd June 1969

	Potential Gradient (Vm^{-1})	Precipitation Current Density ($pA\ m^{-2}$)	Space Charge Density (pCm^{-3})
AVERAGE	-180	12	-55
STANDARD DEVIATION	230	15	71
MAXIMUM	175	105	63
MINIMUM	-805	-7	-390

Time of record 15.22 to 01.14 G.M.T.

Total precipitation charge brought to earth 3 μCm^{-2}

TABLE 8.3 CONTD.

Correlated Parameters	Maximum Cross-Correlation Coefficient	Time Lag for Maximum Correlation
Potential gradient-precipitation current	-0.77***	0
Potential gradient-space charge density	0.88***	0
Precipitation current-space charge density	-0.82***	5min, current leads space charge
Precipitation current-rainfall rate	0.72***	0
Potential gradient-rainfall rate	-0.68***	0
Space charge density-rainfall rate	-0.74***	0

*** Denotes significance at 99.9% level

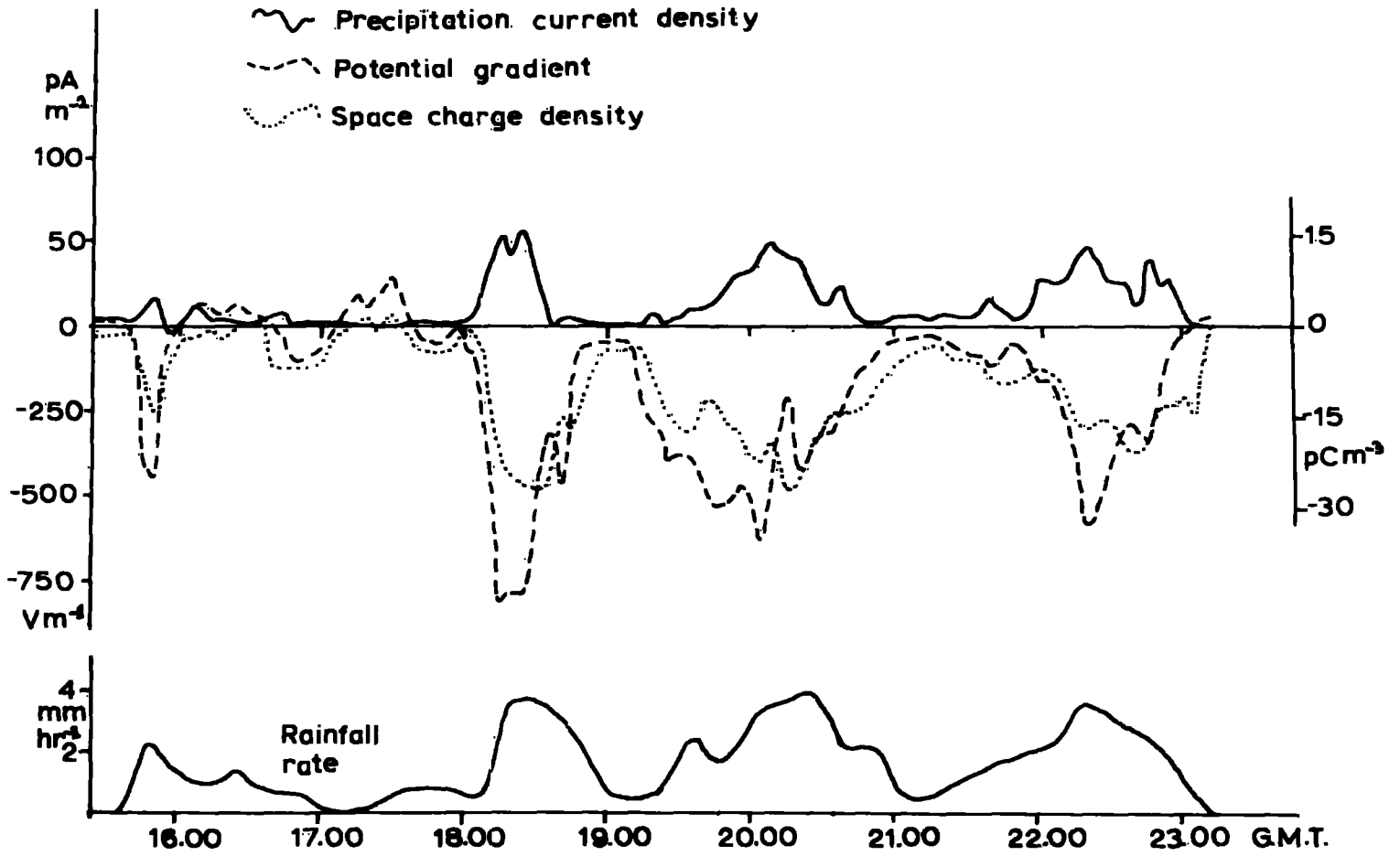

Fig. 8.6 Record of smoothed parameters, 2nd June 1969.

6th May 1969

The record commenced at 13.15 G.M.T. and continued till 16.52. All the atmospheric electric recording equipment was operative throughout the record, which is summarized in Table 8.2. The only significant correlation exists between potential gradient and space charge density. The maximum value is -0.62 for a lead of potential gradient upon space charge density of 10 min. It should be noted that with a resolution time of 5 min, the times of lead and lag can only be approximate. The correlation between potential gradient and precipitation current density is not statistically significant, although it is negative. A plot of the smoothed parameters is shown in Fig. 8.5.

2nd June 1969

This record covered a 10-hour period of quiet rain with little wind from 15.22 to 01.14 on the 3rd June. In addition to the three atmospheric electric parameters, rainfall accumulation was also measured. The record is summarised in Table 8.3, and a plot of the smoothed parameters shown in Fig. 8.6.

Correlation between all the parameters is very high, and all of the coefficients of maximum correlation are significant at the 99.9% level. However, it is essential to realise that correlation between some of the parameters may not be real, and may be the result of inter-relationships between parameters. These relationships will be discussed in section 8.4.

20th June 1969

A continuous record of the atmospheric electric parameters and rainfall accummulation was obtained from 07.20 G.M.T. until 11.31. The record is summarised in Table 8.4, and a plot of the smoothed parameters given in Fig. 8.7.

The correlation between the atmospheric electric parameters is high and of the sign usually expected. The inverse relation between potential gradient and precipitation current density is apparent, as is the direct relation between potential gradient and space charge density. The only significant correlation is between rainfall rate and space charge density, the maximum value being -0.56.

26th June 1969

A record of atmospheric electric parameters and rainfall accumulation was obtained from 18.30 G.M.T. until 22.14. The period was unusual in that the precipitation consisted of very heavy drizzle throughout. The record is summarised in Table 8.5 and a plot of the smoothed parameters is shown in Fig. 8.8.

The only significant correlation exists between potential gradient and space charge density, and the value of maximum correlation, 0.79, is highly significant. The average potential gradient was positive instead of the more usual negative.

TABLE 8.4

LANEHEAD SINGLE-STATION RECORD

20th June 1969

	Potential Gradient (Vm^{-1})	Precipitation Current Density ($pA\ m^{-2}$)	Space Charge Density (pCm^{-3})
AVERAGE	-90	2.3	3
STANDARD DEVIATION	-160	2.8	19
MAXIMUM	180	30	70
MINIMUM	-520	-5	-46

Time of record 07.20 to 11.31 G.M.T.

Total precipitation charge brought to earth $0.04 \mu Cm^{-2}$

TABLE 8.4 CONTD.

Correlated Parameters	Maximum Cross-Correlation Coefficient	Time Lag for Maximum Correlation
Potential gradient-precipitation current	-0.65*	0
Potential gradient-space charge density	0.88**	5min, Potential gradient leads space charge
Precipitation current-space charge density	-0.62*	10min, Precipitation current leads space charge
Precipitation current-rainfall rate	0.21	0
Potential gradient-rainfall rate	-0.40	0
Space charge density-rainfall rate	-0.56*	0

* Denotes significance at 95% level

** Denotes significance at 99% level

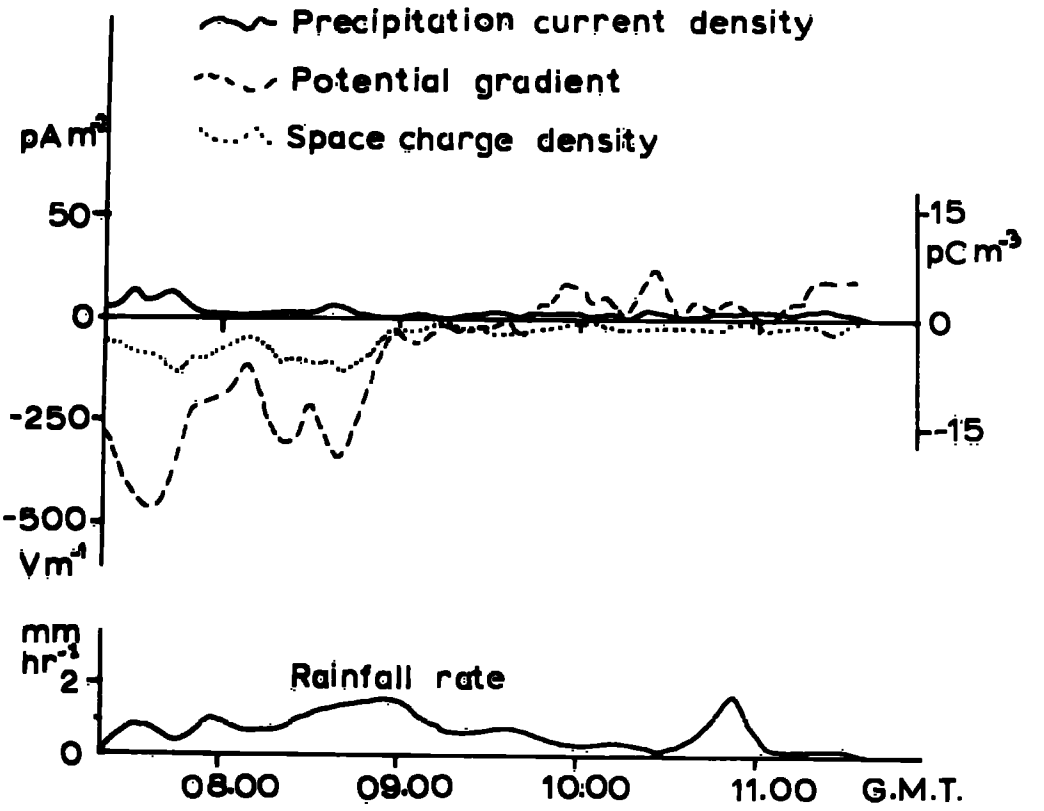

Fig. 8.7 Record of smoothed parameters, 20th June 1969.

TABLE 8.5

LANEHEAD SINGLE-STATION RECORD

26th June 1969

	Potential Gradient (Vm^{-1})	Precipitation Current Density ($pA\ m^{-2}$)	Space Charge Density (pCm^{-3})
AVERAGE	40	4	55
STANDARD DEVIATION	130	13	79
MAXIMUM	260	59	215
MINIMUM	-350	-17	-225

Time of record 18.30 to 22.14 G.M.T.

Total precipitation charge brought to earth $0.05\ \mu Cm^{-2}$

TABLE 8.5, CONTD.

Correlated Parameters	Maximum Cross-Correlation Coefficient	Time Lag for Maximum Correlation
Potential gradient-precipitation current	0.09	0
Potential gradient-space charge density	0.79**	0
Precipitation current-space charge density	-0.07	10min, current leads space charge
Precipitation current-rainfall rate	0.54*	0
Potential gradient-rainfall rate	0.26	0
Space charge density-rainfall rate	-0.31	0

* Denotes significance at 95% level

** Denotes significance at 99% level

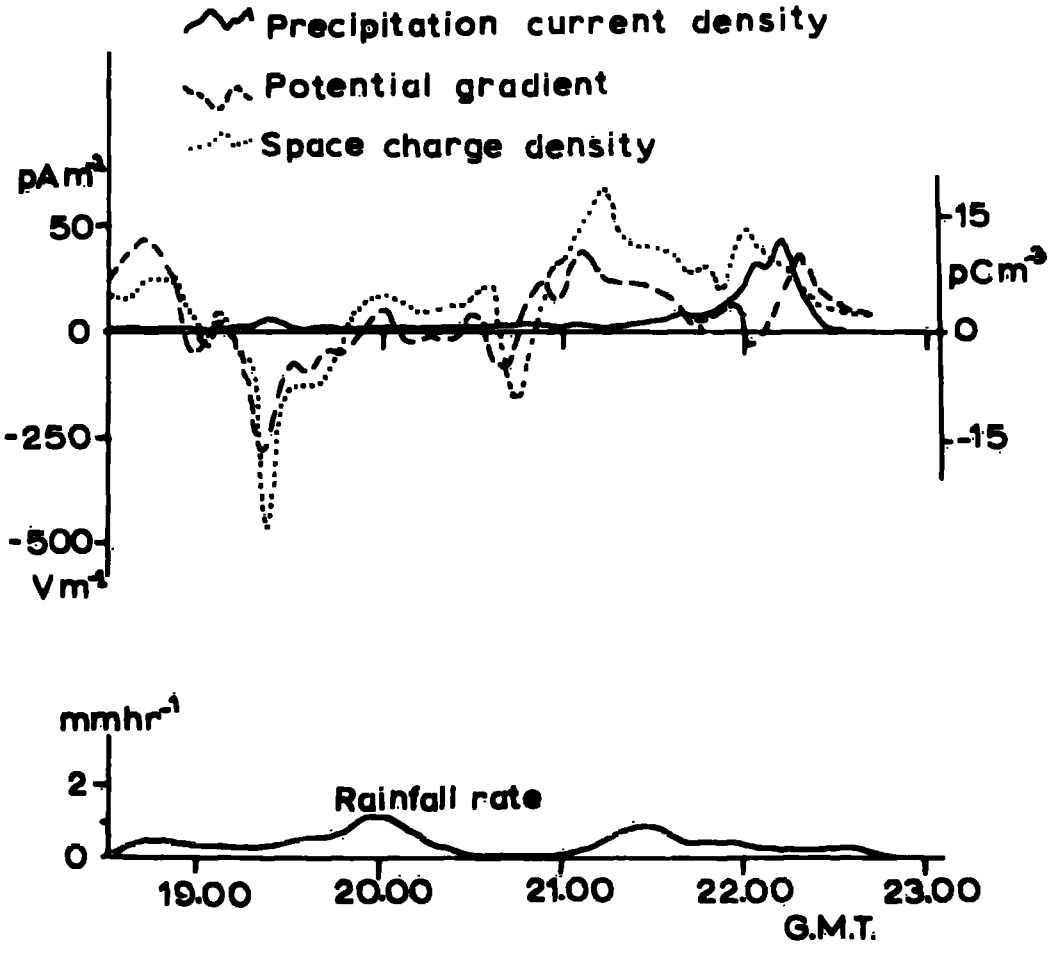

Fig. 8.8 Record of smoothed parameters 26th June 1969.

8.4 Discussion of the Single-Station Results

Three of the five records analysed above show a very strong positive correlation between the smoothed values of potential gradient and space charge density at the ground, the coefficients of maximum correlation being 0.88, 0.88 and 0.79. The space charge densities of the magnitudes observed are sufficient to influence the potential gradient only if they extend upwards to a height of tens or hundreds of metres. On two of these occasions there was strong negative correlation (-0.81 and -0.62 respectively) between precipitation current density and space charge density which suggests that they are both, at least partially, the result of a single process. On these two occasions there was also high correlation between potential gradient and precipitation current density, the maximum values being -0.77 and -0.65 respectively. A reasonable inference from these results would be that a charge separation process operates in the bottom hundred metres or so of the atmosphere, giving charge of one sign to the falling rain and the opposite sign to the air. On the third occasion, however, there was no significant correlation between precipitation current density and space charge density.

The 2nd June and 20th June records showed a fairly well-defined inverse relation between potential gradient and precipitation current density, and the scatter diagrams of the smoothed parameters

are shown in Fig. 8.9. If we assume a linear relationship of the form $F = -AI + B$, the lines of best fit for the two records give $A = 1.43 \times 10^{13}$ and 4.75×10^{13} Ω m, and $B = 51$ and -24 Vm^{-1} respectively. When the precipitation current is zero, one record gives a slightly positive potential gradient, the other gives a slightly negative value, but the numerical values are quite small in both cases. If the relationship is written in the more usual form with F as the independent variable, that is $I = a(F+C)$, the two values of a obtained are 7.0×10^{-14} and 2.1×10^{-14} Ω^{-1} m^{-1} respectively. These values are similar to those obtained by previous workers.

On all of the three occasions that rainfall rate was measured, positive correlation was found between rainfall rate and precipitation current density for the 12-min averages. Two of the correlations, 0.74 and 0.54, are statistically significant. One of the periods (2nd June) also shows high correlation between potential gradient and rainfall rate, and space charge density and rainfall rate, but it seems more likely that these correlations are a result of the inter-relationship between the electric parameters rather than a real correlation. The scatter diagrams for precipitation current density and rainfall rate for the 2nd and 26th June records are shown in Fig. 8.10. If the relationship is written as $I = \alpha R + \beta$, then the two records give $\alpha = 2.75 \times 10^{-5}$ C m^{-3} and 7.62×10^{-5} Cm^{-3} respectively, and $\beta = 0.48$ pAm^{-2} and 3.0 pA m^{-2} respectively. A

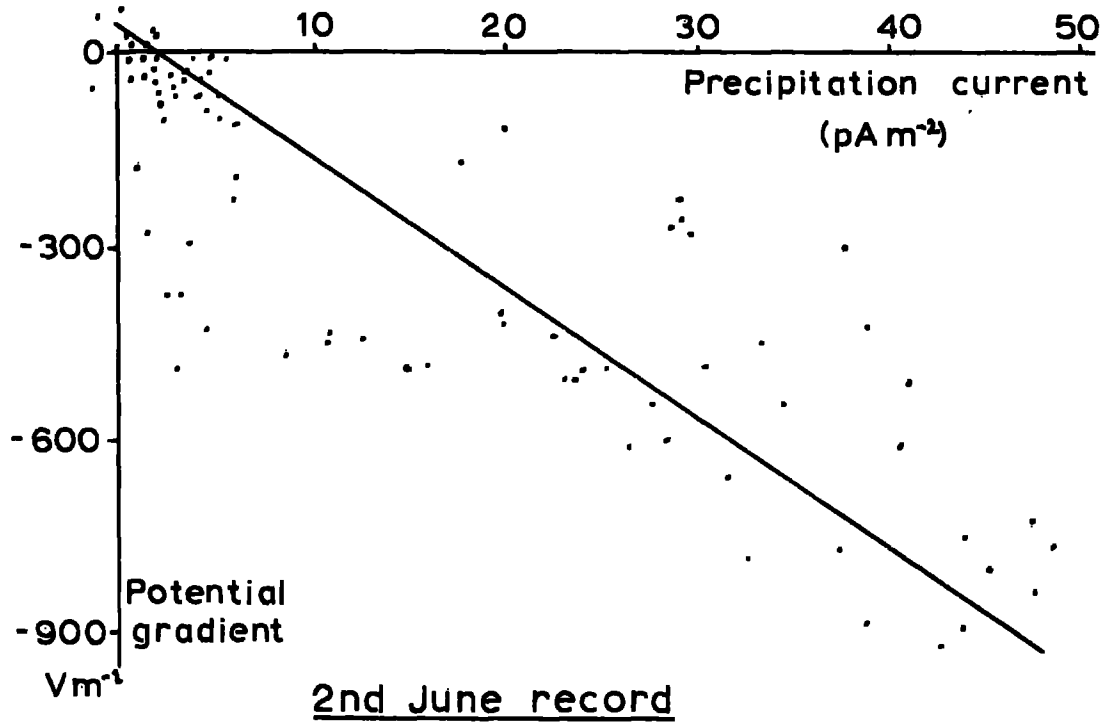

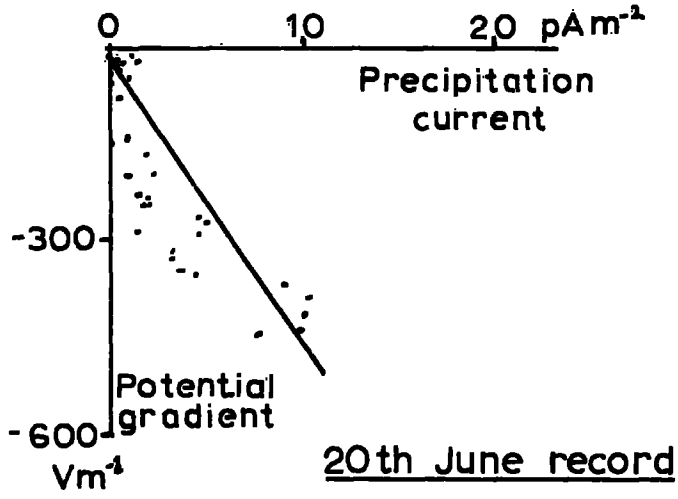

Fig. 8.9 Scatter diagrams of potential gradient versus precipitation current density.

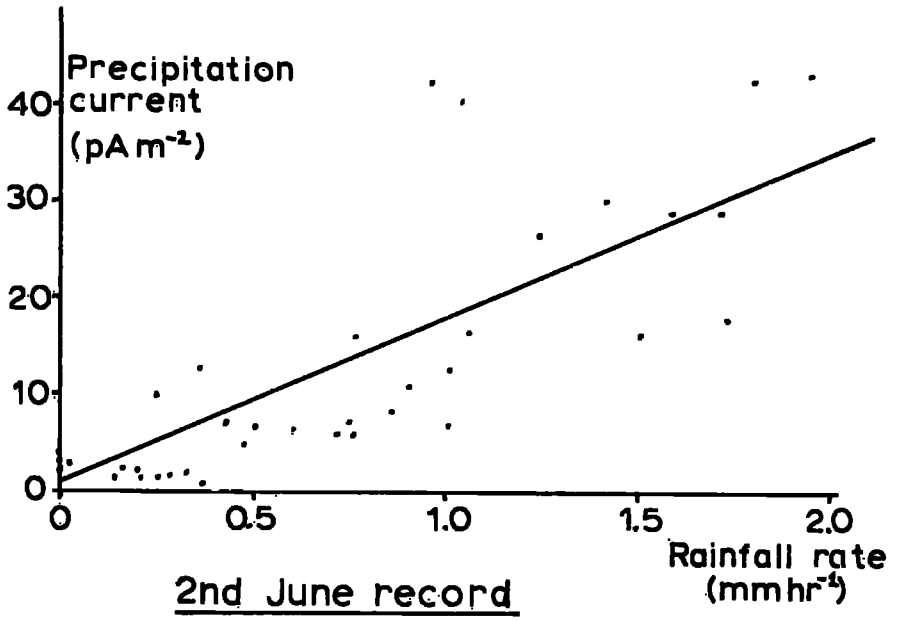

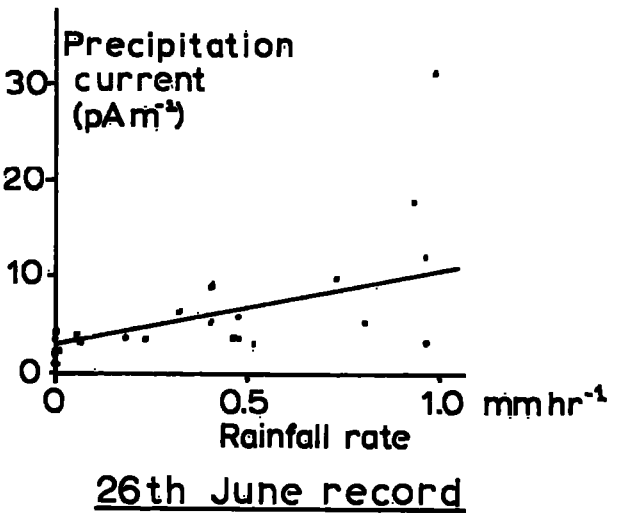

Fig. 8.10 Scatter diagrams of rainfall rate versus precipitation current density.

straight line fit may not be the best one for the scatter diagrams, and an equation of the form $I = \alpha R^2$ may be better.

The above results demonstrate the immense variability of the conditions influencing precipitation electrification and show that any results are very difficult to interpret in a general sense. However, one conclusion that can be made is that the variation of the parameters close to the ground has a great influence on the precipitation electrification, and that a charge separation process in the bottom hundred metres or so of the atmosphere is inferred. This is reflected in the correlation between space charge density and potential gradient at the ground, which requires a relatively thick space charge blanket, and the correlation between space charge and precipitation current. The evidence of Section 8.1 also points to a precipitation charge separation process close to the ground which is in some way dependent upon wind speed. It therefore seems a reasonable inference that drop-shattering, or a similar process, in the lower part of the atmosphere gives rise to at least some of the rain electrification observed at the ground.

The charge separation processes at cloud height seem to be smaller in magnitude and to be more apparent in very quiet, relatively windless conditions. In addition, each charge separation process may depend to a different degree upon rainfall rate, and may even be

different on occasions when the rainfall rate is the same but the drop-size spectra are different. It seems essential that more of the variables will have to be taken into account before a more complete understanding of the processes operating can be obtained.

CHAPTER 9

CONCLUSIONS AND SUGGESTIONS FOR FURTHER WORK

9.1 The Electrical Structure of Nimbostratus Snow Clouds

The experimental work carried out on snow clouds, particularly that of previous workers, enables some general conclusions to be reached. Firstly, in relatively quiet conditions in the absence of blowing snow near the ground, the net precipitation charge will be negative provided the snow is dry. The potential gradient at the ground will usually be positive, suggesting a larger total cloud space charge than precipitation space charge. There is no reason to believe that charge separation takes place other than in the cloud, although it may occur down to ground level if the surface air temperature is below or close to freezing point. There is almost certainly only one charge separation mechanism, and ice-crystal contact electrification seems most likely.

The results of the experimental work described earlier, particularly the cross-correlation between the two stations, suggest that electrification is associated with cloud zones and that within these zones any time variations in the physical processes are relatively slow. Observed variations in electrification are more likely to be a result of movement of the cloud rather than physical development of the cloud zone. That is, the time-scale of changes

within a cloud zone is normally much longer than the time of passage of the zone over a stationary observer. It might be expected that the size of these cloud zones is related in some way to the autocorrelation width described earlier, and they probably therefore have dimensions of the order of several km.

The effects of wind speed upon a snow cloud are almost certainly smaller than those upon a rain cloud, but with dry snow on the ground, blowing snow becomes strongly electrified and renders cloud observation by ground-based apparatus extremely difficult. In addition, due to the low fall speed of snowflakes, the measurement of snow current density with shielded receivers becomes inefficient with wind speeds in excess of a few metres per second.

9.2 The Electrical Structure of Nimbostratus Rain Clouds

The upper portion of a nimbostratus rain cloud is similar to that of a snow cloud, and electrification in these regions almost certainly proceeds in a similar way. Conclusive evidence, for example the potential gradient measurements of Reiter (1955), has shown that quiet snow becomes positively charged on or shortly after melting. This may be due to either or both of two causes, charge separation associated with the change of state, and charge separation due to the breaking of large melted snowflakes into raindrops. Evidence presented by many previous workers has indicated the existence of a

charge separation process close to the ground, particularly evidence of the presence of layers of space charge in the bottom few tens of metres of the atmosphere.

The evidence presented in this thesis has shown that, whereas there is almost certainly charge separation at cloud level, there is a charge separation process operating close to the ground. This process gives a positive charge to the larger raindrops and a negative charge to the air or smaller droplets. Both the potential gradient-space charge correlations and the precipitation current-wind speed correlations indicate that this process operates up to heights of perhaps a few hundred metres, at least in the Pennine region. The evidence is also consistent with the charge separation being a result of drop-shattering in wind gusts close to the ground, a theory first proposed by Simpson (1909). This process may give rise to electrification which is greater than that produced at cloud level. Hence we must now assume that the nimbostratus rain cloud system comprises three charge separation zones, one acting in the solid state at higher levels, the second operating around the melting level in the opposite sense, but with about the same magnitude, and a third process acting from ground level up to an unknown height. All of these processes will depend to some extent upon the cloud activity and the precipitation rate, but the third process is

dependent upon wind speed and probably also the presence of large raindrops (1-4 mm diameter).

The autocorrelation measurements suggest that the horizontal dimensions of cloud across which the electrical parameters are autocorrelated is relatively constant for nimbostratus clouds, and independent of cloud speed. In view of the variability of conditions and of electrification, this result is remarkable. This horizontal distance, the 'autocorrelation width', is of the order of 3-10 km, depending upon the measuring instrument used and its location. For a site with uniform exposure, this autocorrelation width may prove to be a characteristic of nimbostratus clouds and may therefore be used as a criterion for their identification.

The cross-correlation measurements between the two stations showed that variations in the electric parameters are more likely to be a result of cloud movement rather than cloud development. On one occasion, however, simultaneous correlation was found between precipitation current density at the two sites, separated by 5 km, for a very slow-moving cloud system. Thus it seems that large-scale development of the cloud system may contribute to the variations in electrification in very quiet, slow-moving systems. In these systems the general electrification is usually much smaller in magnitude.

9.3 The Proposed Nimbostratus Electrical Model

An electrical model of nimbostratus clouds has been proposed in Chapter 2, and it has been shown that it is consistent with measurements made previously. It should be possible to test the model in greater detail if some of the variables are removed. The snow cloud would appear to be most suitable, since it involves only a single charge separation process, and the precipitation particle fall speed does not depend greatly on particle size. The conductivity within the cloud must be obtained, as well as the approximate cloud dimensions and snow fall speed. It should then be possible to test the model's predictions of potential gradient at the ground with the observed values. It may be possible to observe phase variations between the parameters, although this may be too complicated by mechanical effects to be interpreted easily.

Because of the complex nature of rain cloud electrification it will be extremely difficult to test the model. However, if one of the charge separation processes in the rain cloud is dominant, sufficient approximations may be able to be made to enable a further test of the model. The existence of wide variations in drop sizes and the different raindrop fall speeds greatly complicates matters.

9.4 Suggestions for apparatus

Precipitation electrification is a very complex phenomenon, and the maximum amount of data is therefore required. For this purpose

the continuous automatic recording of data is considered essential, and it is very helpful to have the data in a form which is suitable for computer handling. Because of the large variation in the magnitudes of the parameters, a single instrument with limited range has often proved inadequate. Thus unless instruments with logarithmic response can be developed, much of the apparatus must be duplicated and operated on different ranges to avoid loss of information.

The operation of mobile apparatus for the recording of atmospheric electric and meteorological parameters has been proved possible. However, there are many practical difficulties not encountered with fixed equipment, as well as the problem of variation in site, and it is therefore recommended that the use of mobile equipment should be avoided.

The experience obtained with shielded rain collectors suggests that it may be advisable to mount the collecting surfaces below ground level and to avoid having projections above it. Narrow-spacing wire mesh is a very effective method of eliminating the splashing of raindrops in the vicinity of a collector.

9.5 Suggestions for Further Work

It has been shown that representative measurements of atmospheric electric parameters can be made at a single ground station. In addition, the problems associated with setting up

a network of stations make it an unattractive project. Possibly the most valuable measurements that are required are those made above ground level. The bottom 500 metres of the atmosphere is probably the best region to study, as some of the least understood phenomena take place in this region.

Potential gradient is the simplest parameter to measure, and if this is carried out at several heights, either simultaneously with several instruments or successively with a single instrument, then some estimation of the variation of space charge with height may be obtained. Hence it may be possible to estimate the height of the various charge separation processes. The operation of a tethered balloon or even a kite should make it possible to obtain these measurements relatively cheaply without requiring sophisticated equipment.

Lanehead is probably an ideal site for such an investigation, as it is situated 450m above sea level. This means it is close to freezing level for many of the winter months, and often close to cloud base.

APPENDIX 1

VERTICAL POTENTIAL GRADIENT UNDER CENTRE OF CYLINDER OF UNIFORM CHARGE DENSITY

The vertical potential gradient due to a single charge ρ at a height y above the earth and a horizontal distance of r is given by

$$F = \frac{\rho y}{2\pi\varepsilon_0 (r^2 + y^2)^{3/2}}$$

The vertical potential gradient due to a circle of charge of radius r is therefore $2\pi r$ times this value, and hence the potential gradient due to a horizontal disc of charge of height y is given by

$$F_D = \frac{\rho y}{\varepsilon_0} \int_0^R \frac{r\,dr}{(r^2 + y^2)^{3/2}} = \frac{\rho y}{\varepsilon_0} \left\{ \frac{1}{y} - \frac{1}{(R^2 + y^2)^{\frac{1}{2}}} \right\}$$

$$= \frac{\rho}{\varepsilon_0} \left\{ 1 - \frac{y}{(R^2 + y^2)^{\frac{1}{2}}} \right\} \quad \ldots\ldots\ldots \quad (1)$$

The vertical potential gradient due to a vertical cylinder of depth H, radius R, of uniform charge density ρ, at a height h above the ground (Fig. A.1), is thus given by

$$F_c = \frac{\rho}{\varepsilon_0} \int_h^{H+h} \left\{ 1 - \frac{y}{(R^2 + y^2)^{\frac{1}{2}}} \right\} dy$$

$$= \left[y - (R^2 + y^2)^{\frac{1}{2}} \right]_h^{H+h}$$

$$= \frac{\rho}{\varepsilon_0} \left[H + (R^2 + h^2)^{\frac{1}{2}} - (R^2 + (H + h)^2)^{\frac{1}{2}} \right] \ldots\ldots\ldots \quad (2)$$

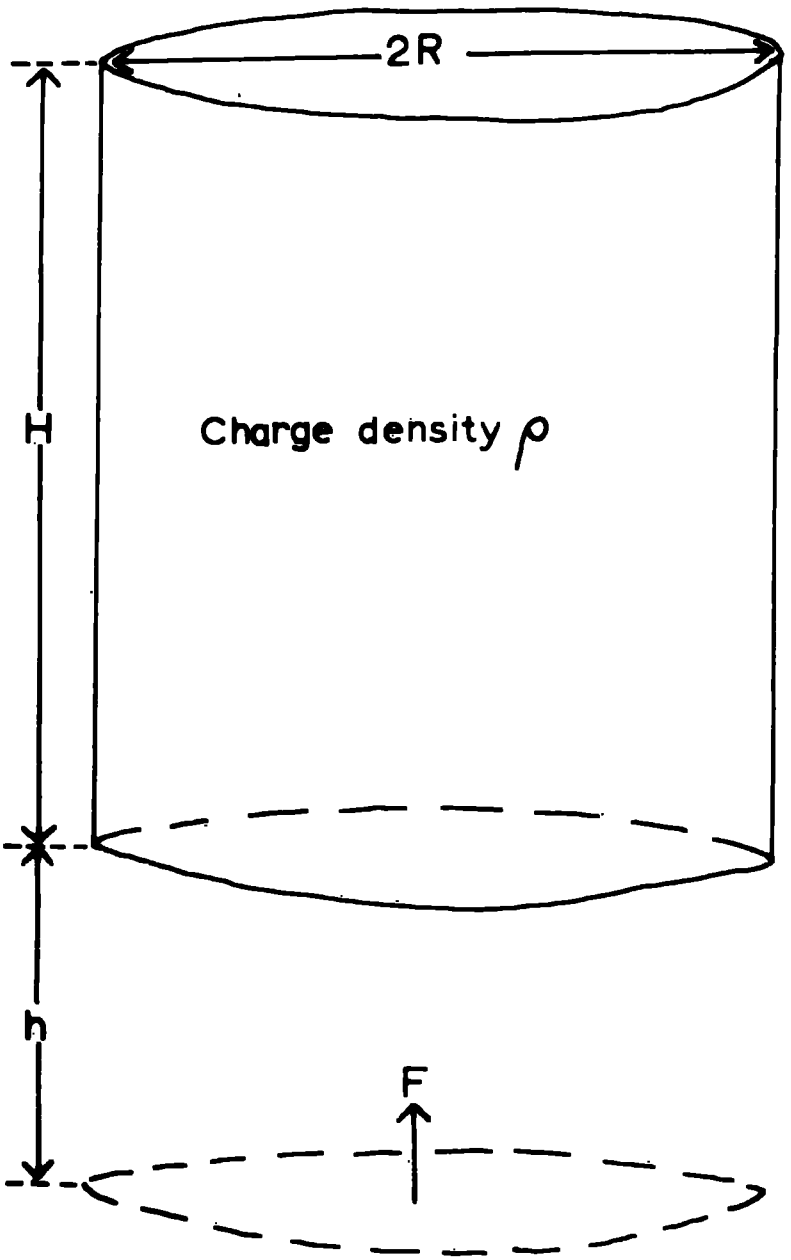

Fig. A.1 Cylindrical cloud model.

VERTICAL POTENTIAL GRADIENT UNDER CENTRE OF CYLINDER OF CHARGE DENSITY LINEARLY DECREASING WITH HEIGHT

As discussed in Chapter 2, if precipitation and cloud charge is being generated in a cloud such that the cloud charge is of uniform density, then the precipitation current density must increase linearly with decreasing height throughout the charging region. For a cloud whose charging region depth is H, base height h, and current density below cloud base I_o, the current density I at a height y above the ground, for $y > h$, will be given by

$$I = \frac{-I_o y}{H} + \left(1 + \frac{h}{H}\right) I_o$$

The precipitation space charge σ at a height y will thus be given by

$$\sigma = \frac{I}{v} = \frac{I_o}{v}\left\{1 + \frac{h}{H} - \frac{y}{H}\right\}$$

where v is the precipitation fall speed. From equation (1), the vertical potential gradient at the ground due to a disc of precipitation space charge at a height y will be given by

$$F_D = \frac{I_o}{\varepsilon_o v}\left\{1 - \frac{y}{(R^2 + y^2)^{\frac{1}{2}}}\right\}\left\{1 + \frac{h}{H} - \frac{y}{H}\right\}$$

The potential gradient at the ground due to the precipitation in the charging region will thus be given by

$$F_e = \frac{I_o}{\varepsilon_o v} \int_h^{H+h} \left\{ \left(1 + \frac{h}{H}\right)\left(1 - \frac{y}{(R^2 + y^2)^{\frac{1}{2}}}\right) - \frac{y}{H} + \frac{y^2}{H(R^2 + y^2)^{\frac{1}{2}}} \right\} dy$$

$$= \frac{I_o}{\varepsilon_o v} \left[\left(1 + \frac{h}{H}\right)\cdot\left(y - (R^2 + y^2)^{\frac{1}{2}}\right) - \frac{y^2}{2H} + \frac{y}{2H} (R^2 + y^2)^{\frac{1}{2}} - \frac{R^2}{2H} \sinh^{-1}\left(\frac{y}{R}\right)\right]_h^{H+h}$$

$$= \frac{I_o}{\varepsilon_o v} \left\{ H/2 - \tfrac{1}{2}\left(1 + \frac{h}{H}\right)\left((H + h)^2 + R^2\right)^{\frac{1}{2}} + \left(1 + \frac{h}{2H}\right)\left(h^2 + R^2\right)^{\frac{1}{2}} - \frac{R^2}{2H} \log\left\{ \frac{H + h + \left((H + h)^2 + R^2\right)}{h + (h^2 + R^2)^{\frac{1}{2}}}^{\frac{1}{2}} \right\} \right\}$$

The potential gradient due to the uniform precipitation space charge below the charging region, from equation (2), is given by

$$F_\rho = \frac{I_o}{\varepsilon_o v} \left\{ h + R - (h^2 + R^2)^{\frac{1}{2}} \right\}$$

Thus the total vertical potential gradient at the ground due to the precipitation space charge is given by

$$F = F_c + F_p$$

$$= \frac{I_o}{2\epsilon_o v} \left\{ H + 2h + 2R + \frac{h}{H} \cdot (h^2 + R^2)^{\frac{1}{2}} \right.$$

$$- \left. (1 + \frac{h}{H})((H + h)^2 + R^2)^{\frac{1}{2}} \right.$$

$$- \frac{R^2}{H} \log \left\{ \frac{H + h + \left((H + h)^2 + R^2\right)^{\frac{1}{2}}}{h + (h^2 + R^2)^{\frac{1}{2}}} \right\}$$

APPENDIX 2

THE FALL VELOCITIES OF PRECIPITATION PARTICLES

SNOWFLAKES

The fall velocity of snowflakes depends to a greater extent upon the crystal structure than upon the dimensions of the snowflake. The only type of snow crystal to exhibit a large dependence of fall speed upon crystal dimensions is graupel, and this is not usually found in nimbostratus conditions. Typical fall speeds of some snow crystals are shown in Table A.1.

TABLE A.1

Structure	Diameter (MM)	Fall Speed (CMS^{-1})
Needle	1.53	50
Plane dendrite	3.26	31
Spatial dendrite	4.15	57
Powder Snow	2.15	50
Rimed crystals	2.45	100
Graupel	2.13	180

RAINDROPS

The terminal velocities of raindrops of various sizes in still air at 1 atmosphere pressure are given in Table A.2.

TABLE A.2

DROP DIAMETER (MM)	TERMINAL VELOCITY (MS^{-1})
0.2	0.72
0.4	1.62
0.6	2.47
0.8	3.27
1.0	4.03
1.2	4.64
1.4	5.17
1.6	5.65
1.8	6.09
2.0	6.49
2.2	6.90
2.4	7.27
2.6	7.57
2.8	7.82
3.0	8.06
3.2	8.26
3.4	8.44
3.6	8.60
3.8	8.72
4.0	8.83

RAINDROP SIZE SPECTRA

The spectrum of drop sizes falling from a cloud varies widely in space and time, depending on many factors, and the spectrum of drops reaching the ground will not be the same as that at cloud level since the smaller droplets will evaporate before reaching the ground. On average, in nimbostratus conditions the spectrum of drop sizes can be fairly well represented by an empirical formula. One such formula, which has been quite widely used, is that derived by Best (1950). The fraction of the liquid water comprising drops smaller in diameter than x is given by

$$F = 1 - \exp\left\{ -\left(\frac{x}{a}\right)^n \right\}$$

where n is typically 2.25. The value of a depends upon rainfall rate R, and a fairly good value is obtained by

$$a = \alpha R^{\beta}$$

where $\alpha = 1.30$ and $\beta = 0.232$.

Two spectra calculated from this formula are shown in Fig. A.2, for rainfall rates of 1 and 4 mm $hr.^{-1}$. In nimbostratus conditions the rainfall rate does not normally exceed 5 mm hr^{-1}.

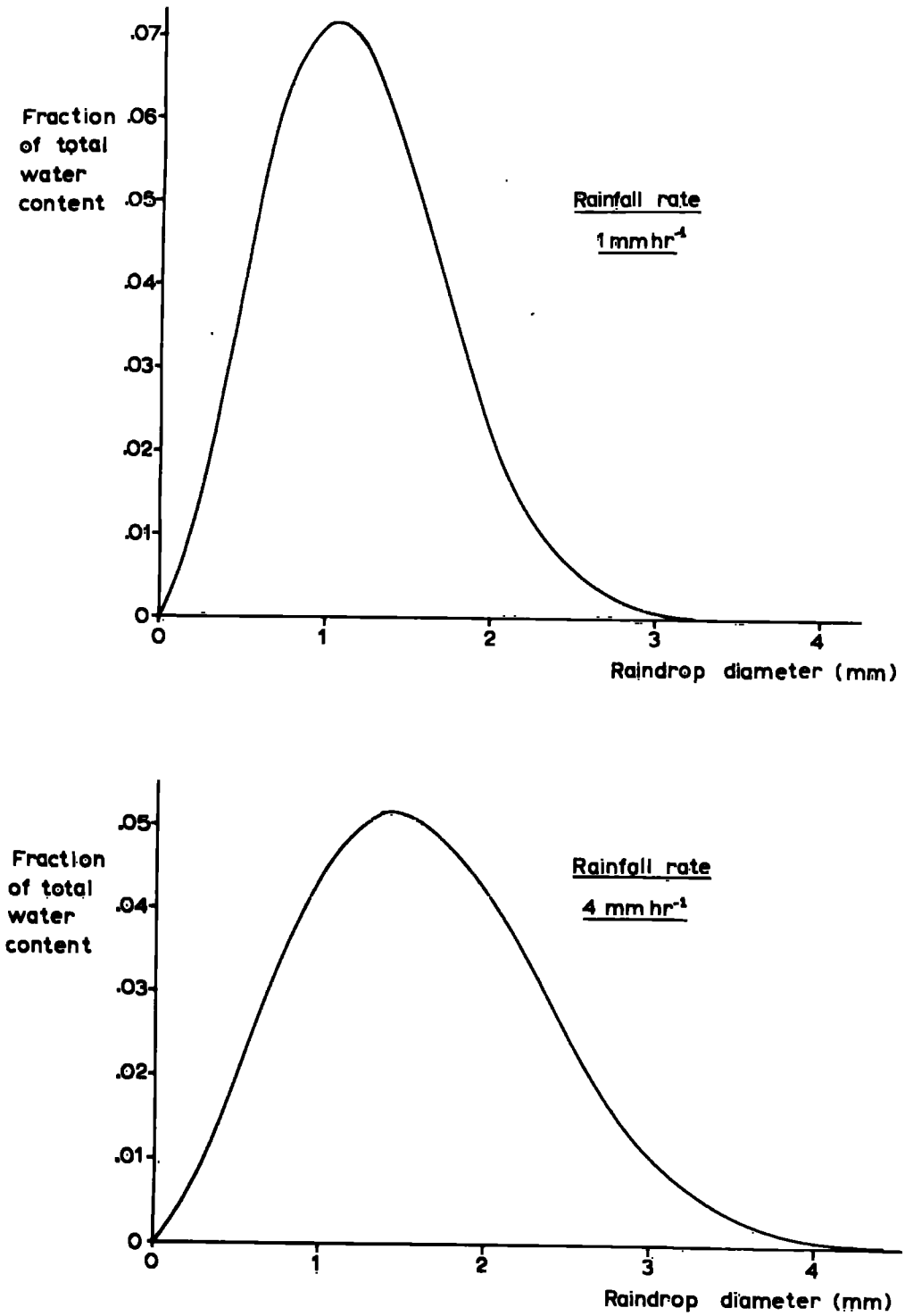

Fig. A.2 Typical raindrop size spectra.

APPENDIX 3

DEVELOPING SNOW CLOUD MODEL EQUATIONS

The vertical potential gradient at the ground due to a cloud system of very large horizontal dimensions compared with its vertical dimensions, containing one charge separation process, is derived below.

If precipitation charging takes place throughout a depth H of the cloud, and the cloud charge density ρ within the charging region is uniform, then if a precipitation current of density I(t) is leaving the cloud base at a time t, the following relationship will hold;

$$H \frac{d\rho}{dt} = -I(t) - \frac{H\rho}{\tau} \quad \ldots\ldots\ldots \quad (1)$$

where τ is the electrical relaxation time. If we further assume the precipitation current to vary sinusoidally, such that

$I(t) = I_o \sin wt$, then integration of equation (1) from t = 0 to t gives

$$\rho(t) = \frac{I_o}{H(w^2 + 1/\tau^2)} \left\{ \frac{1}{\tau} \cdot \sin wt - w \cos wt - we^{-t/\tau} \right\}$$

The potential gradient $F\rho$ at any time t due to the cloud charges will be given by $F\rho = \frac{\rho(t) \cdot H}{\varepsilon_o}$

The precipitation current density at any height h above the ground and above cloud base at a time t will be given by

$I(h) = I_o \sin w\left\{t - \frac{(H^1 - h)}{v}\right\}$ $\quad I(h) = I_o \sin w\left\{t - \left(\frac{H' - h}{v}\right)\right\}$

where H^1 is the cloud base height. The potential gradient due to the precipitation space charge will be given by

$$F = \frac{1}{\epsilon_o} \int I(h)\, dh$$

As an example, H was taken to be 5km, H^1 to be 1km, τ to be 1000s, $T = 2\pi\tau/w = 1000$s, and I(t) was taken to be zero up till $t = 0$ and after $t = 2\pi T$, I_o was taken as $-88.5\ pAm^{-2}$.

In order to calculate the potential gradient due to the precipitation space charge, it is necessary to consider three periods. The first period is from $t = 0$ when the charged precipitation first begins to leave the cloud up to $t = H^1/v$ when the first precipitation reaches the ground. The second period is from $t = H^1/v$ until $t = 2\pi T$, when the precipitation ceases to leave the cloud. The third period is from $t = 2\pi T$ until $t = 2\pi T + H^1/v$, after which no further precipitation reaches the ground.

(a) For the first period, the potential gradient due to the precipitation space charge is given by

$$F = \frac{I_o}{\epsilon_o v} \cdot \int_{H^1 - vt}^{H^1} \sin w\left(t - \frac{H^1 - h}{v}\right) dh$$

$$= \frac{I_o}{\epsilon_o}\left(1 - \cos w\left(t - \frac{H^1 - h}{v}\right)\right.$$

(b) For the second period,

$$F = \frac{I_o}{\varepsilon_o} \int_o^{H^1} \sin w \left(t - \frac{H^1 - h}{v}\right) dh$$

$$= \frac{I_o}{\varepsilon_o} \left(\cos w (t - H^1/v) - \cos w \left(t \frac{-H^1 - h}{v}\right)\right)$$

(c) For the third period

$$F = \frac{I_o}{\varepsilon_o v} \int_o^{H^1 - v(t-2T)} \sin w \left(t - \frac{H' - h}{v}\right) dh$$

$$= \frac{I_o}{\varepsilon_o} \left(\cos w (t - H^1/_v) - 1\right)$$

A computer program was written to calculate the potential gradient due to the cloud charge and precipitation space charge of the system described above, and the result is shown in Fig. 2.6.

MOVING QUASI-STATIC MODEL CALCULATIONS

As a comparison with the results of the developing snow-cloud model as described above, calculations have also been made to compute the potential gradient due to a moving cloud system which also gives rise to a sinusoidal variation of precipitation current density, but which is in steady state. In this case, the cloud system is assumed to consist of a number of bands of cloud. Each cloud band is assumed to be very large in a direction perpendicular to the cloud movement, but relatively narrow in the direction of cloud movement (Fig. A.3). Each band is assumed to be quasi-static equilibrium, as outlined in the model proposed in Chapter 2. The precipitation current density from each band is uniform and the cloud charge density in that band is directly proportional to it. For the purposes of calculation, the precipitation and cloud charges have been assumed to lie along a vertical plane at the centre of the band.

The vertical potential gradient due to a single charge ρ lying in such a plane, at a point a distance x from the plane is given by

$$F = \frac{\rho h^1}{2\pi\epsilon_0(x^2 + y^2 + h^{1}2)^{3}/2}$$

where h^1 is the height of the charge and y the distance from the mid-point of the plane.

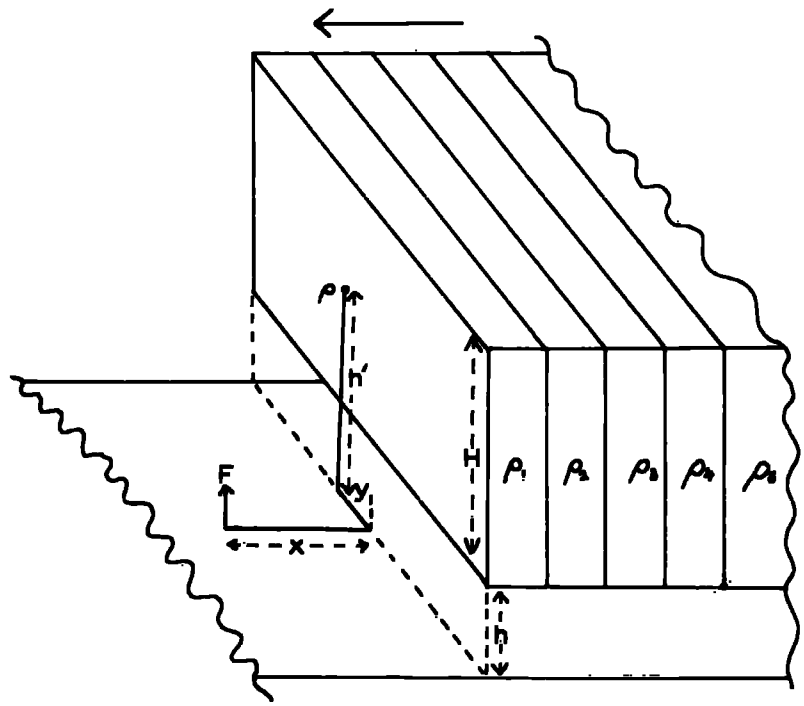

Quasi-static cloud system model

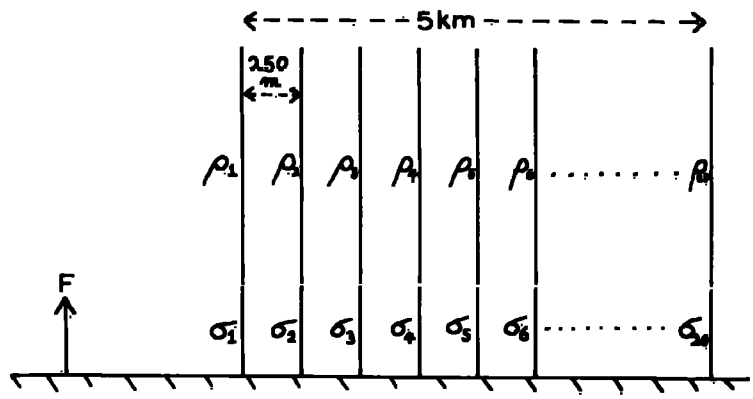

Simplified model for computer calculations

Fig. A.3 Quasi-static electrical cloud model.

The potential gradient due to a plane of charge of density ρ, height h and depth H is given by

$$F_\rho = \frac{\rho}{2\pi\varepsilon_0} \int_{-\infty}^{\infty} dy \int_{h}^{H+h} \frac{h^1 . dh^1}{(x^2 + y^2 + h^{12})^{3}/_{2}}$$

$$= \frac{\rho}{2\pi\varepsilon_0} \int_{-\infty}^{\infty} \left\{ \frac{1}{(x^2 + y^2 + h^2)^{\frac{1}{2}}} - \frac{1}{(x^2 + y^2 + (H + h)^2)^{\frac{1}{2}}} \right\} dy$$

$$= \frac{\rho}{2\pi\varepsilon_0} \left[\log \left\{ \frac{y + (y^2 + x^2 + h^2)^{1/2}}{x^2 + h^2} \right\} - \log \left\{ \frac{y + (y^2 + x^2 + (H+h)^2)^{1/2}}{x^2 + (H+h)^2} \right\} \right]_{-\infty}^{\infty}$$

$$= \frac{\rho}{4\pi\varepsilon_0} \log \left\{ \frac{x^2 + (H + h)^2}{x^2 + h^2} \right\} \quad \ldots\ldots\ldots\ldots \quad (1)$$

The potential gradient due to the space charge σ of the precipitation of the plane at the same distance x is given by

$$F = \frac{\sigma}{4\pi\varepsilon_0} \cdot \log \left\{ \frac{x^2 + h^2}{x^2} \right\} \quad \ldots\ldots\ldots\ldots\ldots \quad (2)$$

where $\sigma = I/_{v}$.

A computer program was written to calculate the potential gradient due to the above system at various distances. The cloud system was taken to have twenty bands, each 250m wide, and the precipitation current density was taken to vary sinusoidally throughout the system, with a maximum current density of $-88.5 pAm^{-2}$ in the centre band. The electrical relaxation time was taken as 1000s, the cloud depth 5km and cloud base 1km. If the cloud

system moves at 5 ms^{-1} the precipitation current density at a point on the ground varies in a similar manner to that in the developing system described above. The results of the calculations are plotted in Fig. 2.6.

REFERENCES

ADKINS, C.J. (1959) The small ion concentration and space charge near the ground Quart. J.R. Met. Soc. 85, 60-4

D'ALIBARD, T.F. (1752) Letter to Acad. de Sci.

APPLETON, E.V. WATSON WATT, R.A. and HERD, J.F. (1926) On the nature of atmospherics III Proc. Roy. Soc. A, 111, 654-77

AWE, O. (1964) Errors in correlation between time series. J. Atmos. Terr. Phys. 26, 1239-56.

BARNARD, V. (1951) The approximate mean height of the thundercloud charges taking part in a flash to ground. J. Geophys. Res. 56, 33-5

BERGERON, T. (1933) On the physics of cloud and precipitation. Gen. Ass. Int. Un. Geod.(Lisbon) pp. 156-70.

BEST, A.C. (1950) The size distribution of rain drops. Quart. J. R. Met. Soc. 76, 16-36.

CHALMERS, J.A. (1947) The capture of ions by ice particles. Quart. J.R. Met. Soc. 73, 324-34.

CHALMERS, J.A.	(1956)	The vertical electric current during continuous rain and snow. J. Atmos. Terr. Phys. 9, 311-21.
CHALMERS, J.A.	(1959)	The electricity of nimbostratus clouds. Recent Advances in Atmospheric Electricity - Pergamon Press.
CHALMERS, J.A.	(1967)	'Atmospheric Electricity', 2nd edition, Pergamon Press.
CHALMERS, J.A. and LITTLE, E.W.R.	(1947)	Currents of atmospheric electricity. Terr. Magn. Atmos. Elect. 52, 239-60.
CHAUVEAU, B.	(1900)	Études de la variation de l'électricité atmosphèrique Annales de B.C.M. 5, 1.
COLLIN, H.L. GROOM, K.N. and HIGAZI,	(1966)	The 'memory' of the atmosphere. J. Atmos. Terr. Phys. 28, 695-7.
COLLIN, H.L. and RAISBECK, I.A.	(1964)	Errors in recorded precipitation current caused by splashing. J. Atmos. Terr. Phys. 26, 1107-13.
DINGER, J.E. and GUNN, R.	(1956)	Electrical effects associated with a change of state of water. Terr. Magn. Atmos. Elect. 51, 477-94.

ELSTER, J. and GEITEL, H. (1885) Über die Elektrizitätsentwicklung bei der Regenbildung. Ann. Phys. Chem. 25, 121-31.

FRANKLIN, B. (1752) Phil. Trans. Roy. Soc. 47, 289.

FRENKEL, J.I. (1944) A theory of the fundamental phenomena of atmospheric electricity. J. Phys., Moscow 8, 285-304.

GISH, O.H. and WATT, G.R. (1950) Thunderstorms and the earth's general electrification. J. Geophys. Res. 55, 473-84.

GRENET, G. (1947) Essai d'explication de la charge électrique des nuages a l'orages. Ann. Geophys. 3, 306-7.

GROOM, K.N. (1966) Ph.D. Thesis, Durham.

GOTT, J.P. (1933) On the electric charge collected by water drops falling through ionized air in a vertical electric field. Proc. Roy. Soc. A, 142, 248-68.

GOTT, J.P. (1935) On the electric charge collected by drops falling through a cloud of electrically charged particles Proc. Roy. Soc. A, 151, 665-84.

GUNN, R. (1935) The electricity of rain and thunderstorms. Terr. Magn. Atmos. Elect. 40, 79-106.

GUNN, R.	(1948)	Electric field intensity inside of natural clouds. J. Appl. Phys. 19, 481-4.
HUTCHINSON, W.C.A.	(1960)	Ice-crystal contact electrification. Quart. J.R. Met. Soc. 86, 406-7.
KASEMIR, H.W.	(1955)	Measurement of the air-earth current density. Wentworth Conf. pp. 91-5.
KELVIN, LORD	(1860)	Atmospheric Electricity Roy. Instn. Lect., Pap. on Elect. and Mag., pp. 208-26.
LANE-SMITH, D.R.	(1967)	A new design of sign-discriminating field mill. J. Atmos. Terr. Phys. 29, 687-99.
LATHAM, J. and MASON, B.J.	(1961)	Generation of electric charge associated with the formation of soft hail in thunderclouds. Proc. Roy. Soc. A, 260, 537-49.
LENARD, P.	(1892)	Über die Elektrizität der Wasserfälle. Ann. Phys. Lpz. 46, 584-636.
MAGONO, C. and KIKUCHI, K.	(1961)	On the electric charge of relatively large natural cloud particles. J. Met. Soc., Japan, 39, 258-68.
MALAN, D.J. and SCHONLAND, B.F.J.	(1951)	The distribution of electricity in thunderclouds. Proc. Roy. Soc. A, 209, 158-77.

MASON, B.J. (1952) The production of rain and drizzle by coalescence in stratiform clouds. Quart. J.R. Met. Soc. 78, 377-85

MASON, B.J. (1953) On the generation of charge associated with graupel formation in thunderclouds. Quart. J.R. Met. Soc. 79, 501-9.

MASON, B.J. (1957) 'The Physics of Clouds', Univ. Press, Oxford.

MASON, B.J. and MAYBANK, J. (1960) The fragmentation and electrification of freezing water drops. Quart. J.R. Met. Soc. 86, 176-85.

MUHLEISEN, R. and HOLL, W. (1953) Elektrische Aufladung fallender Wassertropfen. Geofis. Pur. Appl. 25, 61-70.

MÜLLER-HILLEBRAND, D. (1954) The ion capture on polarised drops. Ark. Geofis. 2, 197-225.

NAKAYA, U. and TERADA, T. (1934) On the electrical nature of snow particles. J. Fac. Sci. Hokkaido Univ. 1, 181.

NOLAN, J.J. (1914) Electrification of water by splashing and spraying. Proc. Roy. Soc. A, 90, 531-43.

OGAWA, T. and BROOK, M.	(1969)	Charge distribution in thunderstorm clouds. Quart. J.R. Met. Soc. 95, 513-25.
PIERCE, E.T.	(1955)	Electrostatic field changes due to lightning discharges. Quart. J.R. Met. Soc. 81, 211-28.
RAMSAY, M.W. and CHALMERS, J.A.	(1960)	Measurements on the electricity of precipitation. Quart. J.R. Met. Soc. 86, 530-9.
REITER, R.	(1955)	Results of simultaneous recordings of atmospheric-electric parameters at six levels between 700 and 3000m above sea level. Zeitshift fur Meteorologie, 9, 116-120 (Translation)
REITER, R.	(1965)	Precipitation and cloud electricity. Quart. J.R. Met. Soc. 91, 60-72.
REYNOLDS, S.E.	(1953)	Thunderstorm precipitation growth and electrical charge generation. Bull.Amer. Met. Soc. 34, 117-23.
REYNOLDS, S.E.	(1954)	Compendium of thunderstorm electricity. U.S. Signal Corp. Research Report

REYNOLDS, S.E. and NEILL, H.W.	(1955)	The distribution and discharge of thunderstorm charge centres. J. Met. 12, 1-12.
SCHONLAND, B.F.J.	(1928)	The polarity of thunderclouds Proc. Roy. Soc. A, 118, 233-51.
SCRASE, F.J.	(1938)	Electricity on rain. Geophys. Mem., Lond. 75.
SHARPLESS, G.T.	(1968)	Ph.D. Thesis, Durham.
SIMPSON, G.C.	(1909)	On the electricity of rain and its origin in thunderstorms. Phil. Trans. A, 209, 379-413.
SIMPSON, G.C.	(1915)	The electricity of atmospheric precipitation. Phil. Mag. 30, 1-12.
SIMPSON, G.C.	(1919)	Brit. Antan. Exped. 1910-13. Meteorology (Calcutta) 1, 302-13.
SIMPSON, G.C.	(1927)	The mechanism of a thunderstorm. Proc. Roy. Soc. A, 114, 376-401.
SIMPSON, G.C.	(1942)	The electricity of cloud and rain. Quart. J.R. Met. Soc. 68, 1-34.
SIMPSON, G.C.	(1949)	Atmospheric electricity during disturbed weather. Geophys. Mem., Lond. 84, 1-51.

SIMPSON, G.C. and ROBINSON, G.D.	(1940)	The distribution of electricity in thunderclouds II. Proc. Roy. Soc. A, 177, 284-329.
SIMPSON, G.C. and SCRASE, F.J.	(1937)	The distribution of electricity in thunderclouds. Proc. Roy. Soc. A, 161, 309-52.
SMIDDY, M. and CHALMERS, J.A.	(1960)	Measurements of space charge in the lower atmosphere. Quart. J.R. Met. Soc. 86, 79-84.
SMITH, L.G.	(1954)	Electric field meter with extended range. Rev. Sci. Instrum. 25, 510-13.
SMITH, L.G.	(1955)	The electric charge of raindrops. Quart. J.R. Met. Soc. 81, 23-47.
VONNEGUT, B.	(1955)	Possible mechanisms for the formation of thunderstorm electricity. Wentworth Conf. pp. 169-181.
VONNEGUT, B. and MOORE, C.B.	(1958)	Preliminary attempts to influence convective electrification in cumulus clouds by the introduction of space charge into the lower atmosphere. Rec. Adv. Atmos. Elect. pp. 317-31.

WHIPPLE, F.J.W. and CHALMERS, J.A. (1944) On Wilson's theory of the collection of charge by falling drops. Quart. J.R. Met. Soc. 70, 103-20.

WILSON, C.T.R. (1916) On some determinations of the sign and magnitude of electric discharges in lightning flashes. Proc. Roy. Soc. A, 92, 555-74.

WILSON, C.T.R. (1919) Investigations on lightning discharges and on the electric field of thunderstorms. Phil. Trans. A, 221, 73-115.

WORKMAN, E.J. HOLZER, R.E. and PELSOR, G.T. (1942) The electrical structure of thunderstorms. N.A.C.A. Tech. Notes, No. 864.

WORKMAN, E.J. and REYNOLDS, S.E. (1950) Electrical phenomena occurring during the freezing of dilute aqueous solutions and their possible relationship to thunderstorm electricity. Phys. Rev. 78, 254-9.

WORKMAN, E.J. and REYNOLDS, S.E. (1953) Structure and electrification. 'Thunderstorm Electricity'. pp. 139-49.

WORMELL, T.W. (1939) The effects of thunderstorms and lightning discharges on the earth's electric field. Phil. Trans. A, 238, 249-303.

WORMELL, T.W. (1953) Atmospheric electricity; some recent trends and problems. Quart. J.R. Met. Soc. 79, 3-50.